Airflow and Temperature Distribution in Rooms with Displacement Ventilation

Jacobsen, T. V.

Publication date:
1993

Document Version
Publisher's PDF, also known as Version of record

Airflow and Temperature Distribution in Rooms with Displacement Ventilation

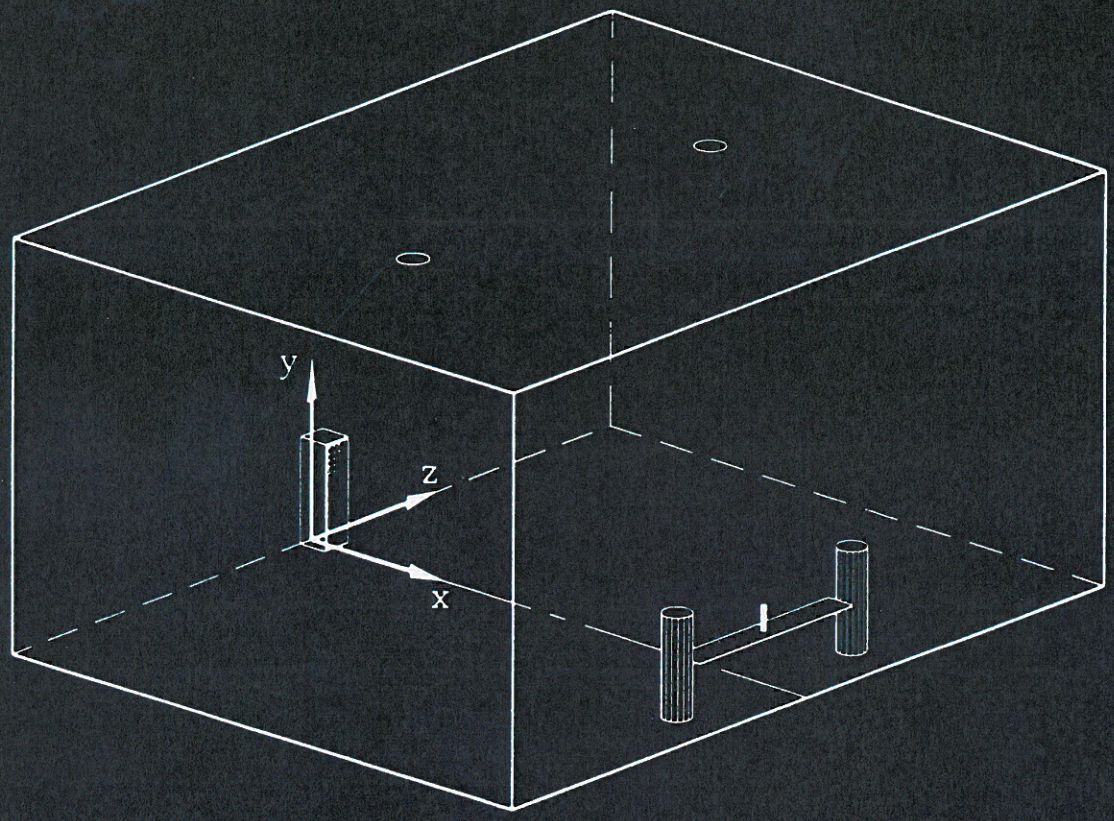

University of Aalborg, Denmark
Department of Building Technology and Structural Engineering

Ph.D.-thesis, Torsten V. Jacobsen, September 1993

ISSN 0902-7513 R9328

Airflow and Temperature Distribution in Rooms with Displacement Ventilation

- Full Scale Measurements, Analytical Models and Computational Fluid Dynamics

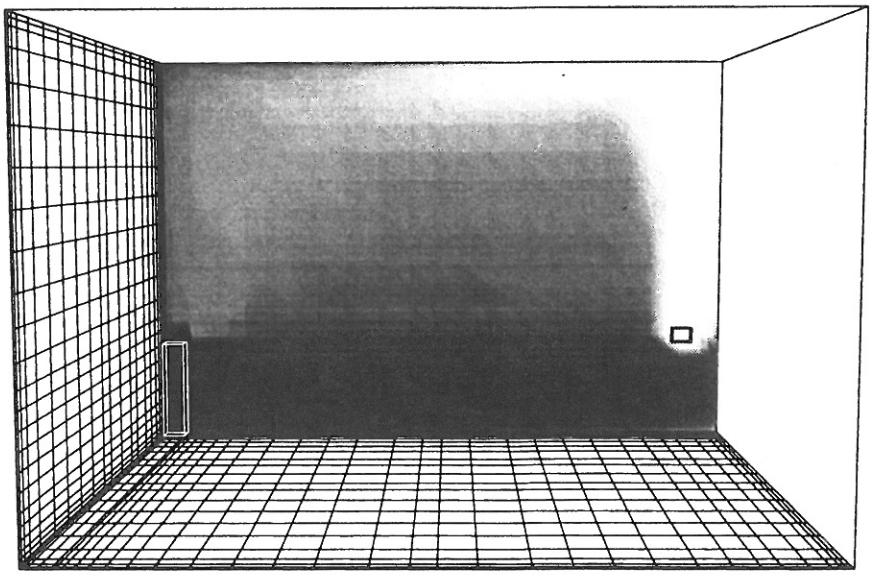

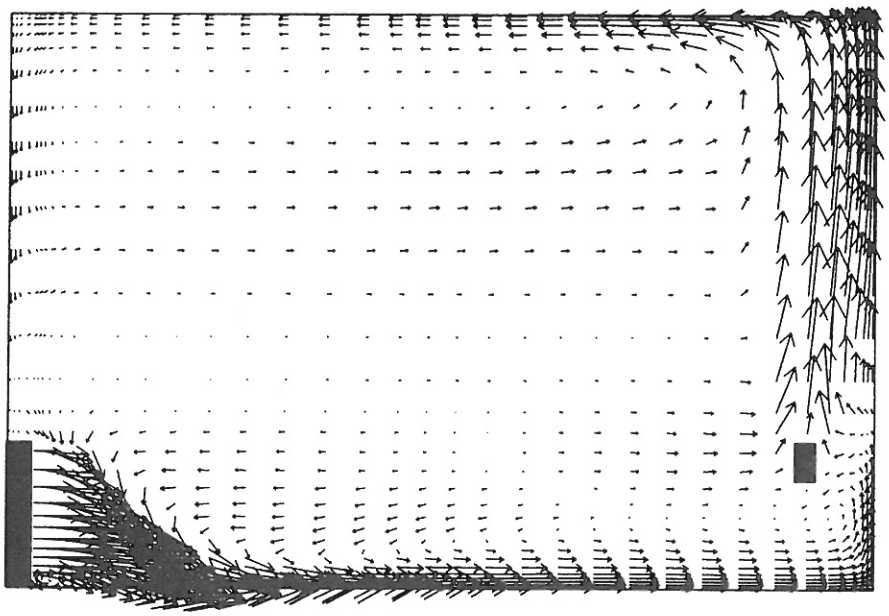

Torsten V. Jacobsen, September 1993.

Preface

The present thesis is submitted in accordance with the current conditions for attaining the danish Ph.D.-degree.

The research project has been carried out from January 1991 to September 1993 at the Institute of Building Technology and Structural Engineering, Aalborg University. It has been jointly funded by the Danish Energy Agency (Energy Research Programme 1991, EFP-91), the Danish Research Academy and The Rockwool Prize 1990. I would like to express my gratitude for the financial support.

The study has been supervised by Prof. Peter V. Nielsen whose guidance and advice is highly appreciated.

My thanks also extends to Prof. Shuzo Murakami, Dr. Shinsuke Kato, Tomoyuki Chikamoto and the rest of the staff at Murakami & Kato Laboratory for their hospitality and support during my stay at the Institute of Industrial Science, University of Tokyo.

Finally I would like to thank colleagues and members of the technical staff for their valuable assistance in completing this report. I would especially like to thank K.E. Hyldgaard for his assistance in the laboratory, N.Hornung for the drawings and K.Svidt for passing remarks on the work.

Torsten V. Jacobsen
September 1993

Abstract

This thesis deals with air flow and temperature distribution in a room ventilated by the displacement principle. The characteristic features of the ventilation system are treated in the whole room but main emphasis is laid on the analysis of the stratified flow region in front of the inlet device.

After a prefatory description of the background and the fundamentals of displacement ventilation the objectives of the current study are specified.

The subsequent sections describe the measurements of velocity and temperature profiles carried out in a full scale test room. Based on experimental data it is investigated if empirical models based on the theory for jets can be modified to apply for the dense air current traversing the floor in front of the inlet device. The semi-analytical expressions yield reasonable approximations for maximum velocities with distance from the inlet device and the vertical velocity profiles. The section is closed by a discussion of the occurrence of two different flow domains for the air flow along the floor. The measurements imply that the flow passes from a supercritical to a subcritical state.

The second part of the thesis mainly concerns itself with the description and application of more advanced models. Computional fluid dynamics (CFD) is applied in terms of a numerical turbulence model. The theory of the k-ϵ model and modifications to include stratification and low-Reynolds number effects are briefly discussed. The numerical solution procedure is addressed and the difficulties associated with the numerical modelling of the low-velocity, stratified flow are treated.

The importance of specifying proper boundary conditions is accentuated. Attention is paid especially to the temperature boundaries and the inlet boundary. It is found that the effect of thermal radiation must be included at the surfaces and different approaches are discussed.

Finally a comparative study between measurements and model results is carried out. Satisfactory model results are obtained provided appropriate boundary conditions are specified. The comparison, however, clearly demonstrates that availability of measured data is of crucial importance. Qualitatively satisfactory results do not ensure quantitative agreement.

Contents

Chapter 1

Introduction

It is the task of the HVAC-engineer to provide an acceptable indoor climate in terms of human health and comfort by means of heating, cooling and ventilation. To obtain satisfactory conditions for any occupant it is desirable to be able to control the environment with respect to distribution of velocities, temperature and contaminants in the entire room. A thorough understanding of the ventilation systems mode of functioning is a prerequisite for obtaining the optimal design and control strategy. The performance of the recently developed displacement ventilation systems differ substantially from that of traditional mixing ventilation systems and it is necessary for the engineer to gain insight into this principle of ventilation.

It is often possible to achieve acceptable conditions by applying general recommendations, simplified empirical models or experience but it is important to realize that the distribution of relevant quantities is ultimately determined by the transport processes that occur in any fluid flow. It is thus crucial to understand the properties of the flow and the underlying coherent physical mechanisms.

The majority of experimental investigations in ventilated rooms which has been carried out are not concerned with the basic fluid mechanics but aim rather at the over all performance of a specific ventilation arrangement or narrow down to local occupational problems. Such investigations are necessary in order to evaluate health and comfort risks in practice but an analysis of the underlying air flow phenomenons is seldom carried out. One way of addressing this issue is to engage in the fundamentals of fluid flow and this has been the incentive to applying computational fluid dynamics (CFD) in prediction of room air flow.

Before actually predicting room air flow at the design stage the accuracy, reliability and general validity of CFD-models should be evaluated by means of sufficiently detailed measured references. A large effort has been done in this area in recent years to verify the models in various types of flow. The low velocity buoyancy affected flow, e.g. flow in a displacement ventilated room, is one such type of flow which currently is subject to extensive research. An improved understanding of this type of flow is needed and

may constitute an important contribution to the ongoing progress of the CFD-method towards widespread application in the analysis of room air flow.

1.1 Flow in a displacement ventilated room

Displacement ventilation is often characterized as a plug or piston flow referring to the air volume being successively and uni-directionally displaced from the inlet towards the outlet. Such a description misleadingly implies that the air flow is uncomplicated. Low velocities, low level of turbulence and buoyancy effects make the flow field rather complicated and locally it exhibits features which are not completely understood neither with respect to the design of the ventilation system nor with respect to the basic physics.

The principle of displacement ventilation is illustrated in fig.1.1.

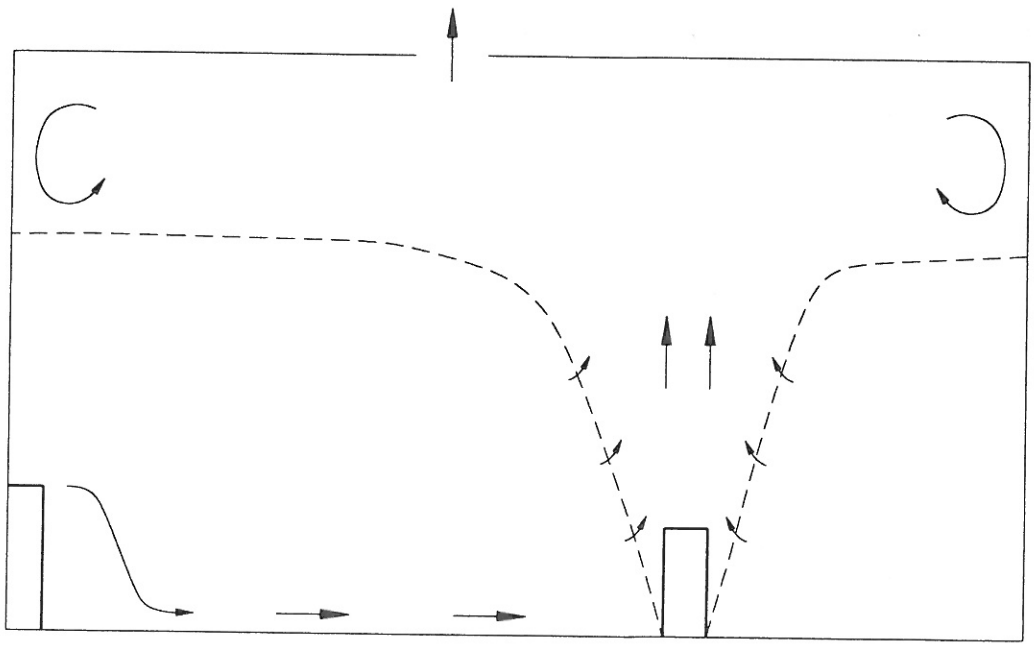

Figure 1.1 The principle of displacement ventilation.

Air with a temperature lower than the surrounding room air is supplied through the inlet device which in this case is wall-mounted. The inlet air enters the room at a rather low velocity and drops to the floor due to gravity forces. The lower part of the room is

is gradually filled by the cool air as if the fluid was water - or to express it differently, the room air in the lower part of the room is displaced.

The heated ascending air above the heat sources constitutes together with the cool injected air the driving forces which are decisive for the performance of the displacement ventilation system. The heat sources including occupants, machines etc., generate thermal plumes which transport warm air to the upper parts of the room. Due to the entrainment of ambient room air the volume flow in the plumes increases with height above the heat source. At a certain level the convective flows induced by the heat sources equal the supply air rate and a more or less distinctly separated upper zone may appear from which the excess heat and contaminants are removed efficiently. The vertical temperature gradient causes a stratified flow to be created and the mixing between horizontal layers is strongly diminished contrary to the intention of traditional mixing ventilation.

Special attention should be paid to the regions close to the inlet, above the heat sources and near the walls. These areas differ from the over all flow pattern and are particulary important to describe since they act as initiators of the air motion.

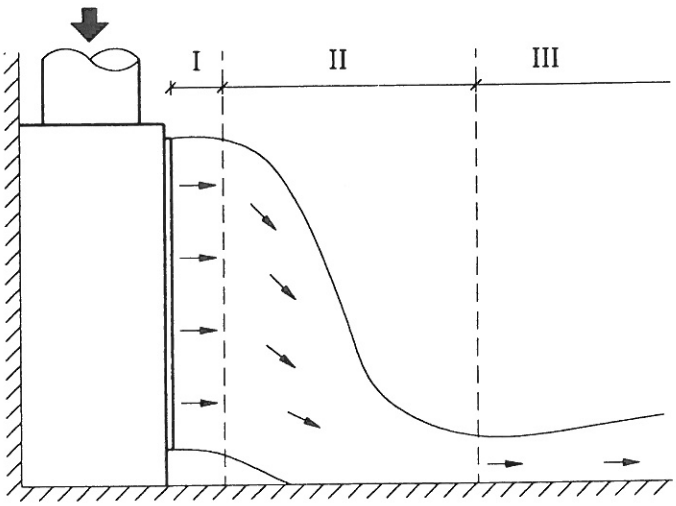

Figure 1.2 Air flow at the inlet device.

The flow in front of the inlet device can be described in three phases as shown in fig.1.2. Phase I is mainly governed by the specific design of the inlet device which determines the initial velocity distribution and induction. In phase II the difference in temperature between the inlet air and the surrounding room air causes acceleration of the cool air towards the floor as potential energy is converted into kinetic energy. A

vertical contraction takes place which subsequently leads to horizontal spreading as the descending air is deflected by the floor. A stratified flow emerges in phase III where the air of the dense cool layer moves with decreasing speed towards the walls. Moving along the floor the cold layer is gradually heated by the entrainment of ambient room air and by heat transfer from the floor. As the cold air reaches the surrounding walls an overlying layer of opposite flow direction may be generated and the characteristic low velocity flow in horizontal layers is developed if not disturbed by secondary air movement induced by obstacles, thermal plumes, human activity etc. The three-phase concept will be addressed in further detail in chapter 3 and 7.

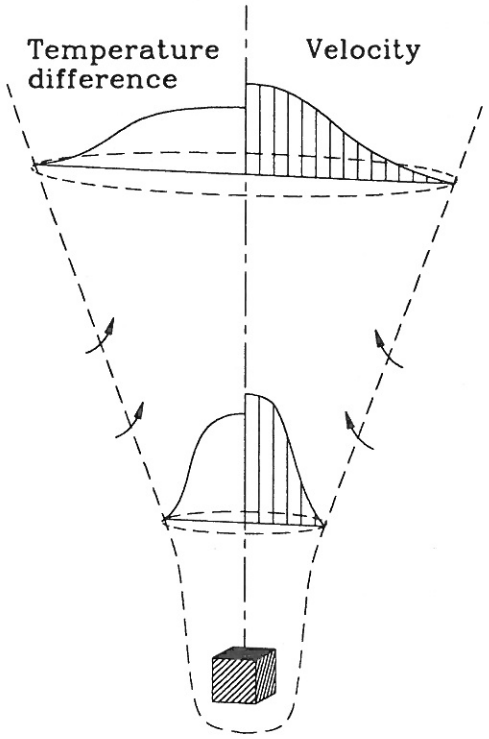

Figure 1.3 Emergence and development of a thermal plume.

The thermal plume emerges from the boundary layer close to the heat source as sketched in fig.1.3. Heat is transferred from the surface of the heat source to the adjacent air and give rise to density differences and the propagation of a boundary layer flow driven by natural convection. In the above immediacy of the heat source the flow converges and merge into the thermal plume. At this intermediate stage a transition takes place and the turbulent plume is established. At the shear layer between the rising plume and the ambient air entrainment occurs. This causes a reduction in the temperature difference between the plume and the surrounding air and subsequently

increasing width of the plume. The ascending air volume either continues its movement to the ceiling where it is deflected or it disintegrates at the level of neutral buoyancy where the driving temperature difference becomes approximately zero. The actual shape of the plume and its maximum height of elevation depends not only on the temperature difference to the ambient air but is affected to a large extent by the geometry of the heat source.

It is obvious that the over all flow pattern in an enclosure is strongly affected by the boundaries and in the case of displacement ventilation it is especially significant. Temperature differences between the inner and outer wall-surfaces induce an ascending or a descending boundary layer flow. In the latter case the vertical flow direction is opposite to the room air flow in general and a considerable transport of warm and polluted air from the upper to the lower part of the room may take place. The near wall flow does in some cases play an important role and may lead to the capsulation of a layer of high concentration of pollutants in the lower part of the room.

The Archimedes number is a key parameter in the development of flow from the inlet device, the plumes above the heat sources and the near wall air currents. It can be regarded as the ratio between buoyancy and momentum forces and it is of crucial importance to the air motion. The following chapters go more thoroughly into the subject.

Rather few investigations of stratified flow, thermal plumes and wall boundary layer flow have been carried out in displacement ventilated rooms but similar flow phenomenons can be found in other contexts, e.g. meteorology and hydraulics, and it is possible to transfer the knowledge from these research areas.

1.2 Background

The invention of displacement ventilation as a self-contained type of ventilation is relatively new but it is strongly inspired by the practice in industrial ventilation with high heat loads. *Baturin 1972* describes how the upward directed flow in a thermal plume can be used in natural ventilation. The thermal plume is the sole driving force which not only transports excess heat towards the outlet in the ceiling but also ensures supply of fresh air through openings near the floor by creating a negative pressure in the lower regions - known as the stack effect. Under favourable conditions a one way

directed flow ,i.e. piston-flow, appears but recirculation of air from the upper to the lower zone can not always be prevented.

The prospect of high ventilation effectiveness on account of relatively high temperature and contaminant concentration at the outlet was an incentive to the development of displacement ventilation. In order to utilize the advantages of the thermally driven flow in a more controlled way cool air is supplied directly into the occupied zone at low velocities.

The first experimental investigation of displacement ventilation for comfort purposes was performed in Norway and Sweden about 10 years ago. *Mathisen & Skåret 1982* point out the advantages of the system in terms of ventilation effectiveness and the disadvantages including high temperature gradients and air velocities in the occupied zone. The design of the air supply device is mentioned as an important and not yet resolved problem. To overcome this problem a wall-mounted low velocity inlet device with high induction is suggested by *Skåret 1986*.

At the same time simple box models were introduced for a displacement ventilated room by a two-zone model by *Skåret 1983* and later by a "filling box model" by *Sandberg and Lindström 1987* and *Sandberg 1988*. The first author pays special attention to ventilation effectiveness and energy consumption while the latter is mainly concerned with the movement in time of the stratification height.

It was realized that the stratified flow which is established close to the inlet device has a pronounced effect on the entire flow field and it is extremely important when comfort conditions are considered. A number of investigators consequently made an effort to describe this particular region.

Nielsen et. al. 1987 measured the velocities in front of different types of inlet devices. The subsequent analysis revealed important correlations with the Archimedes number and an empirical model for the calculation of maximum velocities close to the floor was suggested. The model - which is described in detail in chapter 2 - is elaborated on in *Nielsen 1990* and *Nielsen 1992*. *Sandberg 1989* also presented a model for the stratified flow appearing in front of the inlet device which was based on a different approach applying the theory of dense gravity currents. The theory was developed further in *Sandberg and Blomqvist 1989* and *Sandberg and Mattsson 1991* in the light of extended measurements.

Furthermore, a number of case studies has been undertaken, e.g. *Melikov et. al. 1989* focusing on human comfort, and within the field of practical application of the ventilation principle recommendations are given by *Skistad 1989* and *Jackman 1990.*

The methods applied in the above mentioned work rest on either empirical or confined theoretical basis. The applied models cover specific regions of the flow field and it is obvious to investigate what can be achieved from the more advanced approach of CFD which is capable of predicting the whole flow field.

A few attempts has been made to model velocity and temperature distribution in displacement ventilated rooms. *Sandberg and Holmberg 1990* carried out numerical simulation of a 2D transient case and were followed up by the 3D calculations by *Davidsson 1989* who presented promising results and captured the main flow pattern. In order to evaluate the potential of CFD as a design tool *Lemaire 1991* made a case study of a displacement ventilated room taking into account the effect of radiative heat transfer. Numerical simulation of air flow and temperature distribution in displacement ventilated rooms is also addressed in the work by *Chen 1988* and *Li 1993.*

The use of sophisticated CFD-models to describe the flow field has contributed to the understanding of important flow features but it has also clearly demonstrated that CFD applied to this type of flow is associated with certain shortcomings. The demand for an extended mathematical description of the flow and the requirements for detailed information of boundary conditions is counteracted by the limitations in available computer resources.

1.3 Objectives of this study

The potential and benefits of the displacement principle has been documented for many cases and is widely recognized. Despite the increasing use of the ventilation system the current knowledge of the fundamental physical mechanisms governing the air flow is insufficient.

It is the purpose of the study presented in this thesis to investigate characteristics of flow in a displacement ventilated room in general and in the stratified flow in front of the inlet device in particular. It is the aim to investigate aspects of the flow domain which are decisive and yet poorly understood.

By visualizing the flow field by smoke a line of procedure is adopted for the subsequent measurements. Emphasis is put on performing comprehensive measurements of velocity and temperature profiles which enable a full description of the air flow traversing the floor. Supplementary measurements are carried out in other regions of the room if considered important with respect to boundary conditions and model verification.

The measurements form the basis for evaluating empirical models for velocity and temperature distribution in the 3-dimensional stratified flow and they are intended to be used for comparison with the results obtained by the CFD-model.

The theory of turbulent fluid flow is treated and an adequate method for the numerical solution of the governing equations is chosen. The necessary extensions for simulating non-isothermal flows are added. It is the objective to investigate the effect of modifying the turbulence model and the problems associated with the specification of boundary conditions is dealt with. Especially the effects of stratification and redistribution of heat by radiation is investigated and different approaches to take these effects into account are studied.

It is the aim to describe the flow field and reach conclusions on how well the simple empirical models and the advanced CFD-model applies to the flow field in a displacement ventilated room. It is the intention to demonstrate how the application of different strategies and methods influence the model results and thereby present practical recommendations.

Chapter 2

Measurements

The experimental investigations are carried out in a full-scale room. The purpose is partly to obtain qualitative information about the over all flow pattern and partly to acquire measured data for a detailed analysis of the flow. The flow close to the floor is of primary interest and particulary detailed measurements are performed in this region to enable a description of the development of the dense air current.

The following section describes the set up of the test room, the applied measuring equipment, the line of procedure of the performed measurements and finally some instructive results are presented.

2.1 Configuration of full-scale room

The test room construction consists of an outer steel framework to which walls, floor and ceiling of 20 mm Douglas wood laminates are attached - see the sketch in fig.2.1 and the photos in fig.2.8. Large double glazed windows are mounted at two of the walls to facilitate visual observations. The floor and ceiling are insulated by 10 mm polystyrene and 50 mm glass wool respectively.

The air supply device, exhaust openings and heat sources are arranged in such a way that the middle plane of the room coincides with the middle plane of the inlet device constituting a symmetry plane for all boundary conditions. The purpose is to obtain a symmetrical flow field in order to reduce the required effort of carrying out the measurements and the succeeding analysis.

Two types of heat sources are applied. A heat source with a small surface area and a heat source with a large surface area simulating the human body. This approach aims at generating both diffuse and full penetrating thermal plumes. Three heat sources are placed close to the wall opposite to the inlet device. A small heat source is situated on a table in the centre plane with a large heat source on each side.

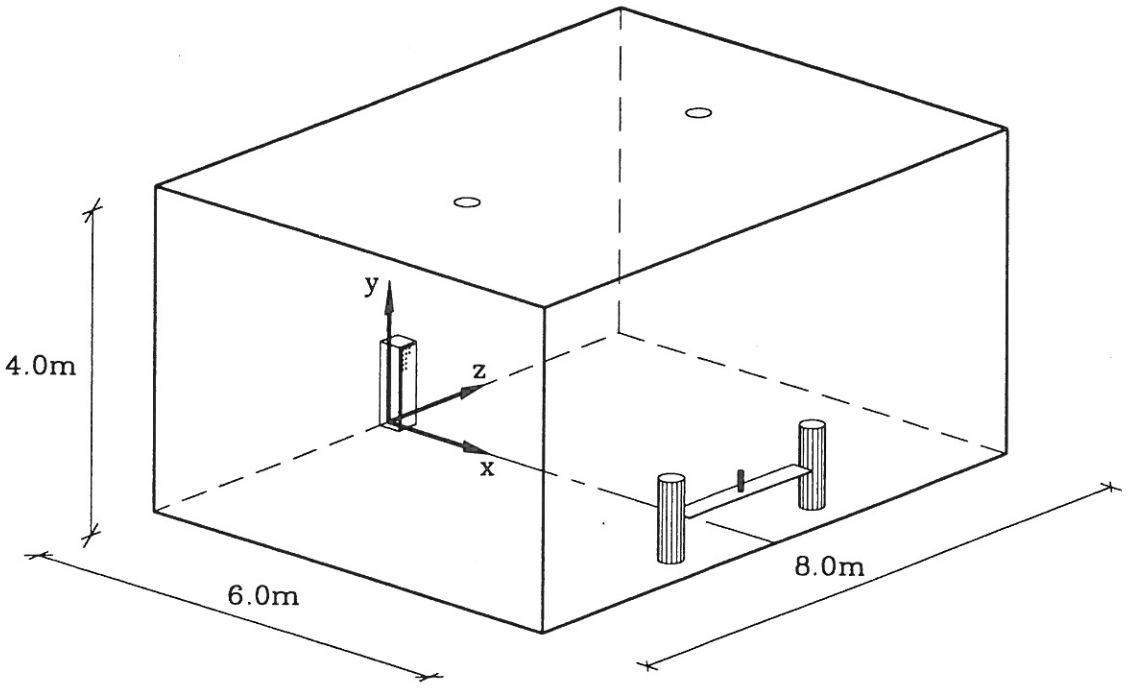

Figure 2.1 Test room arrangement and definition of coordinate system.

The small type of heat source consist of heating coils mounted on a iron base and surrounded by a tube of 15 cm in diameter and the height 20 cm (see fig. 2.8). The air is extracted from the bottom of the tube. It is heated by the coils and leaves the top of the tube as a rather narrow plume. The heat supply is variable up to a maximum of approximately 1000 W.

The larger type is composed of four electric bulbs placed inside an upright black-painted cylinder with a diameter of 40 cm. Contrary to the smaller type of heat source a thin boundary layer is established at the outer surface. The layer thickness increases as it moves in vertical direction and merge into a plume with relatively low velocities. The heat supply is fixed at 100 W to comply with the heat generated by a sedentary occupant.

A low-velocity inlet device of the type, Lindab COMDIF CDE-2010, is placed at the centre-line of the wall. The outside dimensions of the inlet device are given in fig.2.2. The interior of the inlet device (see fig. 2.8) is made up of a spreader which is located in the top where the air enters the inlet device. It is intended to ensure an uniform distribution of injected air. Two vertical flanges are placed at the sides of the box to

contract the air volume in horizontal direction just before it passes through the perforated front plate. A horizontal plate is situated approximately 40 cm above the bottom of the inlet box. Its primary purpose is to deflect the air upwards and there by enhance the initial mixing. In the original version the inlet device is equipped with a second plate but it is removed to obtain a distinct core region in the inlet air. The result of this design of the inlet device is a complex velocity distribution which is addressed in futher detail in the following section and in chapter 7.

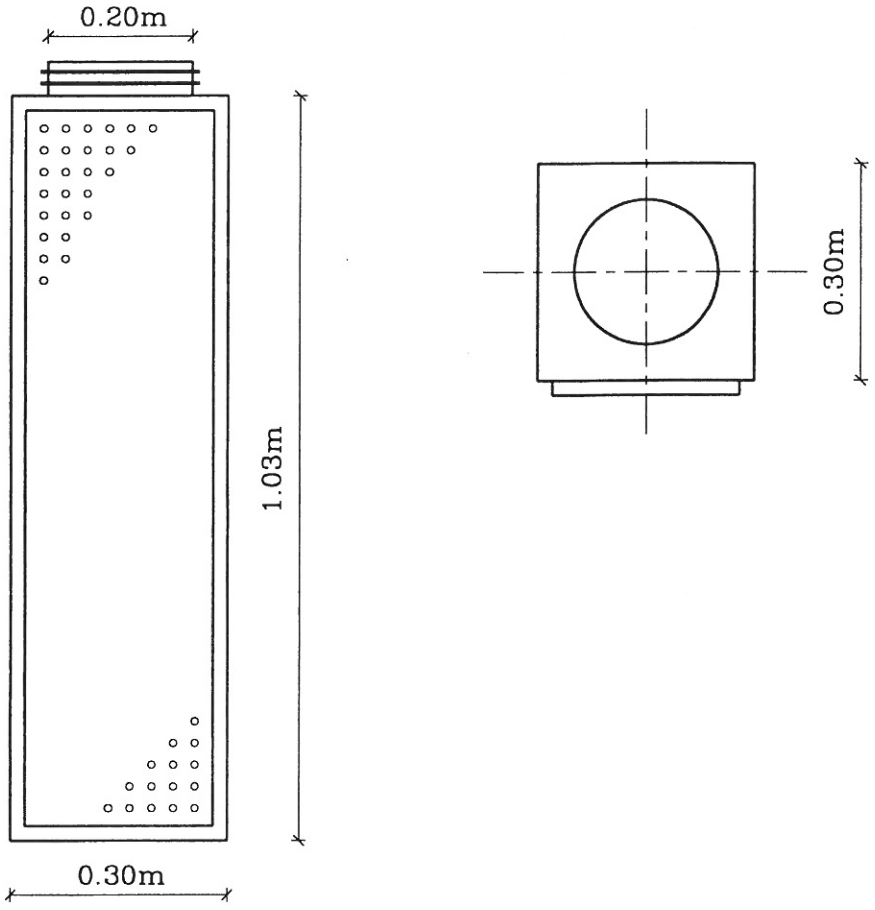

Figure 2.2 Outside dimensions of COMDIF CDE-2012 inlet device.

2.2 Visualizing the flow field by smoke

Smoke is added to the inlet in order to visualize the main features of the flow and subsequently choose a suitable line of procedure for the measurements.

Fig.2.3 shows a sketch of the air flow in front of the inlet device based on the visual impression. A small recirculation zone appears at the base of the inlet device and distinct eddies appear at the upper interface between the jet-like inlet air flow and the surrounding room air. The inlet air is not entering the room uni-directionally - not even under iso-thermal conditions. The direction normal to the inlet surface is prevalent but the velocity vectors are directed downwards in general. Initial spreading in horizontal direction is moreover observed at the circumference of the inlet surface.

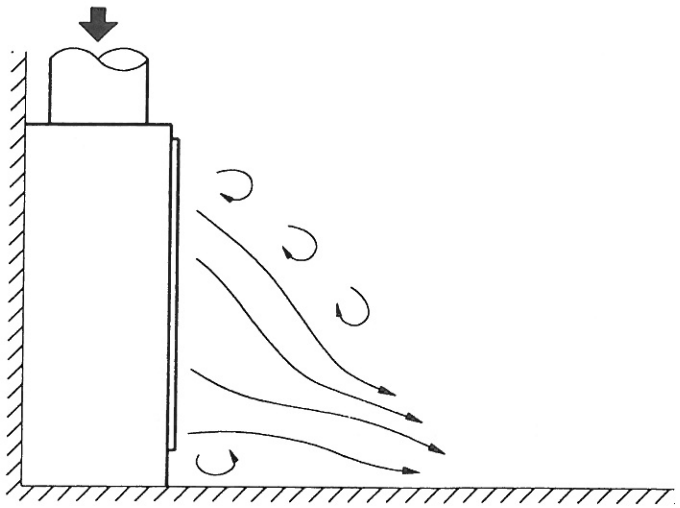

Figure 2.3 Sketch of air flow close to the inlet device.

Under iso-thermal conditions supplied air forms a jet-like flow which penetrates 1-2 m into the room where it disintegrates due to strong dispersion. Even at small temperature differences - and small Arkimedes numbers - the inlet air drops to the floor where it is deflected. It spreads out radially in a thin layer which moves towards the surrounding walls. At larger Archimedes numbers the interface between the cool layer at the floor and the room air becomes even more distinct - presumably due to a more stable stratification. The flow along the floor has a layer thickness of 20-30 cm with a slight decrement for increasing Arkimedes numbers. The streamlines are apparently emanating from the area where the cool air impinges on the floor - less than 0.5 m from the inlet device. The air is moving along straight lines corresponding to an approximately radial flow across the floor - see fig.2.4. It was verified by using smoke ampouls floor and drawing arrows on the floor indicating the flow direction.

Distinct differences between the thermal plumes generated by each type of heat source can be observed. When 200 W is supplied to the small heat source a narrow high velocity plume is formed which reaches the ceiling and is spread in a thin layer -

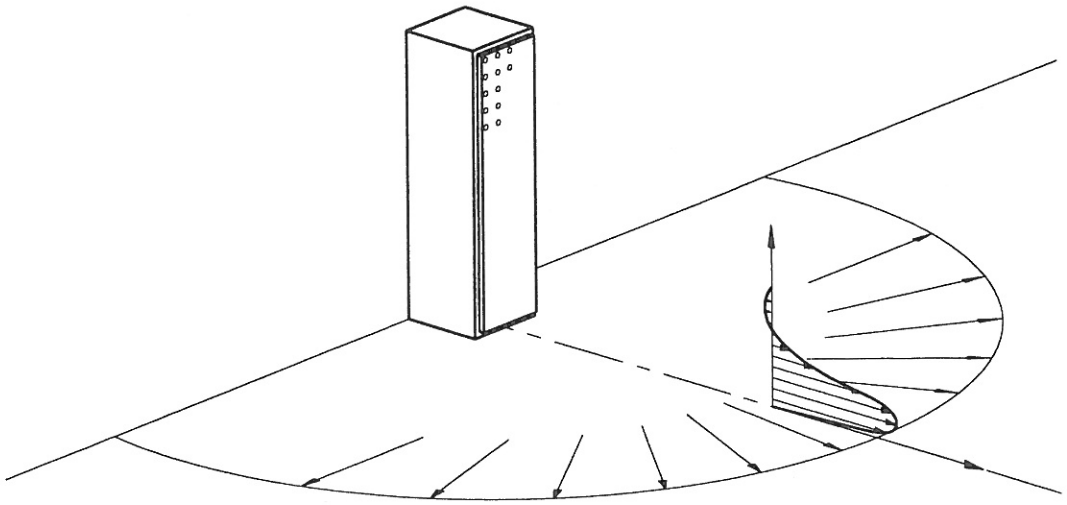

Figure 2.4 Air flow in front of the inlet device.

similar to the air flow in front of the inlet device but with opposite directed buoyancy. The plume is slightly drawn towards the adjacent wall due to the Coanda effect. The large heat sources on the other hand generates wide plumes which are diffused rapidly and rise only 1-2 m. The small distance between the heat sources cause some interaction between the plumes.

It was not possible to detect any significant air flow induced by temperature differences close to the walls but it can not be fully excluded taking into account the sensitivity of the flow to disturbances caused by smoke addition.

2.3 Outline of measured cases and results

The measurements are carried out under steady state conditions. Temperature and velocity profiles are measured in the dense air layer along the streamlines 1.0-3.5 m from the inlet device. In this range the stratified flow is fully established and not disturbed by walls and heat sources. In addition temperature profiles are measured at the walls, in full height of the room and the velocity distribution at the inlet is investigated.

DANTEC hot sphere anemometers and multichannel flow analyzer are employed for the velocity measurements. The predominant flow direction must be determined in advance when this type of anemometers are applied. The probes are calibrated in the range 0.0-1.0 m/s and the lower detection limit is estimated to 0.05 m/s taking into account the effects of convection induced by the hot sphere itself. Values of mean velocity and standard deviation are obtained by integration of sampling intervals of 2-4 minutes. The turbulence intensities derived from the standard deviation are, however, not considered reliable because the thermal mass of the sphere prevents the detection of rapid fluctuations.

Thermocouples, KAYE icepoint reference and FLUKE datalogger are applied for the temperature measurements. The system is calibrated in the range 0-40°C and the expected margin of deviation from the true value is ± 0.2 °C.

Polar coordinates are used for specifying the location of the measuring column as shown in fig.2.5. θ denotes the angle between the streamline and the centre line of the inlet device ($0 \leq \theta \leq \pi/2$) and r denotes the horizontal distance from the centre of the inlet device to the measuring column.

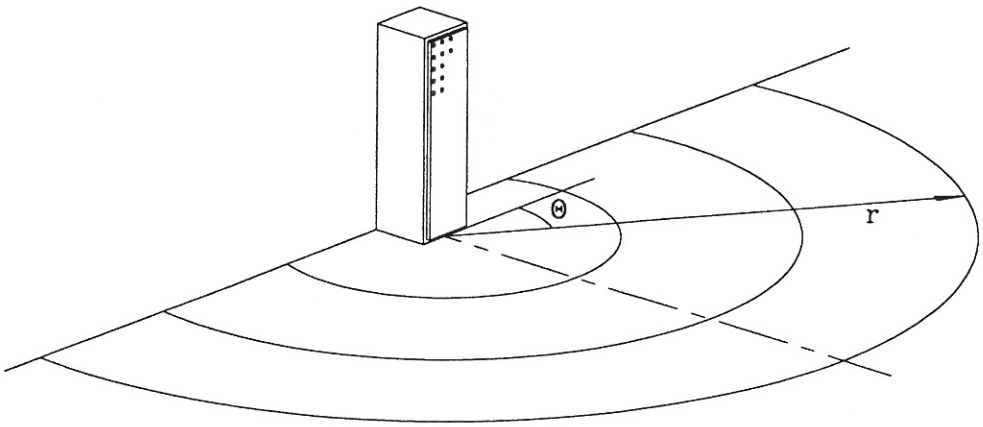

Figure 2.5 Coordinates in radial flow.

Table 2.1 gives a survey of the measured cases including - from left to right - case identification, inlet volume flow, supply air temperature, exhaust air temperature, air temperature in the height 1.10 m above floor level, reduced Arkimedes number, ordinary Arkimedes number and the total number of measured velocity and temperature profiles close to the floor.

case	q_i [m³/h]	T_i [°C]	T_e [°C]	$T_{1.1}$ [°C]	ϕ_{hs} [W]	Ar_r [°Cs²/m⁶]	Ar [-]	no. of prof.
A	300	15.4	21.3	19.7	600	618	1.4	38
B	300	17.9	21.7	20.5	400	383	0.9	14
C	300	12.8	22.8	19.7	1000	986	2.1	14
D	200	14.5	21.4	20.2	460	1850	4.0	10
E	300	22.2	21.6	21.7	0	-72	-0.1	8

Table 2.1 Specification of test cases.

The Archimedes number, Ar, and the reduced Archimedes number, Ar_r, presented in table 2.1 are defined as

$$Ar_r = \frac{\Delta T_0}{q_i^2} \qquad Ar = \frac{\beta g h \Delta T_0}{U_i^2} \tag{2.1}$$

ΔT_0 is the temperature difference between the occupied zone (y=1.10 m) and the inlet, $\Delta T_0 = T_{1.1} - T_i$. U_i and q_i are velocity and volume flow at the inlet surface, respectively. U_i is calculated as q_i/A_i where A_i is the front area of the inlet device. h is the height of the inlet device, β the volumetric expansion factor and g the gravitational acceleration.

The comparatively large number of measurements in case A serve to verify the assumption of symmetrical flow around the mid-plane of the inlet device as illustrated by figure 2.6. It is seen that the differences between velocity profiles in the two streamlines are negligible while some discrepancy is found for the temperature profiles. In spite of the slight disagreement the flow field is treated as symmetrical in the measurements and later in the CFD calculations. Measurements are consequently confined to only one half of the enclosure.

Fig.2.6 is representative in the sense that a similar sequence of profiles can be found along any streamline. The profiles exhibit the characteristics of a buoyancy driven dense current spreading horizontally along a solid surface in a 3-D space. The maximum velocity decreases gradually and the temperature difference between the cool layer and the ambient air is rapidly reduced as the air passes along the floor. This particular type of flow is further analyzed in chapter 3.

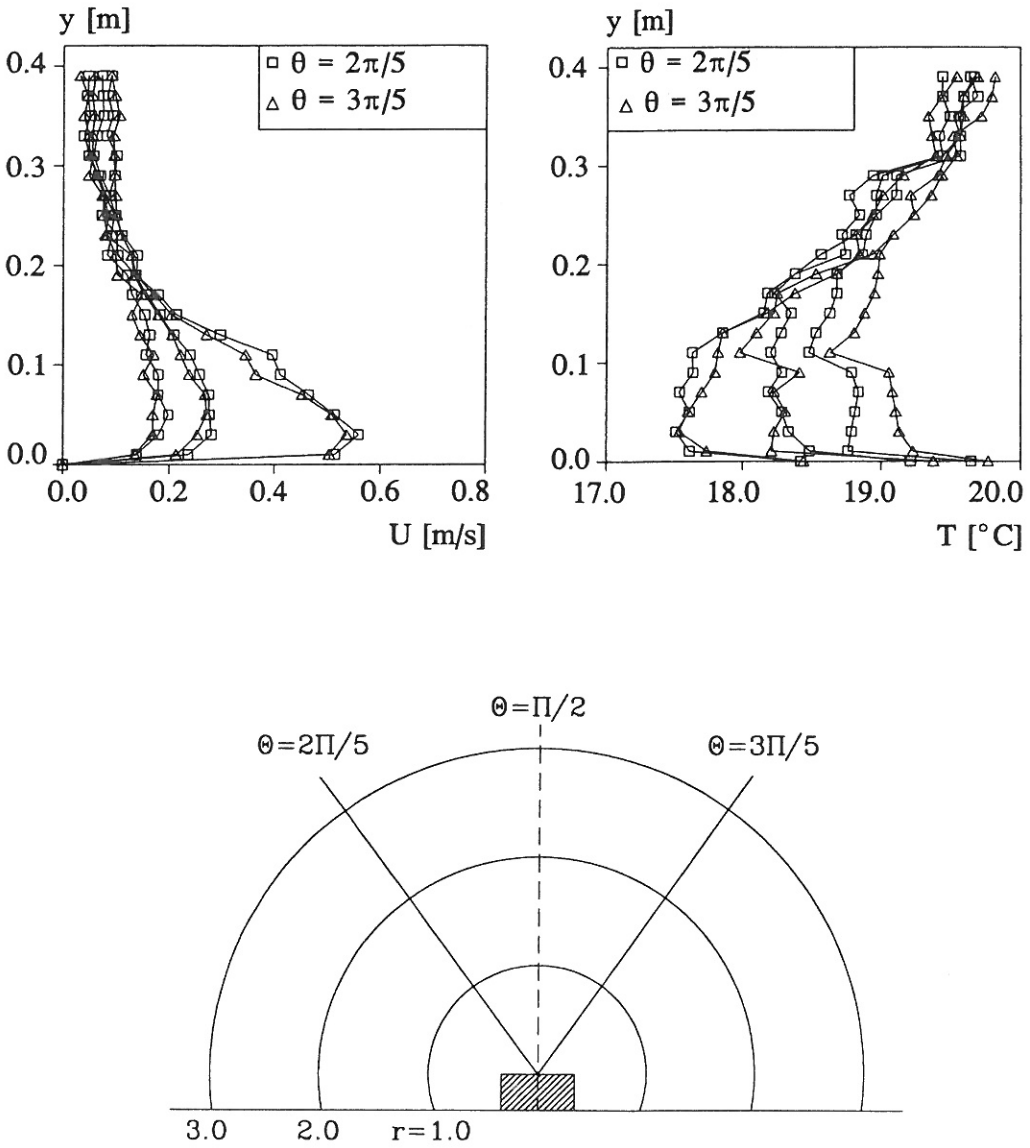

Figure 2.6 Comparison between velocities and temperatures in symmetrical streamlines. The profiles are measured for r=1.0m, r=2.0m and r=3.0m.

Parallel to the measurements close to the floor temperatures are determined at the walls and in the room. Surface temperature profiles are measured at the inside and outside of the walls in two locations. Air temperature profiles in the room are measured in a

location in sufficient distance from the inlet device and the heat sources to avoid pronounced direct disturbances. Fig.2.7 shows the position of thermocouples and resulting profiles.

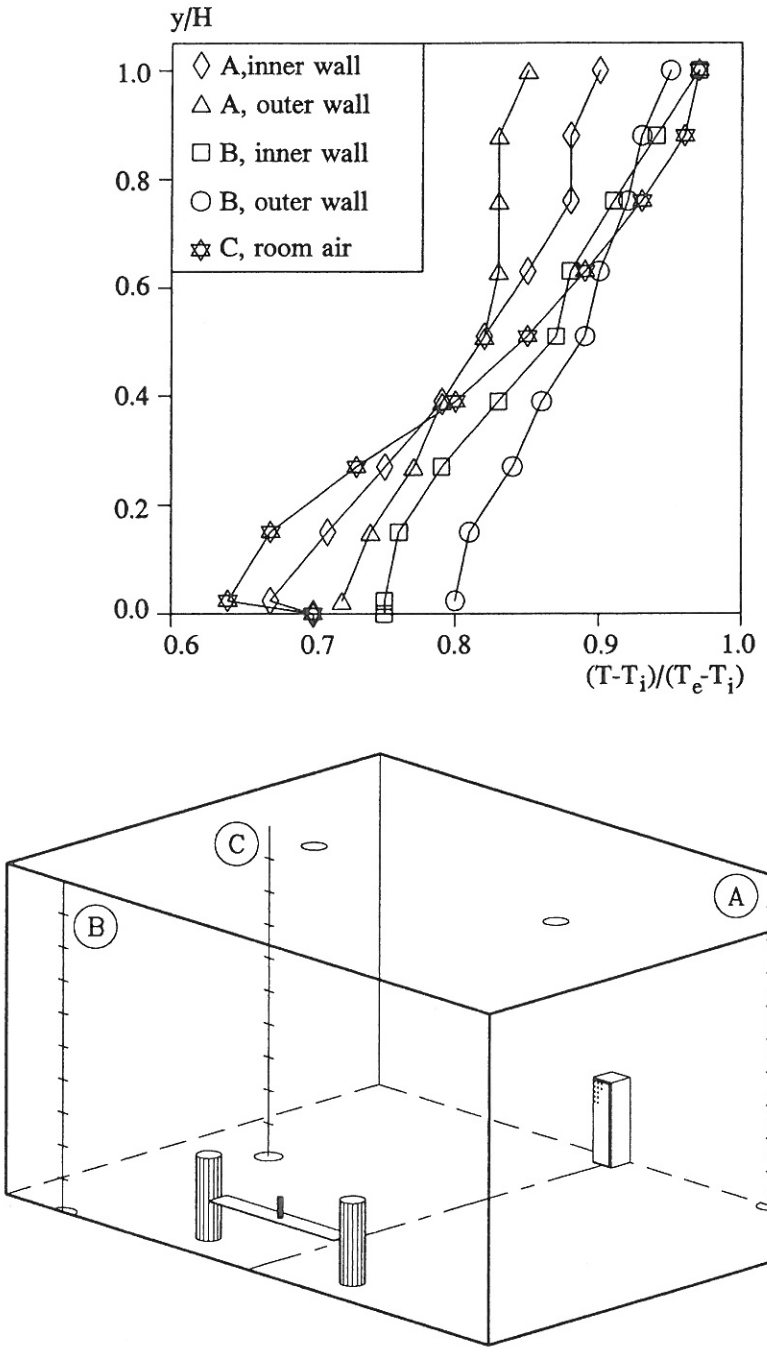

Figure 2.7 Non-dimensionalized vertical profiles of temperature at wall surfaces and of the room air (case A) - the locations are given in the sketch below.

The temperature profiles at the walls are roughly linear. The temperature differences between the inside and the outside of the walls are decisive for the heat transfer through the wall. Moving upwards from floor level it appears from fig.2.7 that heat is supplied to the lower part of the room due to a positive temperature gradient between the outside and the inside. In the upper part of the room the temperature gradient is reversed and heat is removed. This implies that a downwards directed airflow is induced in the vicinity of the wall in the upper part of the room and a corresponding upwards directed flow is generated in the lower part of the room. These air currents - significant or not - are bound to merge close to a neutral level where the temperature difference is zero. The 'neutral height' varies with the location of the measurements which suggests that the air movement is not completely horizontal. According to the measured data it is clearly reasonable to adopt a linear description of the wall temperatures profiles .

The room air temperature profile in fig.2.7 shows a 'stretched S'-like shape which is a common characteristic for displacement ventilated rooms. *Skistad 1989* discusses how the temperature profile is affected by different types of heat sources and inlet devices and recommends a linear approximation of the type :

$$T(y) = \frac{y}{H}(T_e - T_f) + T_f \qquad (2.2)$$

where H is the full height of the room, T_e the exhaust temperature and T_f the floor temperature. The floor temperature is calculated as the inlet temperature plus a fraction of the temperature difference between the exhaust and the inlet. Estimated from fig.2.7 this fraction is close to 0.7 which is considerably larger than value of 0.5 originally suggested by *Skistad 1989*. The modest temperature difference is mainly attributable to the net radiative heat transfer from the ceiling to the floor. The radiative heat loss at the ceiling result in lower temperature at the surface than that of the adjacent air and the radiative heat gain at the floor result in just the opposite effect. In recognition of the non-linearities close to the floor and ceiling *Li et. al. 1993* applied an extended multi-node model for the description of the vertical temperature profile.

Not only the wall boundaries but also the inlet boundary has a pronounced effect on the entire flow field. Velocities are subsequently measured close to the inlet surface. The measurements are, however, associated with difficulties due to the perforated front plate and the strong variation in magnitude and direction of the velocities. In analogy to jet flow a core region is established in front of each of the perforations. Initial entrainment occurs and the velocity differences are rapidly smoothened out. On one hand the anemometers must be placed outside the 'core region' but on the other hand the buoyancy forces acts on the injected air volume and alters the velocity profile in a very

short distance from the inlet surface. The flow direction is furthermore difficult to take into account. The resulting profiles should consequently be regarded as representing the relative distribution of speed rather than exact values of velocity. In fig. 2.8 the arrangement of measuring grid and resulting relative distribution of speed is given.

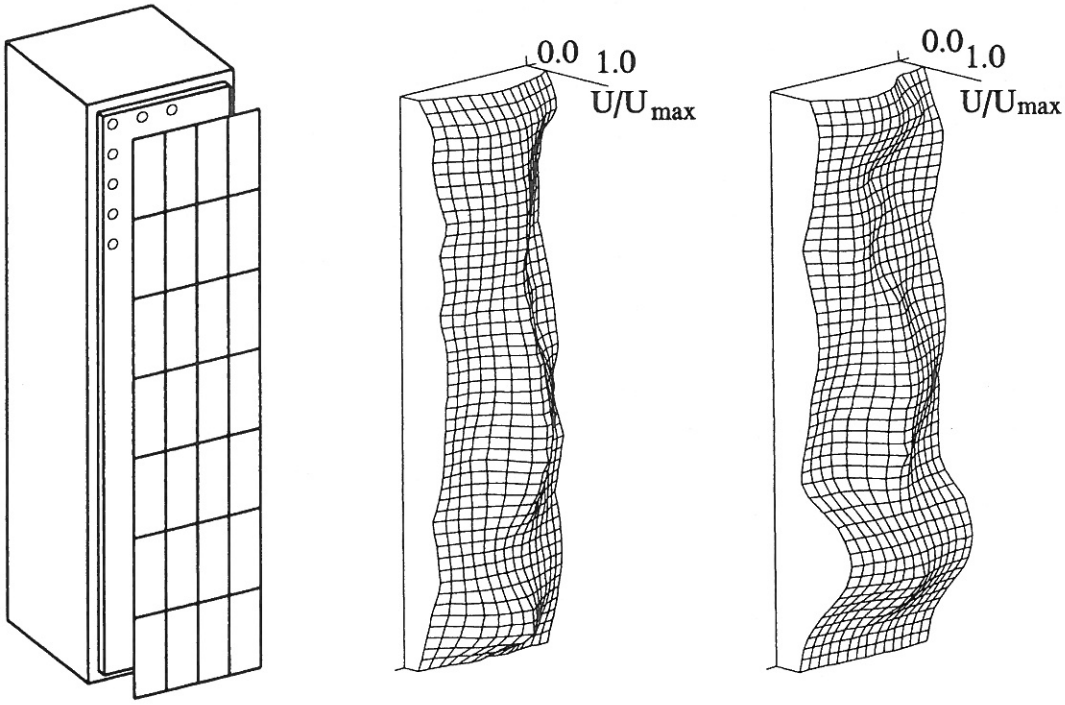

Figure 2.8 Distribution of speed at 2 cm and 8 cm from inlet.

The above plots give qualitative information about the transformation of the inlet velocity profile close to the inlet device. At an early stage after leaving the inlet device the air volume collapses due to initial mixing and buoyancy effects and a distinct outward curve is created at the lower part of the profile. A horizontal spreading is simultaneously induced by the vertical contraction.

Visualization of the inlet airflow by smoke clearly showed that even at the inlet surface the flow is far from uni-directional. The velocity vector is initially downward directed with an angle of approximately $\pi/4$ in the central region of the inlet surface and at the edge an angle of approximately $\pi/3$ in the horizontal plane was observed.

The characteristic stratified flow region is influenced not only by the buoyancy forces acting on the cool air but also to a considerable extent by the design of the inlet device.

In fig.2.9 photos of the full-scale room and the experimental set up are shown.

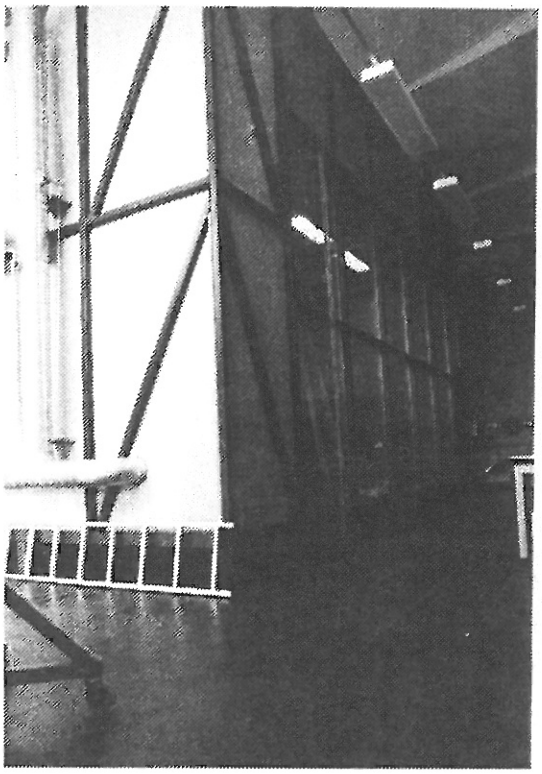

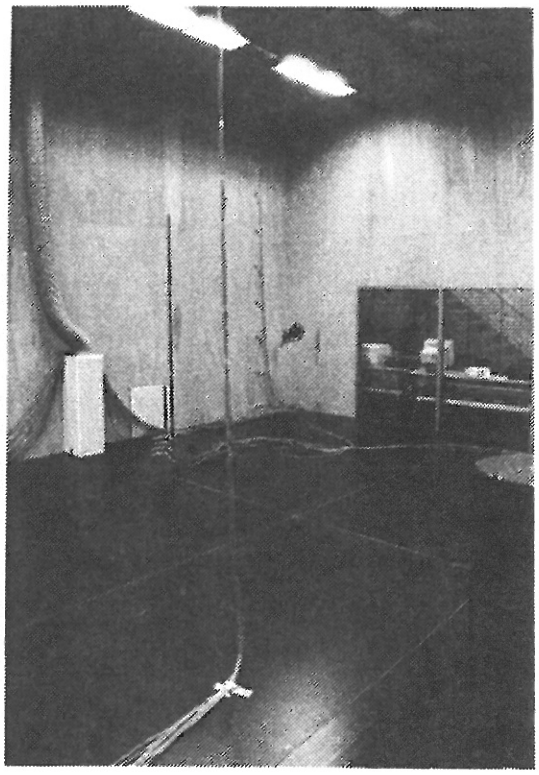

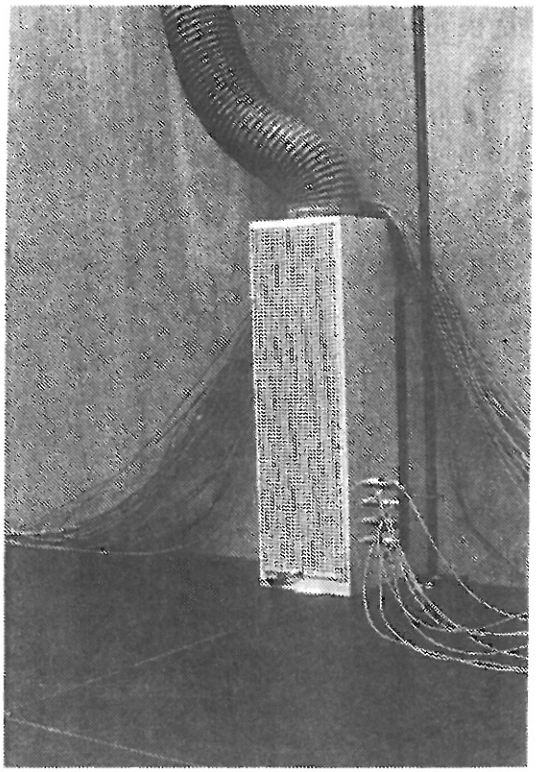

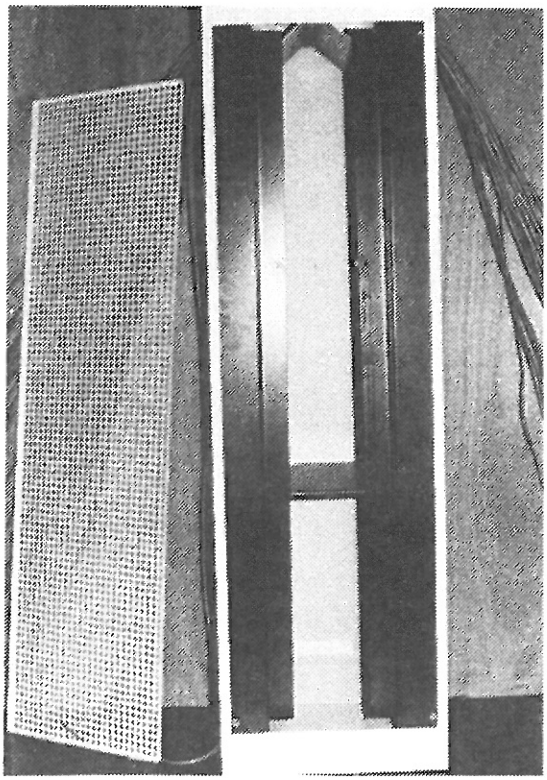

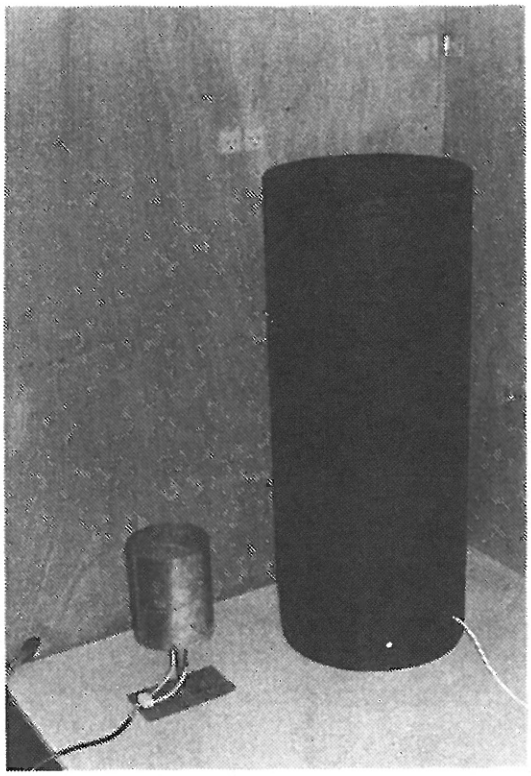

Figure 2.9 Arrangement of full-scale room. In succession the photos show the exterior and the interior of the room, the inlet device and the heat sources.

Chapter 3

Analysis of velocity and temperature profiles

A number of semi-analytical expressions has been used as guide lines in the design of mixing ventilation systems. Expressions for calculating maximum velocities and temperatures as functions of the distance from the diffuser has been derived. The formulas are based on the assumption of conservation of momentum and self-similarity of velocity and temperature profiles in the jet and have proved useful for practical applications.

This chapter investigates proposals for simplified expressions describing the flow from the inlet device in a room with displacement ventilation - with reference to the measured data.

3.1 Decay of maximum velocities

The inlet air is forced downwards as it enters the room. It is deflected by the floor and a stratified flow is developed close to the floor. The dense air layer is restricted by the rigid floor surface and a free shear layer to the surrounding fluid. The height of the layer is typically 20-30 cm and the maximum velocity is usually found 2-5 cm above floor level. When centreline maximum velocities in the flow are plotted against the distance from the inlet device a sequence of acceleration followed by deceleration is identified - see fig. 3.1.

The highest velocity is found close to the point of impingement with the floor which is located less than 1.0 m from the inlet device for the Archimedes numbers considered in the measured cases. The decay of maximum velocities in front of the inlet device has been treated by *Sandberg and Blomqvist 1989*, *Nielsen et. al. 1988* and later by *Nielsen 1992*. In all cases an exponential relationship has been recognized but while the first author takes a theoretical approach the latter employs empiricism.

The theory of *Sandberg and Blomqvist 1989* is based on an assumption of energy conservation and a progressive transformation of potential energy into kinetic energy.

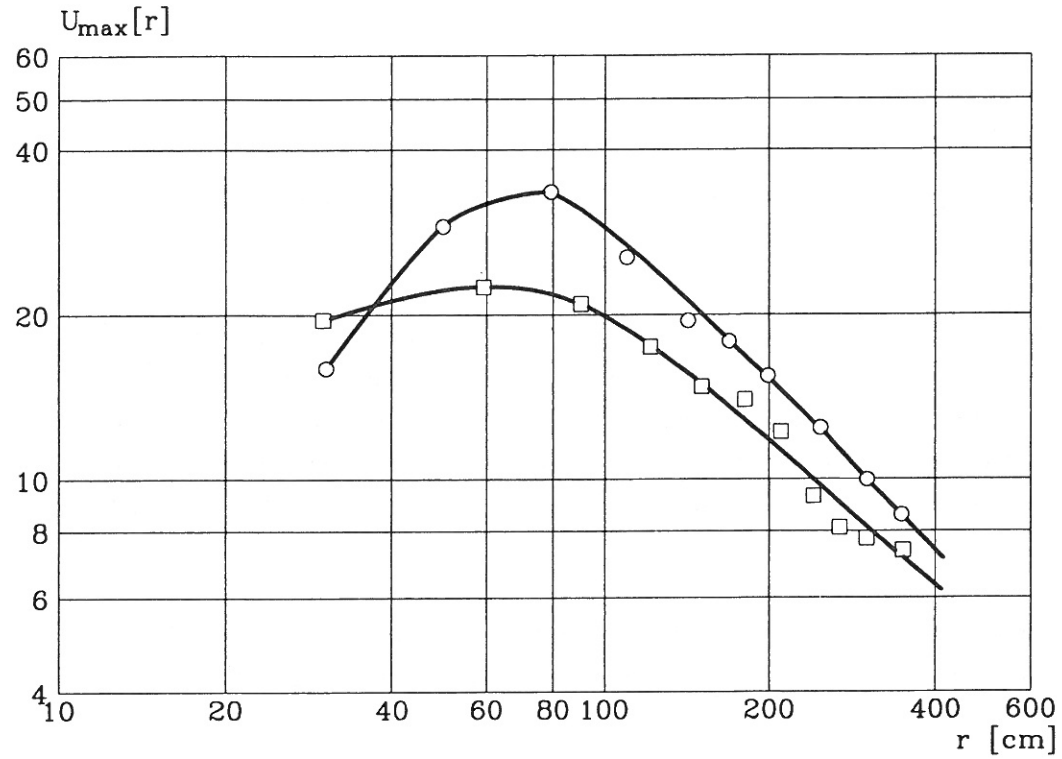

Figure 3.1 Maximum velocities versus distance from inlet device for two different inlet devices (*Nielsen et. al. 1988*).

The flow is regarded as a gravity current and a velocity component perpendicular to the main flow direction is introduced to take the horizontal spreading into account. It is possible to derive the expression presented in eq.(3.1) provided the temperature difference between the cool layer and the surrounding room air is constant, the vertical velocity components are negligible and the height of the near floor layer is constant from the impingement with the floor to the collision with the walls.

$$\frac{U_{max}(r)}{U_0} = \exp\left(\frac{-2V_g hr}{q_i}\right)$$

$$U_0 = \sqrt{U_i^2 + g\frac{T_r - T_i}{273 + T_r}H} \qquad (3.1)$$

$$V_g = K_v\left(g\frac{T_r - T_i}{273 + T_r}h\right)$$

where $U_{max}(r)$ is the maximum velocity with distance r from the inlet device. U_0 is the velocity where the air volume impinges on the floor. U_0 is composed of a contribution

from inlet velocity U_i and a term representing the velocity increment due to gravitational acceleration. V_g is the lateral velocity component responsible for the horizontal spreading and K_v is a constant. T_r-T_i is the temperature difference between room air and supply air at the inlet device. H is the height from the upper edge of the inlet device to the floor, h is the height of the air layer in proximity of the floor and q_i is the supply air rate.

Eq.(3.1) gives an instructive interpretation of the air flow in vicinity of the floor. The weakness of applying these formulas is the assumption of no entrainment and heat exchange with the surroundings. The demand for constant height of the dense layer and constant temperature difference between the air layer and its surroundings imposes further constraints and limits the range of applicability. The strongly idealized conditions makes it difficult to choose a proper value of the constant K_v and the use of eq.(3.1) should be confined to the region far from the inlet device where the above mentioned requirements are approximately satisfied.

The suggestion by *Nielsen et. al. 1988* for calculation of maximum velocities in the centre line of the inlet device reads

$$\frac{U_{max}(r)}{U_i} = K^*(Ar_r)\left(\frac{\sqrt{A_i}}{r+r_0}\right)^n \qquad (3.2)$$

A_i is the area of the supply surface. r_0 is the distance from the inlet device to a virtual origin and n an exponent. K^* is a constant depending on the Archimedes number and the specific inlet device. Eq.(3.2) originates from similar expressions for an isothermal 3-D wall jet but with the distinction that the non-linear dependency on Archimedes number is incorporated through K^*.

The smoke experiments and regression analysis on measured data demonstrate that r_0 is approximately zero for the type of inlet device in question. The value of the exponent n varies in the range 0.93-1.05 and is subsequently fixed to 1.0. It is furthermore assumed that q_i and U_i are proportional and eq.(3.2) subsequently reduces to

$$\frac{U_{max}(r)}{q_i} = K(\theta,Ar_r)\frac{1}{r} \qquad (3.3)$$

It is necessary to introduce a new constant K to replace K^* in eq.(3.2). The constant is written as a function of the reduced Archimedes number, Ar_r, and the streamline ang-

le,θ. Eq.(3.3) is in principle formulated only for the centre line ($\theta=\pi/2$) but here it is adopted for all streamline directions.

Nielsen 1992 elaborates on the velocity decay in the flow in front of the inlet device and gives an interpretation of eq.(3.3) based on physical reasoning. It is argued that in a fully radial flow with negligible entrainment and approximately constant layer thickness the velocity decay with distance from the inlet device is determined by the expansion in area of the flow front - calculated as the increment in circumference of a semicircle. The maximum velocity is thus inversely proportional to the distance from the inlet device and n subsequently equals 1.0.

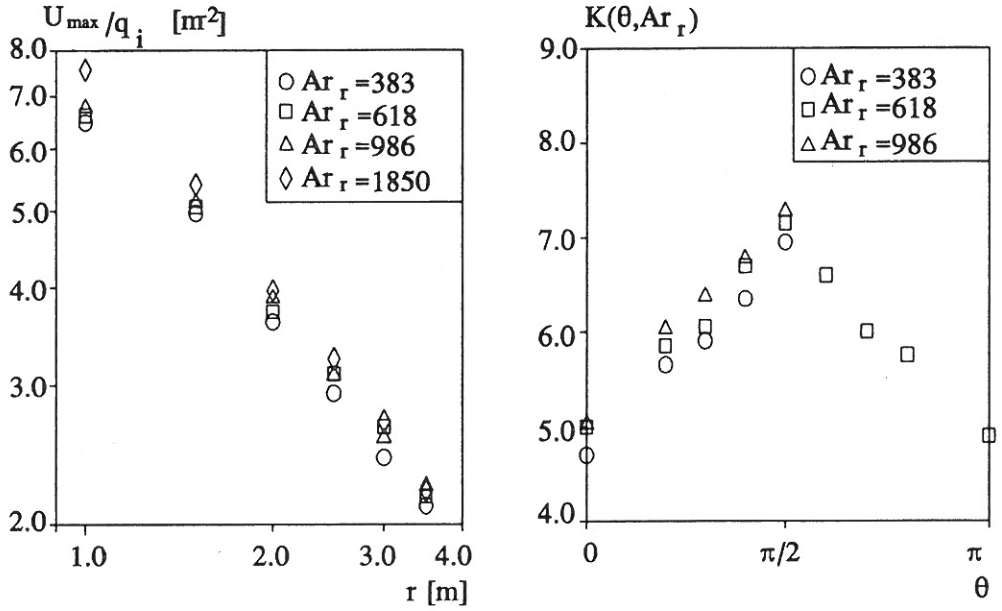

Figure 3.2 Velocity variation in the centre line ($\theta=\pi/2$) with distance from inlet device and $K(\theta,Ar_r)$ variation with streamline angle for different Ar_r-numbers.

Fig. 3.2 (left) shows that eq.(3.3) constitutes a good approximation to the measured maximum velocities in the centreline. Even though the range of Arkimedes numbers is rather narrow the plot indicates increasing maximum velocities with increasing Ar_r.

The right side of the figure shows the K-values calculated for different streamline angles. It appears that the distribution is systematical and symmetrical around the centre line of the inlet device. This suggests that the range of validity of eq.(3.3) can be

extended to all streamline directions but to draw any final conclusions additional data are required. The K-values apparently increase with increasing Archimedes number. The curves of K-distributions are approximately parallel. This does not necessarily apply to cases with considerably larger or smaller Archimedes number. E.g. under isothermal conditions - which can be regarded as an extreme case with respect to Archimedes number - the flow pattern in front of the inlet device is not radial.

3.2 Velocity and temperature profiles

Applying jet-like expressions leads to satisfactory estimates of the maximum velocities in the near wall layer and a similar approach is chosen to approximate the vertical distribution of velocity and temperature.

In analogy to turbulent jets the velocity profiles in the near wall layer are supposed to be similar and a shape function of a wall jet is thus applied. The expression derived by *Verhoff 1963* includes the free jet boundary to the surrounding fluid and the turbulent boundary layer adjacent to the wall.

$$\frac{U(y)}{U_{max}} = A\left(\frac{y}{b}\right)^{\frac{1}{7}}\left[1-erf\left(B\left(\frac{y}{b}\right)\right)\right] \qquad (3.4)$$

where the constants A and B equals 1.48 and 0.68, respectively, erf is the error function and b is the height of the profile defined as the level where the velocity equals 0.5 U_{max}.

Equations for heat transfer can often be deduced from the momentum transport. For turbulent jets the following relation between temperature and velocity is proposed by *Schlichting 1955*.

$$\left(\frac{\Delta T(y)}{\Delta T_{max}}\right)^{m} = \frac{U(y)}{U_{max}} \qquad (3.5)$$

$\Delta T(y)$ is the temperature difference between room air and the temperature in the height y above the solid surface. ΔT_{max} is the maximum temperature difference between room air and the cool layer. *Mathisen 1989* argues that 2.0 is an appropriate value of the exponent, m, in a displacement ventilated room. It is confirmed by regression that the second power actually gives the best obtainable fit when all T-profiles are included.

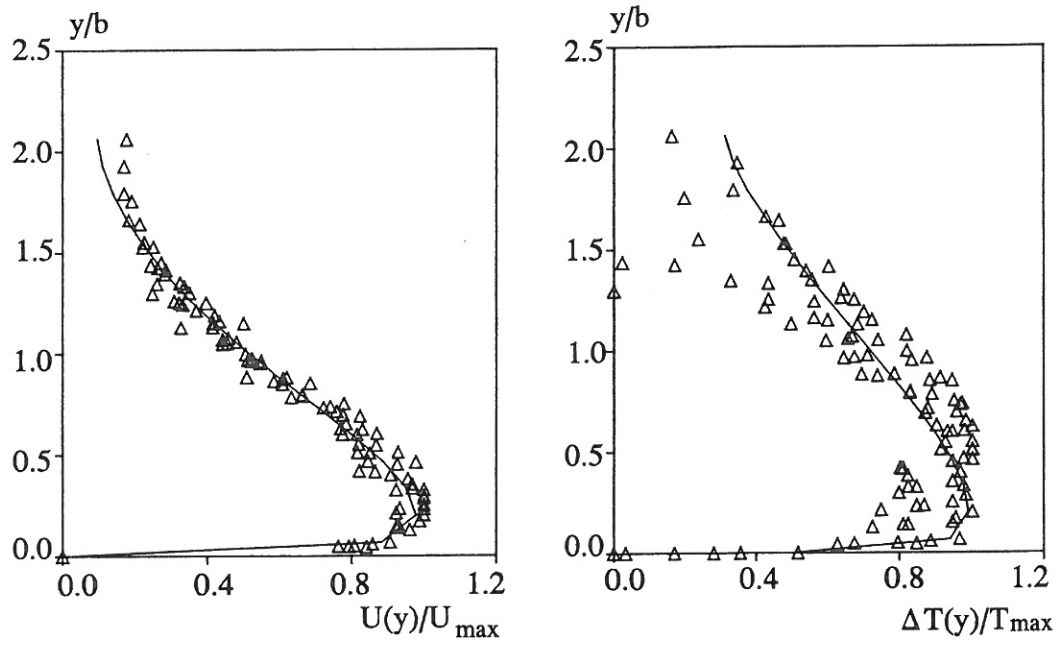

Figure 3.3 Measured velocities and temperatures compared with theoretical profiles, eq.(3.4) and eq.(3.5) (Ar_r=618 °Cs^2/m^6).

The comparison between eq.(3.4) and the measured velocities in fig.3.3 (left) show good agreement in general with a slight divergence for y/b > 1.5. This is probably caused by secondary flow in terms of air motion in the ambient room air.

The temperatures are more scattered and they do not fit the theoretical expression in the same convincing way as the velocities. The divergence does not occur solely at single points but the entire profile shape is progressively altered as the layer moves across the floor. The temperature distribution is distorted and the approach of universal profiles is not valid. A closer study reveals a slowly increasing discrepancy with distance from the inlet device and increasing θ-values. The disagreement is probably attributable to the radiative heat transfer to the floor and to some extent to wall effects. The walls affect the flow and the geometry of the room play an important role.

The use of equations (3.3),(3.4) and (3.5) is restricted to the area outside the initial zone where the characteristic profiles are not yet fully developed, and outside the zones near to the walls where deceleration occurs. The conclusions based on fig.3.3 can be extended to the Ar_r-number range which is considered (~ 300-1900 °Cs^2/m^6).

3.3 Entrainment and effects of stratification

The type of flow which is established in front of the inlet device is characterized as a stratified flow implying that an interface exist between a lower dense layer and an overlying light layer. The development of the layer is determined by the interaction between the dense air current, the above shear layer, the below solid surface and the interchange of radiative energy. The dynamics of stratified flows has been treated by a large number of authors e.g. *Turner 1979*, *Launder 1975* and *Pedersen 1986*.

At the density interface buoyancy forces constitute a stabilizing force which counteracts the vertical exchange of heat and momentum induced by destabilizing effects of shear stress. On microscale the entrainment rate of light air into the dense layer is closely connected to the interfacial turbulence and on macroscale it can be described in terms of density and velocity profiles.

Turner 1979 working with an inclined plume below a roof over a stationary fluid, *Pedersen 1986* working with dense bottom currents in coastal hydraulics and *Sandberg 1991* working with gravity currents in rooms all suggest that the flow field is subdivided into a subcritical and a supercritical region. Under subcritical conditions disturbances caused by internal waves or the surrounding walls are able to propagate upstream while this is hindered under supercritical conditions. The concept of subcritical and supercritical flow is universal even though the transition between the two types of flow is expressed differently by applying Richardson number, Ri, densimetric Froude number, F_Δ, or Archimedes number, Ar. In this context a local Archimedes number, Ar_l, is convenient

$$
\begin{aligned}
Ar = Ri = \frac{1}{\sqrt{F_\Delta}} = \frac{g\beta\Delta Tl}{U^2} \\
Ar < 1 \Rightarrow supercritical \\
Ar > 1 \Rightarrow subcritical
\end{aligned}
\qquad (3.6)
$$

$$
Ar_l = \frac{g\beta\Delta T_{max} b}{U^2_{max}}
$$

where the variables appearing in the expression for Ar_l are given by the local profiles of velocity and temperature. The height of the profile, b, is used as the characteristc length scale.

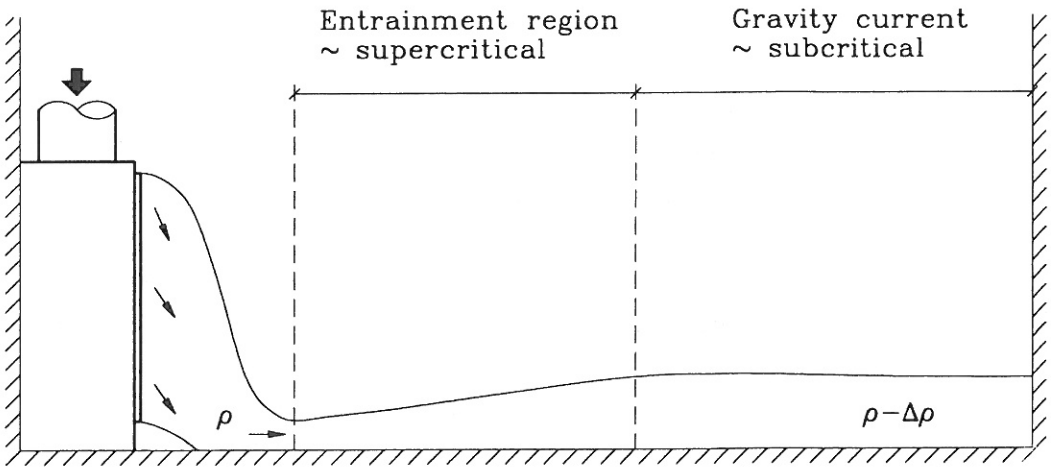

Figur 3.4 Schematic diagram of flow across the floor (after *Wilkinson and Wood 1971*).

The Arkimedes number increases with distance from the inlet device and at a critical value a transition takes place. In analogy to a hydraulic jump it is referred to as a density jump. The location of the density jump is determined by the upstream conditions and the downstream control - in this case the walls. A density jump has not been identified experimentally in a displacement ventilated room. Measurements, however strongly implies that two interlinked characteristic flow domains prevail and a region of transition thus exists.

Sandberg 1991 investigates the super- and subcritical domains in gravity currents in rooms and proposes a velocity scale based on a buoyancy flux parameter for the supercritical region close to the inlet device. As the dense current traverses the floor the Archimedes number increases, the flow conditions become subcritical. For this region of the flow a velocity scale depending on the inlet conditions (U_0 in eq.(3.1)) is applied.

In the subcritical domain the vertical mixing is strongly inhibited and the entrainment rate can be used as a qualified indicator for locating the density jump. It is possible to calculate entrainment rates for the flow as the increment of volume flow through sections of the cool air layer. Provided that the flow from the inlet device can be regarded as fully radial and that the air is entrained through the face, A_e, an entrainment velocity can be estimated as shown in fig.3.5.

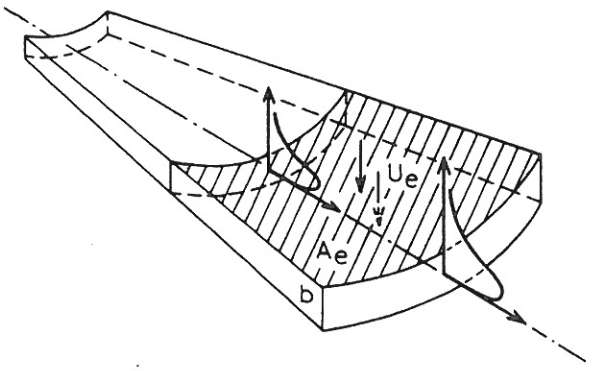

Figure 3.5 Entrainment velocity in radial flow from inlet device.

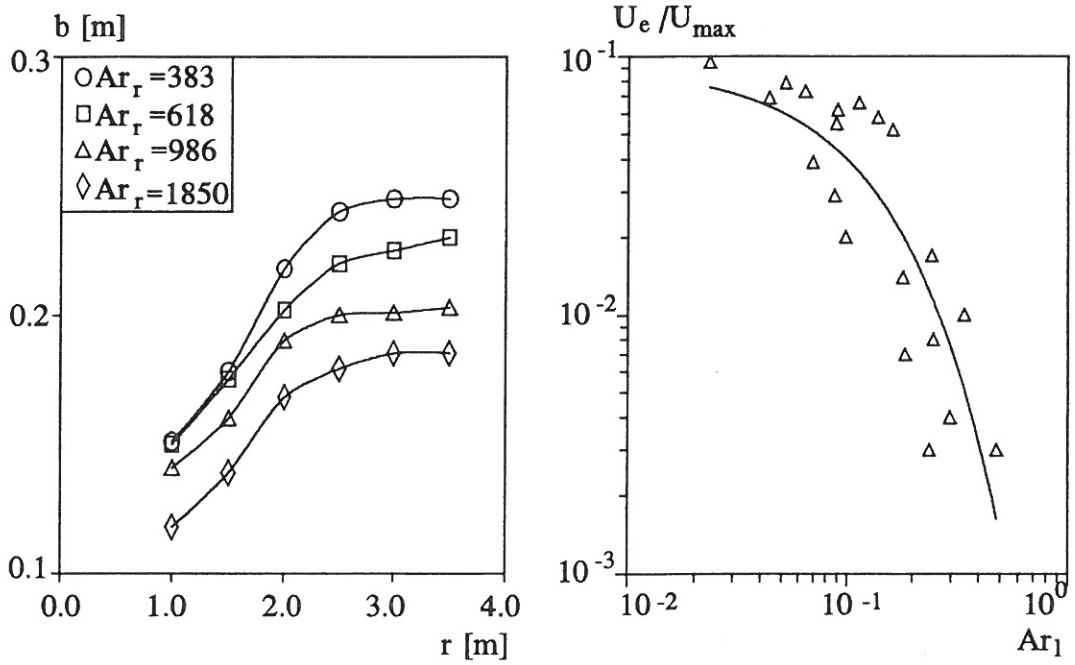

Figure 3.6 Growth of cool layer height with distance from inlet device and decay of entrainment velocities with local Archimedes number in centreline.

The two plots of fig.3.6 agree in the sense that decreasing growth rate of layer thickness correspond to decreasing entrainment velocities. In the zone close to the inlet device the entrainment velocities are of the same order of magnitude as an isothermal jet. As the injected air mixes and spreads out the Ar_l increases and the entrainment velocity falls rapidly. The entrainment velocity becomes extremely small for $Ar_l > 0.1$ ($r > 2.0$-4.0 m). *Pedersen 1986* and *Turner 1979* describe a similar abrupt decrement

of entrainment rate as the flow becomes subcritical. The measurements seem to support the hypothesis of two flow domains of distinctly different properties.

It should be kept in mind that the geometry of the room and the inlet device is of crucial importance to the flow field. The location of the transition region is to a large extent affected by the upstream flow given by the specific inlet conditions and the downstream control which is determined by the distance to the walls if no other obstacles are present.

Further experimental investigations with the main purpose of describing the mechanism of a density jump are necessary to draw any final conclusions. Nevertheless there are strong indications that such a transitional phenomenon play an significant role in this type of flow. The hypothesis of two fundamentally different flow domains is an important aspect of the air flow along the floor and it should be considered in the further development of the description expressed in eq.(3.1)-(3.5).

Chapter 4

Turbulence modelling

The air flow in ventilated rooms is mainly considered to be turbulent implying a motion influenced by random fluctuations in time and space. This causes the instantaneous measured value of a given scalar in the flow field to exhibit a wide range of variation and unpredictability. Turbulence is initiated by small disturbances which are amplified and lead to the generation of 3-D eddies. Due to viscous losses the turbulent motion is damped and it can not maintain itself but obtains energy from shear stress generated by velocity gradients of the mean flow or buoyancy.

The detailed nature of turbulence is complex and makes it extremely difficult to develop a model of general validity which is feasible with respect to the mathematical solution procedure. Taking the origin and full development of the turbulent eddies into account by direct numerical solution (DNS) of the Navier-Stokes equations, which govern turbulent fluid flow, requires a calculation effort which is unattainable for practical use even by the standards of modern high performance computers. This approach is confined to a very limited range of application and has no prospect of being employed in practical investigations of the air flow in ventilated rooms in a foreseeable future.

Another, but yet similar, method is the large eddy simulation (LES). The Navier-Stokes equations are solved for the large scale motion and a subgrid scale model is added for the small scale motion and the computing cost is thereby reduced. *Murakami et. al. 1992* demonstrate convincing prediction accuracy by LES in the flow around buildings but the computing cost associated with the calculation of indoor air flow is very high.

Two problems are encountered in the development of applied methods for turbulent flow. The incomplete knowledge of the laws governing the transport of mass and heat in a turbulent flow and the limited available means for solving the differential equations makes the task of modelling the flow field difficult. However, from a practical point of view the main feature of turbulence is its effect on diffusion processes in the flow and a description based on mean values of relevant quantities has proven itself useful for estimating heat and mass transfer.

By time averaging of the Navier-Stokes equations the problem becomes that of assessing the Reynold stresses which contain the fluctuating part of the motion. It is the sole purpose of turbulence models to make a proper approximation of these specific terms. Several suggestions has been presented and a review of the methods can be found in e.g. *Rodi 1980* or *Nallasamy 1987*. Without recapitulating these methods in further detail it is important to state that a crucial progress was made by the introduction of two-equation models - of which the k-ϵ model is widely used today. The reason why the k-ϵ model has been applied in many different types of flow is that it constitutes a good compromise between prediction accuracy and required computing time for solving the governing equations.

This chapter mainly describes the basic idea of the k-ϵ model and finally discusses its potential and shortcomings in relation to the flow calculations in a displacement ventilated room.

4.1 The flow equations

A conventional assumption dealing with turbulence is that statistically the instantaneous value of a variable, i.e. velocity or temperature, can be expressed as the sum of a mean quantity and a fluctuating quantity. The instantaneous value of velocity components expressed in tensor notation thus reads

$$U^*_i = U_i + u_i \tag{4.1}$$

The mean value U_i is obtained by averaging in time. The averaging period of time is by definition larger than the time scale of the fluctuating motion and shorter than the transient long term motion of the mean flow.

The purpose of adopting decomposition of the variables become evident when a 3-D incompressible, non-isothermal flow field is considered. Inserting eq.(4.1) in the conservation equations for mass, momentum (Navier-Stokes) and any scalar property - in this case temperature - yields

$$\rho \frac{\partial U_i}{\partial x_i} = 0 \tag{4.2}$$

$$\rho\left(\frac{\partial U_i}{\partial \tau}+U_j\frac{\partial U_i}{\partial x_j}\right) = -\frac{\partial P}{\partial x_i}-\frac{\partial}{\partial x_j}\left(\rho\overline{u_i u_j}-\mu_l\frac{\partial U_i}{\partial x_j}\right)+g_i\rho\beta(T-T_{ref}) \quad (4.3)$$

$$\rho\left(\frac{\partial T}{\partial \tau}+U_j\frac{\partial T}{\partial x_j}\right) = -\frac{\partial}{\partial x_j}\left(\rho\overline{u_j t}-\lambda\frac{\partial T}{\partial x_j}\right) \qquad i,j \in [1..3] \quad (4.4)$$

where P, T, ρ, g, β, μ_l and λ denote pressure, temperature, density, gravitational acceleration, volumetric expansion factor, molecular viscosity and heat conductance, respectively.

In accordance with the Boussinesq assumption the density of the fluid is considered to be constant and density differences are only included in the calculation of buoyancy. Eq.(4.3) and eq.(4.4) both consist of first derivatives in terms of the transient and convective term on the left hand side and a second derivative in terms of the diffusion term on the right hand side.

The terms containing mean flow quantities are separated from the terms involving the fluctuating quantities in eq.(4.2)-eq.(4.4). The purpose of a turbulence model is to model the fluctuating part - the Reynold stresses. To close the system of equations the hypothesis of eddy viscosity was conceived.

4.2 Eddy viscosity concept and k-ϵ model

The idea of eddy viscosity is based on the conception of turbulence consisting of eddies of variable length scale. From large low-frequency eddies of a length scale comparable to the physical space of the flow domain to small high frequent eddies determined by viscous forces in the fluid. Energy is provided from the mean flow to the large eddies which are gradually diminished and finally dissipated when the length scale is sufficiently reduced. This view of turbulence corresponds only to some extent to the physical reality but it has nevertheless been useful. As it appears from eq.(4.5) the eddy viscosity concept - or Boussinesq approximation - facilitates simplifications and thus convenient reductions of eq.(4.2)-(4.5).

$$\rho\overline{u_i u_j} = -\mu_t\left(\frac{\partial U_i}{\partial x_j}+\frac{\partial U_j}{\partial x_i}\right) + \frac{2}{3}k\rho\delta_{ij} \tag{4.5}$$

where k is the turbulent kinetic energy and δ_{ij} the Kronecker delta which takes the value 1.0 for i=j and 0.0 for i≠j to comply with the definition of k given below.

The assumption that the Reynolds stresses in analogy with viscous stresses are dependent on the mean velocity gradients makes it possible to operate with an eddy - or turbulent - viscosity, μ_t.

Scalars are transported by turbulent motions and an analogy between momentum and heat transfer is assumed. Corresponding to the concept of eddy viscosity the scalar flux is expressed as an eddy diffusivity depending on the mean gradient. The including temperature fluctuations is subsequently approximated by

$$\rho\overline{u_j t} = -\frac{\mu_t}{\sigma_t}\frac{\partial T}{\partial x_j} \tag{4.6}$$

where σ_t is the turbulent Prandtl number.

Instead of approximating the individual Reynolds stresses the task is now reduced to finding an expression for the turbulent viscosity. This simplification is possible only because the fully developed turbulence is considered to be isotropic. The more advanced Reynolds stress models are characterized by solving the equation for each stress component and they are thereby able to capture anisotropic features of the turbulence. The eddy viscosity concept, however, offers a more convenient final formulation of the governing equations as demonstrated in the succeding section.

The turbulent viscosity can be regarded as being proportional to the local velocity and length scales of the eddies. In the k-ϵ model the velocity scale is calculated from the turbulent kinetic energy, k, contained in the eddies responsible for the turbulent mixing and the length scale is related to the dissipation rate of turbulent kinetic energy, ϵ.
The turbulent kinetic energy is a measure of the magnitude of velocity fluctuations and is defined as :

$$k = \frac{1}{2}\left(\overline{u^2}+\overline{v^2}+\overline{w^2}\right) \tag{4.7}$$

The turbulent dissipation rate is defined as :

$$\epsilon = \frac{\mu}{\rho}\overline{\left(\frac{\partial u_i}{\partial x_j}\frac{\partial u_i}{\partial x_j}\right)} \tag{4.8}$$

k and ϵ are subjects to the transport and diffusion processes as other scalars in the flow field. *Chen 1988* gives a thorough description of how the momentum equations of eq.(4.3) are manipulated to derive the final standard form of the k and ϵ equations.

Launder & Spalding 1974 argues from comparison with experimental data that the definition of length scale inherent in the k-ϵ model makes it superior to other two-equation turbulence models and thus preferable

$$l = \frac{k^{3/2}}{\epsilon} \tag{4.9}$$

This leads to the Kolmogorov-Prandtl relation for the turbulent viscosity where the empirical parameter C_μ is assumed constant in the standard high Reynolds number version of the k-ϵ model

$$\mu_t = \rho c_\mu \frac{k^2}{\epsilon} \tag{4.10}$$

4.3 The governing differential equations and their interpretation

A complete set of equations can be presented by introducing eq.(4.5) and eq.(4.6) in eq.(4.2)-(4.4). The governing equations read :

Continuity :

$$\rho\frac{\partial U_i}{\partial x_i} = 0 \tag{4.11}$$

Momentum :

$$\rho\left(\frac{\partial U_i}{\partial \tau}+U_j\frac{\partial U_i}{\partial x_j}\right) = -\frac{\partial P}{\partial x_i}+(\mu_t+\mu_l)\frac{\partial^2 U_i}{\partial x_j^2}-\rho\beta g_i(T-T_{ref}) \qquad (4.12)$$

Temperature :

$$\rho\left(\frac{\partial T}{\partial \tau}+U_i\frac{\partial T}{\partial x_i}\right) = \left(\frac{\mu_t}{\sigma_t}+\frac{\mu_l}{\sigma_l}\right)\frac{\partial^2 T}{\partial x_i^2} \qquad (4.13)$$

Turbulent kinetic energy :

$$\rho\left(\frac{\partial k}{\partial \tau}+U_i\frac{\partial k}{\partial x_i}\right) = \left(\frac{\mu_t+\mu}{\sigma_k}\right)\frac{\partial^2 k}{\partial x_i^2} - \rho\epsilon + \underbrace{\mu_t\frac{\partial U_i}{\partial x_j}\left(\frac{\partial U_i}{\partial x_j}+\frac{\partial U_j}{\partial x_i}\right)}_{P_k} \underbrace{- \beta g_i\frac{\mu_t}{\sigma_t}\frac{\partial T}{\partial x_i}}_{G_k} \qquad (4.14)$$

Dissipation rate :

$$\rho\left(\frac{\partial \epsilon}{\partial \tau}+U_i\frac{\partial \epsilon}{\partial x_i}\right) = \left(\frac{\mu_t+\mu_l}{\sigma_\epsilon}\right)\frac{\partial^2 \epsilon}{\partial x_i^2} + \frac{\epsilon}{k}(c_1 P_k + c_3 G_k - c_2\rho\epsilon) \qquad (4.15)$$

The above listed system of equations consists of coupled non-linear partial differential equations which apart from the continuity equation have the same general structure. The common features are the convective and transient terms on the left hand side of the equations and the diffusive term on the right hand side. The remaining terms on the right hand side are collectively called the source term responsible for the local generation and destruction of the considered quantity.

The set of equations can only be solved analytically if drastic restrictions are imposed, i.e. by transforming them into ordinary differential equations in 1-D or 2-D flow

situations. To solve the equations numerically is far more relevant in the context of air flow simulation and the numerical solution procedure is outlined in chapter 5. At this point it is sufficient to point out that the generalized form of the equations makes it possible to construct an effective computer algorithm.

Attention should be paid in particular to the buoyancy terms appearing in the eq.(4.12), eq(4.14) and eq.(4.15) respectively. If a positive temperature gradient is encountered corresponding to a stable stratification the source terms in the k and ϵ equations serve to reduce the turbulent viscosity and thereby decrease the vertical momentum flux. If on the other hand an unstable region is present in the flow field it will result in increased mixing. The suppression of turbulent mixing in a stable environment with considerable temperature gradients is very important in non-isothermal room air flow.

The k-ϵ model of eq.(4.11)-(4.15) contains seven constants C_μ, C_1, C_2, C_3, σ_t, σ_k and σ_ϵ. Standard values are recommended partly from measurements partly from computer optimization

C_μ	C1	C2	C3	σ_k	σ_ϵ	σ_t
0.09	1.44	1.92	0.0/1.44	1.0	1.3	0.9

Table 4.1 Constants in equations for turbulent flow.

The constants listed in tab.4.1 are not universally valid but dependent on the flow situation. The variation of C_3 and σ_t in buoyancy affected flow has been addressed by many authors.

C_3 is treated as an empirical function of the Richardson number by *Rodi 1980*. *Viollet 1987* distinguishes between unstable conditions where $C_3=C_1$ and stable conditions where $C_3=0$ in reactor flow analysis. *Murakami et. al. 1987* show that the latter approach yields fair accordance between measurements and model predictions in a horizontal nonisothermal 3-D jet in a room.

σ_t is typically assigned a constant value in the range 0.7-1.0 in heat transfer calculations in room air flow but in reality it depends of the type of flow. *Yuan et. al. 1992* reviews a number of functions for σ_t describing the transition from free flow in the interior of the flow field to the boundary layer flow at the walls and *Nielsen et. al. 1979* apply a σ_t depending on a buoyancy parameter in room air flow.

In room air flow the effects of laminarization and stratification are of primary importance. Viscous forces influence the flow field significantly not only at the walls but also in stagnant regions in the free flow. *Skovgaard 1991* found that even in rooms with mixing ventilation low-Reynolds number effects can be expected. Low velocities and thermal stratification prevail throughout the flow domain in a displacement ventilated room and further intensifies the need of proper modelling of viscous effects. The description of transition between turbulent and laminar flow is not fully supported mainly due to the lack of experimental information. The existing knowledge become even more limited when the flow is influenced by buoyancy, see e.g. *Turner 1979*.

In recognition of the popularity of the k-ϵ model efforts have been made to offer remedies of general validity for these effects. With few exceptions the proposed modifications have been made for low-Reynolds number effects and stratification effects separately.

Low-Reynolds models are originally developed for the analysis of near wall behaviour but later versions have been extended to free flows. In the eddy viscosity model an exponential decay function is multiplied to the turbulent viscosity of eq.(4.8) to damp the turbulent mixing. For example the damping function of *Jones and Launder 1972* based on the turbulent Reynolds number, R_t reads

$$\mu_t = f_{R_t}\, \rho C_\mu \frac{k^2}{\epsilon}$$

$$f_{R_t} = \exp\left(\frac{-3.4}{(1+R_t/50)^2}\right) \qquad R_t = \frac{\rho k^2}{\mu_t \epsilon} \tag{4.16}$$

Davidsson 1989 applied this function in a 2-D buoyancy driven cavity and reported promising results which were in agreement with experimental data. *Dagestad 1991* concludes that in a stably stratified channel flow the low-Reynolds extended k-ϵ model improves the obtained results in the free shear flow as well as in the near wall region.

Chikamoto et. al. 1992 apply the k-ϵ model to predict the air flow and temperature distribution in an atrium with pronounced thermal stratification. A damping function for buoyancy effects is proposed. A damping function, f_b, depending on the buoyancy parameter, b, is proposed. b is the ration between the generation of k by buoyancy and the dissipation rate.

$$\mu_t = f_{R_t} f_b \rho C_\mu \frac{k^2}{\epsilon}$$

$$f_b = \begin{cases} 0.0 \text{ for } b \le -10 \\ 1 + b/10 \text{ for } -10 < b < 0 \\ 1.0 \text{ for } b \ge 0 \end{cases} \qquad b = \frac{G_k}{\epsilon} \tag{4.17}$$

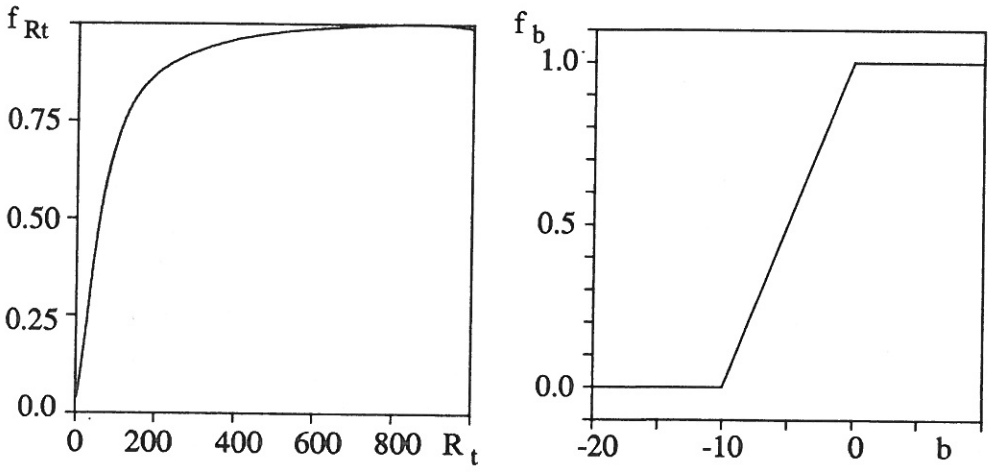

Figure 4.1 Damping functions.

The model describes the progressing collapse of turbulence in stably stratified free flow in an atrium with high heat load. The damping function, f_b, presented here has not yet reached its final form. An obstacle for the general implementation of this damping functions is the fact that turbulent fluctuations are diminished in all directions to comply with the assumption of isotropic turbulence. In reality only the vertical exchange of heat and mass should be reduced. The task involves the derivation of a valid algebraic expression from the Reynolds stress equations which is to be implemented only for the vertical direction and there by adopting a pseudo non-isotropic turbulence model. One main problem in this process is to describe the effects of buoyancy and laminarisation separately.

The use of the damping functions has one serious drawback. When f_{Rt} is introduced a high number of grid nodes are required close to the walls where large gradients occur. The increased local grid refinement entails heavily increased computing cost which

makes this type of damping function infeasible for 3-D applications. The effect of applying f_{Rt} in the free flow while ignoring it at the walls may, however, favour prediction accuracy.

4.4 Capabilities and limitations of the k-ϵ model

In relatively simple flows characterized by full turbulence, simple geometry, one or two predominant flow directions and the absence of body forces numerous successful predictions by the k-ϵ model have been reported. In complex flows some weaknesses become apparent and they will be addressed in the following with reference to the present work.

Leschziner 1992 describes a number of shortcomings of the eddy viscosity closure which include flow affected by buoyancy, acceleration/deceleration, impingement, stream-line curvature, separation, reattachment, rotation and three-dimensionality. Some of these features are present in room air flow in general and in flow in a displacement ventilated room in particular. Strong buoyancy forces prevail in the regions close to the inlet device and at the heat sources where acceleration, deceleration impingement and separation take place and subsequently leads to pronounced three-dimensionality of the flow.

The reason why the k-ϵ model fails to include the above mentioned features with sufficient precision should mainly be found in the inherent eddy viscosity hypothesis but also the equation for dissipation of turbulent energy is disputable.

The suppression of turbulent mixing at a density interface is not correctly accounted for by the k-ϵ model and it may lead to poor estimates of diffusion and excessive erosion of the gradients. In a well-mixed layer bounded by a stable density interface and a solid surface the fluctuations in vertical direction are strongly reduced and the turbulent eddies are stretched. The turbulence becomes anisotropic which is inconsistent with the eddy viscosity assumption. The vertical exchange of heat and momentum is consequently not correctly assessed. In a stratified flow this is not merely a local problem but it may in fact influence the flow field in general.

Rodi et. al. 1989 characterize the ϵ-equation as a weak element of the k-ϵ model due to its lack of universality. To derive a manageable equation of ϵ from the Navier-Stokes

equations it has been necessary to make simplifications in terms of empirical approximations which compromise the generality of constants in the model.

Another serious drawback is encountered at the stagnation point of an impinging flow. The production of turbulent kinetic energy by shear, P_k of eq.(4.14), is based on the eddy viscosity assumption and result in too high estimates of turbulent kinetic energy and turbulent viscosity.

The above mentioned difficulties suggest the application of more advanced turbulence models. Among the most widely used alternatives are second moment closure models such as the differential stress model (DSM), which contain separate transport equations for all independent stresses and fluxes, or the more economical algebraic stress model (ASM), where differential equations are converted into algebraic relations but anisotropic features are retained.

Murakami et. al. 1992 carry out comparative studies between the k-ϵ, ASM and DSM models in non-isothermal jet flow in an enclosure. The ASM and DSM show by far the best agreement with measurements when Reynolds stresses and heat fluxes are considered, but the difference between the models is less conspicuous when mean velocities and temperature gradients are compared. This clearly demonstrates that the benefit of applying advanced models depends on the specific purpose of the simulation and the accepted deviation from what is considered the main properties and key-parameters of the flow.

Leschziner 1992 states that in general the most considerable improvements by turning to more advanced turbulence models are achieved in swirling and rotating flows while more modest improvements can be expected in buoyancy affected flows.

The benefit of applying more advanced models in terms of greater prediction accuracy should be weighed up aganst the immense increment of required computing time and the stability problems which are likely to impede the solution procedure. It is also important to realize that the discrepancies between measurements and model results are not entirely attributable to the turbulence model but also depend on the specification of the boundary conditions and the numerical errors inherent in the numerical solution scheme.

In spite of poor accuracy of the model predictions in some types of flow the arguments against applying the k-ϵ model are not convincing when practical engineering investigations of room air flow are carried out. The previous discussion, however,

strongly implies that adequate precautions should be taken and physical understanding of the flow phenomenons and validation by experimental data are indispensable elements in a critical evaluation of the results.

Chapter 5

The numerical method

A general numerical method for solving equations for heat transfer and fluid flow is presented by *Patankar 1980*. The numerical procedure aims at solving equations on the common convection/diffusion form. A thorough description is provided by the author and the objective of this chapter is not to give a comprehensive account of the computational method but rather to give a brief outline and highlight elements which are considered to be of special interest to the present work.

The numerical method is employed in the development of a computer algorithm. The work is based on the TEAM computer code (Turbulent Elliptic Algorithm Manchester, University of Manchester 1984). The code is extended to take into account non-isothermal flow, radiative heat transfer and the description of boundary conditions is improved. The code share its structure with the well known TEACH code and the only major difference between the codes is the layout of the computational grid. The structure of the TEAM code is given in appendix B.

The topics treated in this chapter do not apply only to the specific computer programme used in this study but they are also relevant to the large share of fluid flow codes which are more or less based on the practice of *Patankar 1980*.

5.1 Discretization of the governing equations

The equations presented in chapter 4 describe the continuous variation of the variables U,V,W,T,k and ϵ throughout the flow domain. To solve the set of governing differential equations numerically they are converted into a set of algebraic difference equations by discretization. In this work a finite volume approach has been applied to promote a direct physical interpretation of the approximations made by discretization but an identical set of algebraic equations can be derived using a description based on finite differences.

The finite volume approach implies that the flow domain is subdivided into a number of control volumes - or computational cells - as shown in fig.5.1.

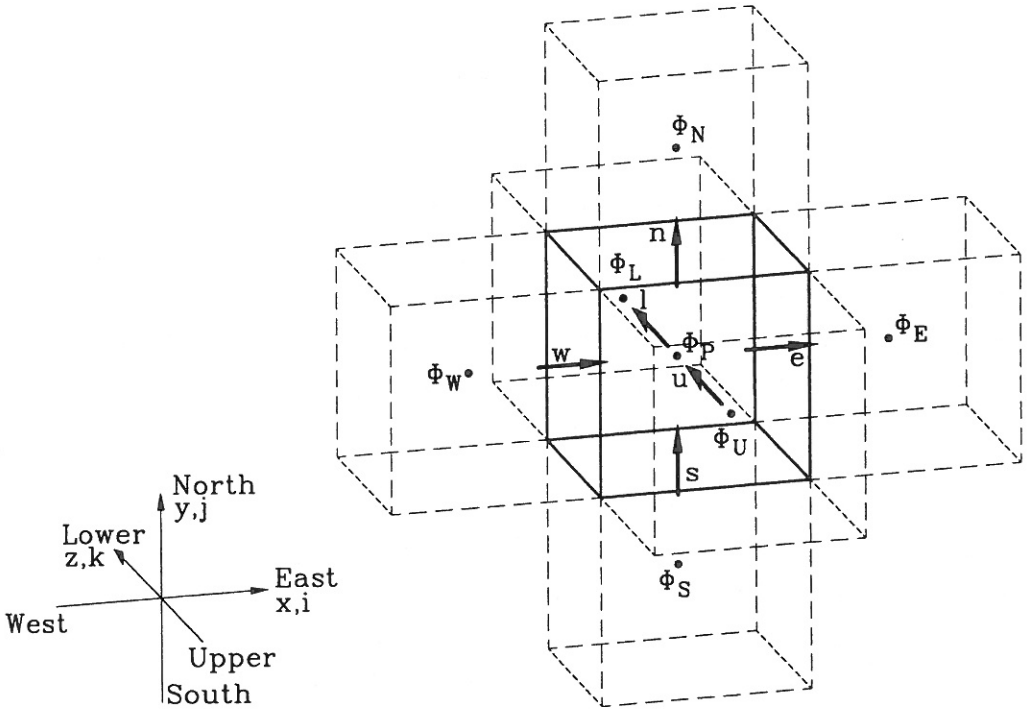

Figure 5.1 3-D sketch of a computational volume and its neighbouring cells. The arrows illustrate the net inflow or outflow through the cell faces.

If ϕ is used to denote any of the involved flow variables it is possible to obtain a general formulation of the convection-diffusion equation. By integration of the ϕ-equation over a flow volume it is possible to attain the following expression

$$\begin{aligned}
&\left((\rho U)_e\phi_e - \frac{\Gamma_{\phi,e}}{\Delta x_{EP}}(\phi_E-\phi_P)\right) - \left((\rho U)_w\phi_w - \frac{\Gamma_{\phi,w}}{\Delta x_{WP}}(\phi_P-\phi_W)\right) \\
&+ \left((\rho V)_n\phi_n - \frac{\Gamma_{\phi,n}}{\Delta y_{NP}}(\phi_N-\phi_P)\right) - \left((\rho V)_s\phi_s - \frac{\Gamma_{\phi,s}}{\Delta y_{SP}}(\phi_P-\phi_W)\right) \\
&+ \left((\rho W)_l\phi_l - \frac{\Gamma_{\phi,l}}{\Delta z_{LP}}(\phi_L-\phi_P)\right) - \left((\rho W)_u\phi_u - \frac{\Gamma_{\phi,u}}{\Delta z_{UP}}(\phi_P-\phi_U)\right) \\
&= \iiint_V (S_u + S_p\phi_p)dV
\end{aligned} \tag{5.1}$$

The transport by convection and diffusion across each of the cell faces is summed on the left hand side of eq.(5.1). On the right hand side the linearized source term, $S_\phi = S_u + S_p\phi_p$, is integrated over the cell volume.

A major difficulty is how to make an accurate estimate of the variable at the cell faces - ϕ_w, ϕ_e, ϕ_n etc. It is necessary to make an assumption concerning the ϕ-profile between the grid nodes and subsequently choose a suitable interpolation method. With the purpose of simplification a 1-D spatial ϕ-distribution in a uniformly spaced grid is considered

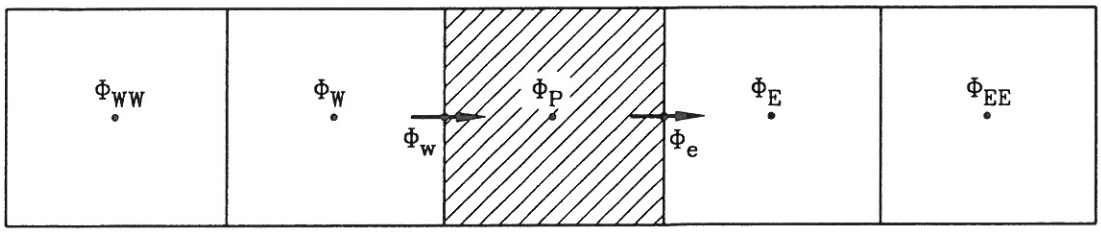

Figure 5.2 1-D finite volume

The approximation of e.g. ϕ_w is derived on basis of a Taylor series expansion which reads

$$\phi_w = \phi_P - \frac{\Delta x}{1!}\frac{\partial \phi}{\partial x} + \frac{\Delta x^2}{2!}\frac{\partial^2 \phi}{\partial x^2} - \frac{\Delta x^3}{3!}\frac{\partial^3 \phi}{\partial x^3} + h.o.t. \qquad (5.2)$$

where h.o.t. is an abbreviation for higher order terms.

Similar expressions can be set up for the value of ϕ at the remaining cell faces. If the equations are rearranged and combined formulations for the first and second order derivatives in the convective and diffusive terms can be derived.

The accuracy of an approximation based on eq.(5.2) depends on the highest order term included. A large number of methods for approximating the cell face values has been suggested and in principal they all originate from the Taylor series.

In the field of CFD upwind and central difference schemes have traditionally been used. These two schemes are very simple and certain restrictions must be imposed. The strengths of the schemes have been combined in the HYBRID scheme (*Spalding 1972*). The HYBRID scheme is composed of an upstream approximation for convection

dominated flow and a central difference approximation for flow with considerable influence of diffusion. Later the QUICK scheme (*Leonard 1979*) was introduced and recently a large number of higher order variants has been developed concurrently with the increasing available computer speed (*Matsuo et. al. 1992*). To choose a capable approximation method is akin to the choice of turbulence model in chapter 4. It is basically a question of making an appropriate compromise between computing speed, desired accuracy and numerical stability when a tolerable grid refinement is applied.

The difference shemes are presented in eq.(5.3)-(5.6).

Upwind :

$$\begin{aligned} \phi_w &= \phi_W \quad for \quad (\rho U)_w > 0 \\ \phi_w &= \phi_P \quad for \quad (\rho U)_w < 0 \end{aligned} \tag{5.3}$$

Central :

$$\phi_w = \frac{1}{2}(\phi_W+\phi_P) \tag{5.4}$$

HYBRID :

$$\begin{aligned} \phi_w &= \phi_P \quad for \quad Pe_w < -2 \\ \phi_w &= \frac{1}{2}(\phi_P+\phi_W) \quad for \quad -2 < Pe_w < 2 \\ \phi_w &= \phi_W \quad for \quad Pe_w > 2 \end{aligned} \tag{5.5}$$

$$Pe_w = \frac{(\rho U)_w \Delta x_{ew}}{\Gamma_{\phi,w}}$$

QUICK :

$$\phi_w = \phi_P + \frac{\phi_P-\phi_W}{2} - \frac{1}{8}(\phi_P-2\phi_W+\phi_{WW}) \tag{5.6}$$

where the cell Peclet number - or cell Reynolds number -, Pe, is the ratio between convection and diffusion. The Peclet number is a key parameter when the accuracy of the schemes is assessed. When geometric weight factors are introduced for a non-uniformly spaced grid similar, but more extensive, expressions can be derived.

The discretization introduces errors which entail differences between the numerical solution and the exact solution of the partial differential equations. The numerical errors arising in the computation is mainly caused by the truncation error while the round off error of the computer normally is negligible. The truncation error is attributed partly to the limited order of accuracy of the discretization scheme and partly to the grid layout. The errors in the approximation of the first derivative in the convection term and the second derivative in the diffusion term leads to overestimation of diffusivity - collectively referred to as numerical diffusion. This unphysical effect tends to erode gradients and may cause unreliable results. Improved accuracy can be obtained by applying approximations of higher order accuracy. *Matsuo et. al. 1992* test several advanced higher order schemes in laminar airflow and demonstrate their advantages in terms of prediction accuracy compared with the upwind scheme. *Leschziner 1992* also advocates the use of high order accurate schemes but common to the authors is the recognition of the severe inherent stability problems which may cause numerical oscillations and breakdown of the calculations.

In the present work the HYBRID scheme is adopted to avoid stability problems. By refining the grid in areas with large gradients it is in principle possible compensate for insufficiency of the approximation method but the numerical errors can not be completely avoided in practical problems. It is possible to rearrange eq.(5.1) when the HYBRID approximation is introduced. A more compact version appears when coefficients containing the joined effect of diffusion and convection are introduced

$$\phi_p \left(\sum_{nb} a_{nb} - S_p V \right) = \phi_p \left(a_p - S_p V \right) = \sum_{nb} (\phi_{nb} a_{nb}) + S_u V \qquad (5.7)$$

$$a_W = (\rho U)_w A_w \qquad for \quad Pe_w < -2$$

$$a_W = ((\rho U)_w + \frac{\Gamma_e}{\Delta x_{WP})} A_w \qquad for \quad -2 < Pe_w < 2$$

$$a_W = 0 \qquad for \quad Pe_w > 2$$

The nb-index in eq.(5.7) indicates neighbouring cells - east, west, north, south, upper and lower. An expression for the coefficient, a_W, is given and a similar formulation is valid for the coefficients of the other cell faces. V is here used for the cell volume.

5.2 Pressure correction

A remaining problem is how to calculate the pressure term in the governing equations and ensure that the continuity equation is satisfied. To calculate the effect of the pressure field on the velocity field a pressure gradient across the computational cell must be estimated. A pressure field obtained by discretization in the grid layout of fig.(5.1) will satisfy the continuity equation but it may lack physical realism according to *Patankar 1980* who presents examples of highly non-uniform pressure fields which may be the result of applying this line of procedure.

A usual way to handle the problem is to use a staggered grid causing the velocity components and pressure to be calculated in different locations. By employing displaced separate grids for each velocity component an alternating sequence of grid nodes for velocity and grid nodes for other scalars including pressure is established as shown in fig.5.3. The difficulties mentioned above can now be eliminated. The additional cost of this approach is the necessity of performing interpolations in more than one grid.

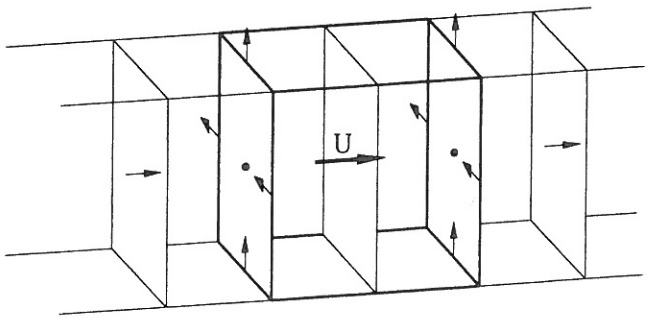

Figure 5.3 Lay out of staggered grid in the x-direction for the computation of the U-velocity component.

Despite the staggering both velocity components and other variables are in principle handled as described in the previous section with the exception that the interpolations are performed in separate grids. A special treatment is, however, required to extract a

pressure equation and among several available methods the SIMPLE algorhitm has been adopted in the present work.

Eq.(5.7) applies to any variable, ϕ, including the U-velocity component in the momentum equation. Despite the grid staggering a similar expression is derived focusing on the location of U

$$a_w U_w = \sum_{nb} a_{nb} U_{nb} + (S_u + S_p U_w) V + (P_w - P_p) A_w \qquad (5.8)$$

where the pressure gradient is not included in the source term but is expressed as the pressure force acting on the faces of the control volume.

The task of solving the set of coupled non-linear equations is carried out by iteration. At an intermediate stage in the process of obtaining the final solution the value of a variable is only preliminary. The final value can be regarded as the sum of this preliminary value and a correction. With this convention the pressure and in this case the U-velocity component reads

$$P = P^* + P' \qquad U = U^* + U' \qquad (5.9)$$

where the superscript * denotes preliminary values and $'$ the correction.

When the equation containing values of the preliminary velocity and pressure field is subtracted from eq.(5.8) containing the final values a correction equation appears

$$a_w U'_w = \sum_{nb} (U'_{nb} a_{nb}) + (P'_W - P'_P) A_w \qquad (5.10)$$

In the SIMPLE method the first term on the right hand side is omitted. This simplification leads to a convenient reduction of the required numerical operations and it does not exert any influence the final solution. By rearranging eq.(5.10) an equation for pressure correction is obtained

$$U_w = U^*_w + \frac{A_w}{a_w} (P'_W - P'_P) \qquad (5.11)$$

An expression for the pressure term, P′, is needed to complete eq.(5.10). It can be derived by inserting eq.(5.10) into the integrated continuity equation. The obtained equation can be arranged on the standard convection-diffusion form according to eq.(5.7).

$$a_p P'_p = \sum_{nb} \left(a_{nb} P'_{nb} \right) + (S_u + S_p P'_p) V \qquad (5.12)$$

The expression for pressure correction enables the solution of momentum equations in accordance with the demand for mass conservation. The system of interlinked equations is then solved iteratively by stepwise calculating coefficients and solving the set of algebraic equations for one variable at a time. In each iteration cycle the pressure correction equation is solved and subsequently the U-velocity component is adjusted to comply with eq.(5.11). The other velocity components are treated in the same way.

5.3 Solution procedure and convergence

To obtain a solution for eq.(5.7), eq.(5.8) and eq.(5.10) initial values of the involved variables must be specified. The resulting velocity and temperature fields are obtained by repeatingly calculating coefficients and solving the set of linear algebraic equations. Progressively the information at the imposed boundary conditions are propagated and the variable values are adjusted throughout the flow domain. It is assumed that the preliminary solution is gradually converging to a final solution. During the iterative calculation an indicator is needed to check for convergence and if so to determine at what rate. The residuals are used for that purpose.

$$R_\phi = \sum_{1}^{N} \left(\sum_{nb} (\phi_{nb} a_{nb}) + (S_u + S_p \phi_P) V - a_p \phi_P \right) \qquad (5.13)$$

The over all residual, R_ϕ, is given by eq.(5.13) where N denotes the total number of control volumes. In the case of convergence the residuals are reduced and after a number of iterations only a fraction of their initial value remains. Further iterations will lead to negligible changes of any of the variables and it is assumed that a solution for the dependent variables in accordance with the governing equations and the boundary conditions is reached. If the calculation is stopped before the residuals for each variable is sufficiently reduced the continuity restraint may not be satisfied and some regions of the flow domain may not have fully 'settled'. It is thus crucial to choose a proper termination criterion which does not imply excessive computing effort.

An universal stop-criterion can not be given but must be determined with respect to the type of flow and required prediction accuracy. In the present work the residuals are normalized by inlet values for momentum and mass. It was tested that a stop criterion of a few percent did not cause any significant changes of the flow field compared to a stop-criterion of a few per mille. The largest contributions of individual control volumes to the over all residual are often found in confined parts of the flow domain - typically in regions with considerable gradients.

In a 3-D low velocity buoyancy affected flow divergence is often encountered or the convergence rates decline rapidly - strongly impeding the solution procedure. Physical and numerical reasoning may prove itself useful in speeding up convergence. The task of iteratively solving non-linear interlinked equations by a linearized set of equations is affected by various factors as :

- *grid lay out and refinement*
- *discretization scheme*
- *pressure correction method*
- *source term linearization*
- *matrix solver and number of sweeps*
- *relaxation coefficients*

The former two items differ from the latter four in the sense that they also affect the prediction accuracy. By applying a coarse computational grid convergence is enhanced but the solution can only be regarded as grid independent for a sufficiently fine grid. The use of non-uniformly spaced grid offers the opportunity of increasing the number of grid nodes in regions of specific interest and where the occurrence of large gradients requires it. The grid layout has consequently been motivated by desired prediction accuracy in certain regions of the room and not by the difficulties involved in achieving tolerable convergence rates.

As mentioned earlier the HYBRID scheme was applied because of its simplicity and tractable features concerning convergence. The HYBRID scheme suffers from overshots in the diffusion term but it can be compensated by grid refinement. The numerical models ability to converge is severely deteriorated by applying higher order schemes and in this specific case it has not been possible to obtain a solution by QUICK. Special measures are required to adjust the QUICK scheme to this particular type of flow.

It is possible to linearize the source terms in the equations in various ways. It is often a non-linear function of the dependent variable and an unfavourable representation tends to enhance instabilities and prolong the time required to achieve convergence. It is essential that all negative terms are included in the S_p-term while the positive terms are put into the S_u-term. Otherwise it may result in unphysical values of dependent variables. This practice is particulary important to the k and ϵ equations because they are strongly influenced by the source term.

Compared to other pressure correction methods (e.g. SIMPLER and PISO) SIMPLE is characterized by lower convergence rate and less computing effort for each iteration. The benefit of applying more advanced methods diminishes with increasing flow complexity. Flow in a displacement ventilated room is strongly buoyancy affected. The velocity-temperature coupling by the buoyancy term in the momentum equations is mainly responsible for slow convergence and the velocity-pressure coupling which is extensively accounted for by the SIMPLER and PISO methods is of less importance.

Many methods have been developed for solving system of linear equations. The use of direct solution methods tends to be unfit because of large requirements to storage and computing speed. The iterative nature of the solution method suggests an indirect method and consequently the Tri-diagonal Matrix Algorhitm (TDMA) with alternating sweep directions is applied. To utilize the information of the calculated coefficients the number of sweeps performed by the TDMA algorhitm must be adjusted. On one hand the coefficients are only preliminary and too much effort spent on several sweeps is inexpedient but on the other hand poorly determined values of the variables causes propagation of errors to the succeeding iterations. In view of the slowly converging temperature field only 1-3 sweeps has been applied depending on the variable to be solved.

To obtain a steady state solution two different approaches are possible. In the stationary version of the numerical model it is necessary to introduce underrelaxation factors in order to prevent divergence. The change of a variable from the previous (old) to the current (new) iteration cycle is modified as

$$\phi_P = \phi_{P,old} + \alpha_\phi(\phi_{P,new} - \phi_{P,old}) \qquad 0<\alpha_\phi \leq 1 \qquad (5.14)$$

where α_ϕ is the underrelaxation coefficient.

When eq.(5.14) is inserted in eq.(5.7) the general discretization equation can be put into the following form

$$\phi_p \left(\frac{a_p - S_p V}{\alpha_\phi} \right) = \sum_{nb} (\phi_{nb} a_{nb}) + S_u V + (1 - \alpha_\phi) \phi_{p,old} (a_p - S_p V) \quad (5.15)$$

The underrelaxation coefficients must be optimized. In other words the α_ϕ-values are maximized without causing divergence. In the present work values in the range 0.1-0.6 have been applied. During a calculation the underrelaxation coefficients can be increased to speed up convergence but it often leads to amplification of numerical instabilities and divergence.

In a transient version of the model, time dependent terms are included in the source terms for all variables. Divergence is avoided by adjusting the time step. A steady-state solution is obtained by using the time step as an underrelaxation parameter. If no long term air movements, e.g. gravity waves, occur a solution is in principle attainable by choosing a sufficiently small time step. If a small time step is used the transient term in the governing equations become dominant corresponding to heavy underrelaxation and numerical oscillations are suppressed. Tests with a transient model and a slightly modified pressure correction method (SIMPLEC, *Van Doormal and Raithby 1984*) show stable but slow convergence. The stationary model with specification of individual underrelaxation coefficients for each variable yields higher convergence rates. In the present work an optimal set of underrelaxation coefficients is chosen by trial and error.

The large majority of engineers working with CFD has experienced divergence or intolerable slow convergence but unequivocal recommendations of general validity can hardly be given due to the complexity of the equations and the immense number of interlinked numerical operations. The choice of adequate measures for optimizing the efficiency of the numerical method is not only a question of flow type but may even be case dependent.

Chapter 6

Boundary conditions

Boundary conditions are required along all the domain boundaries for all dependent variables in order to complete the system of equations. The boundary conditions are unique to a specific flow situation and thus decisive to the obtained results. For a number of years investigations of room air flow by CFD has been carried out using simplified boundary conditions and mainly focusing on the internal flow. The task of improving the representation of the boundaries has, however, attracted attention in recent years.

Different types of boundary conditions are used for surfaces of the room, symmetry plane, inlet and outlet. In this chapter the subject is treated in further detail and special attention is paid to the description of temperature boundaries at the surfaces and the inlet boundary in recognition of their pronounced importance to the air flow in a displacement ventilated room.

6.1 Boundary layers at walls and obstacles

In the layer close to a solid surface the fluctuating motion in transverse direction is suppressed and molecular viscosity plays a dominant role. Large gradients prevail and a large number of grid nodes are required to model this region, e.g. with a low-Reynolds number model. To avoid a very fine near wall grid the traditional way of linking the near wall viscous layer to the free turbulent flow by a wall function is far more relevant to practical applications in 3-D. The wall functions offer the opportunity of reducing the required processing time and still maintain a sufficient number of grid nodes in regions of the flow where the solution is expected to depend on the grid resolution.

The wall function is derived from assumptions of boundary layer similarity. It was originally developed for channel flows with high velocities and production of k at the boundary but here it is assumed applicable to boundary layers in rooms where the air

flow is omnidirectional, the velocities generally low and the boundary layer relatively thick. Fig.6.1 shows a sketch of a wall boundary layer.

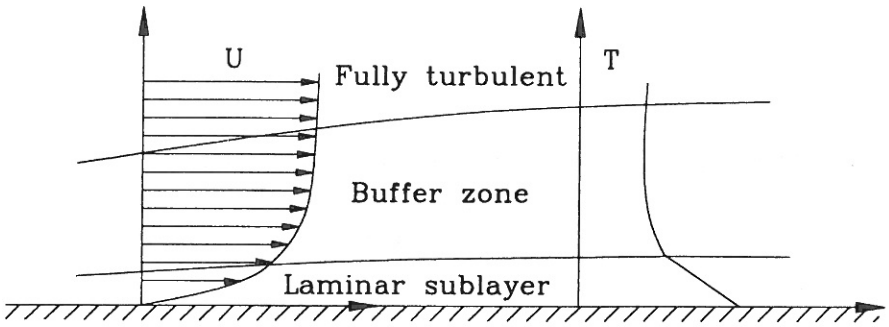

Figure 6.1 Schematic representation of velocity and temperature profiles in a turbulent boundary layer at a wall.

The momentum equation at a grid node, P, adjacent to the wall is adjusted by subtracting the friction exerted by wall shear stress. If local equilibrium of turbulent energy is assumed in an attached boundary layer flow near the wall a generalized logarithmic relation is derived (*Patankar et. al. 1967*)

$$U^+ = \frac{\ln(Ey^+)}{\kappa}$$

$$\Updownarrow$$

$$\tau_w = \frac{\rho\kappa U_p U^*}{\ln(Ey^+)} \qquad (6.1)$$

$$U^+ = \frac{U_p U^*}{U_f^2} \qquad y^+ = \frac{\rho U^* y_p}{\mu_l} \qquad U_f = \sqrt{\frac{\tau_w}{\rho}}$$

where U^+ and y^+ are dimensionless velocity and wall distance, respectively. U^* is a velocity scale and U_f the friction velocity. τ_w is the wall shear stress and y_p the distance from the wall to the first grid point. E and κ are empirical constants. The value of E is 9.0-9.7 for a smooth wall and κ takes the value 0.40-0.44.

It is important to ensure that the first grid node is situated in the turbulent region (see fig.6.1) by arranging the grid with respect to the y^+-values. In practical application the y^+-values do not always comply with this demand since the magnitude of velocities

often vary dramatically along a solid surface. When y^+ becomes small a laminar relation is employed

$$\tau_w = -\mu_l \frac{U_p}{y_p} \tag{6.2}$$

The value of turbulent kinetic energy at the first grid node, k_p, is found by the regular kinetic energy equation with some modifications. There is no transport of k across the wall and the near wall flow is considered as a Couette flow and the calculation of the generation term is reduced.

In the vicinity of the wall the length scale, l, calculated from k and ϵ varies linearly with the distance to the wall and the near wall dissipation rate is accordingly prescribed and not obtained from the ordinary ϵ - equation, see e.g. *Nallasamy 1987.*

$$\begin{aligned} l &= \frac{k^{3/2}}{\epsilon} = \frac{\kappa y_p}{C_\mu^{3/4}} \\ \epsilon_p &= \frac{U_f^3}{\kappa y_p} = \frac{C_\mu^{3/4} k_p^{3/2}}{\kappa y_p} \end{aligned} \tag{6.3}$$

6.2 Boundary conditions for the temperature equation

Conduction through the walls and radiative exchange of energy between the surfaces of the room is often of considerable importance to the overall temperature distribution and particulary to the vertical temperature gradient in a room with displacement ventilation. It is important to choose proper boundary conditions for temperature in order to account for supplied and redistributed heat. It is possible to handle the temperature boundary on different levels of increasing complexity. The simplest possible approach is to neglect radiation and heat flux by assuming adiabatic walls. Alternatively heat fluxes are prescribed at all surfaces - thereby indirectly incorporating radiation and heat conduction. This method suffers from the lack of very detailed experimental information and estimates of heat flux may involve severe uncertainties since they must be performed without sufficient knowledge about the local air flow.

Describing the heat fluxes as a function of local flow parameters offers further improvement. If a measured temperature distribution is prescribed at the surfaces the task narrows down to calculating convective heat transfer coefficients, α_w. Assuming analogy between momentum and energy transport a logarithmic relationship is derived in accordance with eq.(6.1).

$$\begin{aligned} T^+ &= \frac{c_p \rho U^*}{\alpha_w} \\ &\Updownarrow \\ \alpha_w &= \frac{c_p \tau_w}{T^+ U_p} \frac{\ln(Ey^+)}{\kappa} \end{aligned} \tag{6.4}$$

where T^+ is the dimensionless temperature and c_p is the specific heat of air at constant pressure.

The traditional and widely used version of the logarithmic wall function was formulated by *Launder and Spalding 1974*

$$U^+ = \begin{cases} y^+ & y^+ < 11.6 \\ 2.3\ln(y^+)+5.1 & y^+ > 11.6 \end{cases}$$

$$T^+ = \begin{cases} \sigma_l \, y^+ & y^+ < 11.6 \\ \sigma_t(U^+ + P) = \sigma_t(2.3\ln(y^+)+3.2) & y^+ > 11.6 \end{cases} \tag{6.5}$$

$$U^* = C_\mu^{1/4} k^{1/2} = U_f$$

where P is a function of the ratio between laminar and turbulent Prandtl numbers. When σ_l=0.71 and σ_t=0.9 the value of P is -1.8.

The weaknesses of this type of wall function is pointed out by several authors - see e.g. *Chen 1988*, *Yaun et. al. 1992* or *Takemasa et. al. 1992* . It fits the exact solution very well for $y^+ > 30$ while the approximation in the range $8 < y^+ < 30$ is relatively poor. A second drawback is that the wall function is developed for high Reynolds number forced convection and wall heat flux can not be exactly accounted for in mixed or natural convection flow. Furthermore the traditional wall function is grid dependent which causes decreasing convective heat transfer coefficients with increasing distance from the wall to the first grid point in the flow domain. Remedies in terms of adjusting the traditional wall functions has been suggested by a number of authors - some of the suggestions are plotted in fig.6.2-6.3.

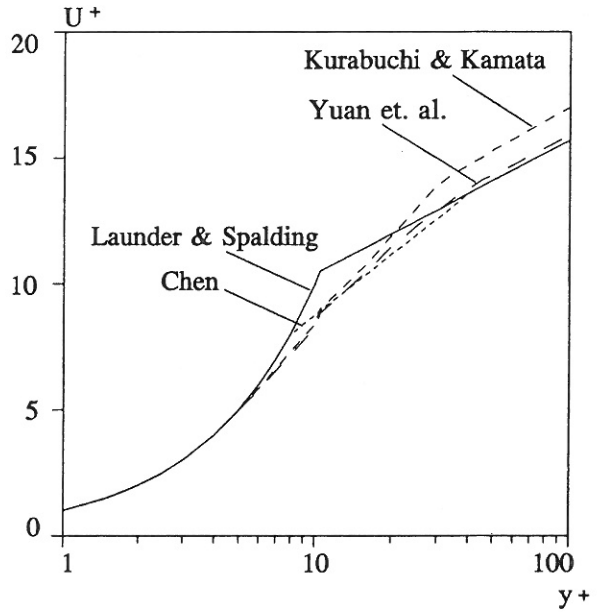

Figure 6.2 Correlation between U^+ and y^+ for different wall functions.

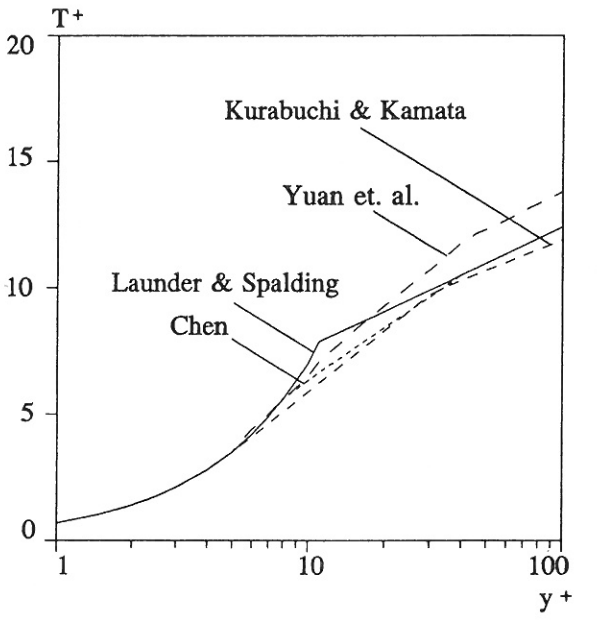

Figure 6.3 Correlation between T^+ and y^+ for different wall functions.

Chen 1988 working with indoor air flow improves the performance of the original wall function by curve fitting. A logarithmic curve segment is introduced to represent an

intermediate buffer layer between the laminar and the turbulent region. The extra curve segment substitutes the traditional wall function in the range $8 < y_+ < 40$.*Kurabuchi and Kamata 1989* developed a three layer wall function similar to the traditional one for a vertical plate with natural convection. The wall function of *Yuan et. al. 1992* is a four layer model which incorporates the variation of σ_t with y^+. The different proposals for wall functions are written on common form in appendix A.

If the distance from the wall to the first grid node is chosen in the range 0.5-1.0 cm in a displacement ventilated room the y^+-values typically lies in the range from 5 to 40 where the predictions made by traditional wall function are questionable. The use of wall functions is particularly interesting with respect to the heat flux at the floor. The total heat transfer from the floor to the room air is essential in establishing the correct vertical temperature gradient and thus to the room air flow. The effect of applying three or four-layer wall functions is discussed in chapter 7.

6.3 Radiation

Radiative heat transfer plays an important role in the temperature distribution in the room and this section discusses how to account for the heat exchange between the surfaces of room.

The effects of radiation are implicitly accounted for by the specification of measured temperatures at the walls, floor and ceiling but too low convective heat transfer coefficients may cause an underestimation of the heat exchange between solid surfaces and room air. It is investigated whether the introduction of a radiation model leads to any improvement of the prediction accuracy. The walls are treated as adiabatic and it is assumed that the heat loss or gain at a solid surface is transferred to the adjacent air volume by convection.

The traditional way of modelling thermal radiation in an enclosure is to subdivide the surfaces of the room into a number of subsurfaces and calculate the mutual interchange between all pairs of surface elements. To obtain a tolerable accuracy a fine discretization of the surfaces is needed. The computational effort used for calculating the shape factors and the storage requirements are considerable. *Lockwood and Shah 1981* and *Li 1992* shortly review existing techniques for calculating radiative heat exchange and conclude that zone methods and the Monte Carlo method suffer from limited accuracy and computational inefficiency. The uneconomical computational

performance is particularly inexpedient when the radiation model is incorporated as an integrated part of the CFD-model since the temperature field is continuously altered during the iterative process and the radiation model must update the radiative heat transfer. The discrete transfer model (DTM) is characterized by ease of application and relatively high computational efficiency. The degree of accuracy achieved by the DTM-model is adjustable as described in the following. It is developed to enter into a model for flow and heat transfer predictions in a combustion chamber by *Gosman et. al 1980.* The DTM-model has recently been successfully implemented for prediction of thermal radiation in rooms by *Lemaire 1991* and *Li 1992.*

The first step in applying the DTM-method is to subdivide the surfaces into a number of subsurfaces - see fig.(6.4). The hemisphere surrounding a point P on a subsurface is divided into a number of segments by discretization with respect to the horizontal angle, θ, and the vertical angle, ϕ. The radiation transferred from a subsurface is regarded as rays leaving P and passing through the center of each segment of the hemisphere. It is traced through space until it intersects a subsurface at a point Q.

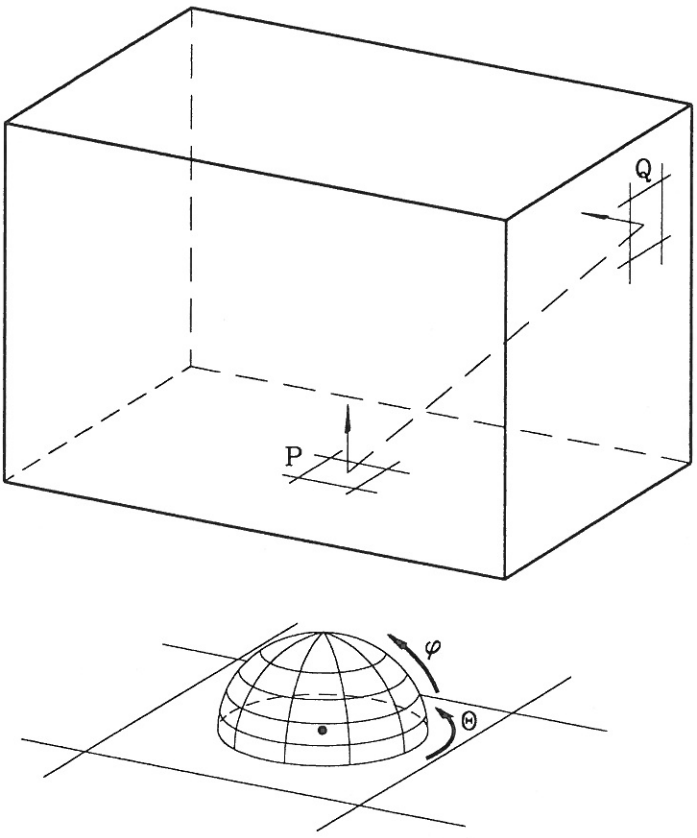

Figure 6.4 Radiative exchange between subsurfaces and spatial discretization of the hemisphere surrounding a point on the subsurface.

The area of the segment is defined by the solid angle dΩ and the total number of rays, n, is calculated as

$$n = n_\phi n_\theta = \frac{\pi}{2d\phi}\frac{2\pi}{d\theta} = \frac{\pi^2}{d\phi d\theta} \tag{6.6}$$

where n_ϕ and n_θ are the number of divisions of vertical and horizontal angle, respectively - $d\phi$ and $d\theta$ are the corresponding increments.

The intensity of a representative ray leaving P and arriving at a point, Q, at another surface is found by integrating the radiative heat transfer equation with respect to the distance, s, travelled by the ray. The derived recurrence relation reads

$$I_{out} = I_{in}e^{(-\kappa s)} + \frac{\sigma T^4}{\pi}(1-e^{\kappa s}) \tag{6.7}$$

where I_{in} and I_{out} are the intensities entering and leaving a control volume. κ is the absorption coefficient for air and σ the Stefan-Boltzmann constant. This implies that the intensity of a ray is progressively altered in an absorbing/emitting medium. Moderately humid air, with the temperature and the carbon dioxide concentration normally encountered in occupied rooms, is usually assumed transparent and no radiative energy is deposited as the ray traverses the room. The intensity of a ray leaving a subsurface is equal to the intensity arriving at the receiving subsurface and eq.(6.7) can be omitted. Instead attention is paid to the calculation of intensity at the point P.

$$I_P = \frac{q_+}{\pi} = (1-\epsilon_P)\frac{q_-}{\pi} + \frac{\epsilon_P \sigma T^4}{\pi} \tag{6.8}$$

where q_- and q_+ are the fluxes towards and away from the surface and ϵ_p is the emissivity. It is seen that the heat flux from the surface is composed of a term containing the emitted energy and a term containing the reflected part of the incoming radiation. The incoming flux is calculated for each individual ray by summing up the contributions from each individual ray.

$$q_- = \sum_{i=1}^{n} I_{Q_i \to P}\, d\Omega \tag{6.9}$$

where $I_{Qi \to P}$ denotes the intensity of the ray from the point Q_i arriving at P - see fig(6.5).

When the surfaces of the room are not black iteration is needed to determine q_- and q_+ from eq.(6.8).

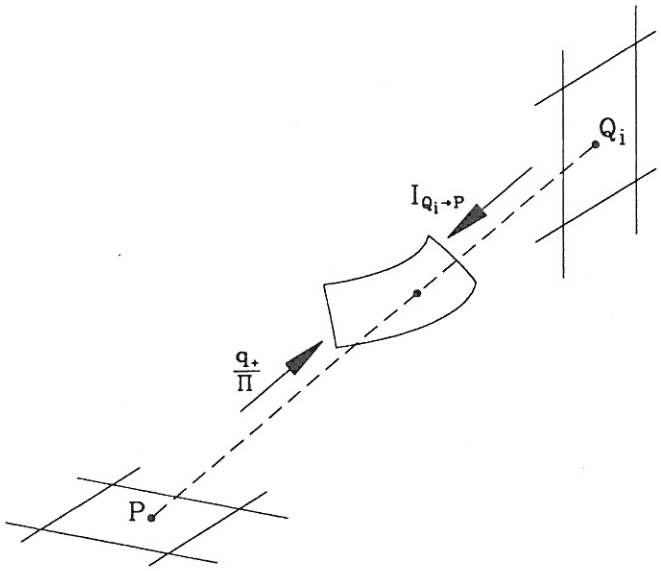

Figure 6.5 Radiative exchange between subsurfaces through a segment of the hemisphere.

The performance of the DTM-model is tested separate from the CFD-code by comparison with the Monte Carlo algorithm. The test case is selected to provide an estimate of the radiative heat loss from the heat sources to the surrounding room surfaces under conditions corresponding to the full-scale measurements. All surfaces of the room are considered grey with an emission coefficient of 0.95. A vertical linear temperature profile is prescribed at the walls and the temperatures at floor and ceiling are assumed constant

Surfaces	Area [m^2]	Emis.coeff.	Temp [o C]
Floor	48.0	0.95	19.2
Ceiling	48.0	0.95	21.3
Walls	112.0	0.95	19.2+2.1y/H
Small heat source	0.2	0.95	60.0
Large heat sources	2.8	0.95	40.0
Inlet device	1.4	0.95	16.0

Table 6.1 Data for calculation of radiative heat transfer.

The accuracy of the predicted radiative heat transfer obtained by the DTM-model depends on the spatial discretization in terms of number of subsurfaces and emitted rays. The surfaces of the room are subdivided into 1104 elements and table 6.2 shows the results of the Monte Carlo and the DTM radiation model where n_ϕ and n_θ are given and 'sym.' denotes results obtained for one half of the symmtrical set up.

In the Monte Carlo model 5000 radiant bundles are emitted per surface element in random directions and a statistical approach is used for calculating the shape factors between the subsurfaces of the room (see e.g. *Omori et. al. 1990*). The Monte Carlo method is not exact due to statistical errors but here it is used as a reference to the results obtained by the DTM-model. It should be noticed that the estimates of temperatures and emission coefficients prescribed in the model to some extent deviate from true values and thus influence the accuracy of predicted radiative heat transfer. This does, however, not prevent a comparative test.

Surfaces	Monte Carlo	DTM (5×5)	DTM (10×10)	DTM (sym.) (10×10)
Floor	-388	-430	-418	-392
Ceiling	332	318	327	311
Walls	-111	-123	-121	-120
Small heat source	117	120	118	118
Large heat sources	128	130	129	124
Inlet device	-22	-23	-22	-22

Table 6.2 Radiative heat transfer in a displacement ventilated room obtained by the Monte Carlo method and the DTM-model.

The accordance between the two models is surprisingly good even with few rays in the DTM-model. When the number of emitted rays is increased minor improvements are observed. In spite of the discrepancies the results suggest that sufficient accuracy can be achieved by relatively few rays and thus low computational cost.

When the DTM-model is included in the CFD-model only half the full scale room is modelled. It is tested if the performance of the radiation model is notably altered by the introduction of a symmetry plane. The mid-plane is set up as perfect reflecting implying

that the angle of incidence equals the angle of reflection. A ray impinging on the symmetry plane is redirected and traced to a solid surface. The results of the full room modelling are not fully reproduced but a fair agreement is obtained.

When the radiation model is used as a coherent part of the CFD-model it is activated to update the radiative heat transfer after the temperature field has been calculated. It is uneconomical to perform radiation calculations for each iteration and at the early stages of the iterative procedure it may cause numerical instabilities. At first a converged solution is obtained without radiation and then it has been found expedient to call the radiation subroutine in the computer code for every 10th iteration.

6.4 Description of inlet and outlet boundaries

Skovgaard 1991 investigates the airflow in an iso-thermal room by a k-ϵ model. It is demonstrated that the boundary conditions at the diffuser are decisive and it is particularly important to specify the correct inlet momentum flow in order to achieve acceptable results concerning both overall flow pattern and maximum velocities in the occupied zone.

This does not necessarily apply to a displacement ventilated room. When cool air is supplied directly into the occupied zone through a wall-mounted inlet device it is necessary to ensure rather low velocities. The inlet device for displacement ventilation subsequently differs from a jet diffuser with respect to the inlet surface area which is much larger for the former.

Nielsen et. al. 1988 illustrate by measurements of velocity distribution at the inlet surface the vast variation for velocity level and direction between different types of inlet devices. The design of the interior inlet device and the inlet surface itself strongly influences the actual distribution and the initial mixing with surrounding room air. This suggests that boundary conditions should be chosen very carefully for the individual types of inlet devices. It should, however, be pointed out that the velocity field undergoes drastic changes in a short distance from the inlet surface due to the dominating buoyancy forces and the effect of a specific boundary condition may entirely or at least partially vanish.

Different inlet boundary conditions has been tested in order to determine to what extent the specification of inlet boundary influences the velocity and temperature field in front

of the inlet device. Measurements and smoke observations described in chapter 2 is used in the development of suitable boundary conditions. The direction and distribution of the velocities and the turbulent quantities at the inlet has been treated. The model results obtained by different inlet boundary conditions are presented and discussed in further detail in chapter 7.

The inlet boundary is implemented in accordance with the geometry of the inlet device. A number of computational cells are defined as solids and velocities are prescribed at the front surface. The different descriptions of the inlet boundary from the simple to the more advanced are :

- A uniform inlet velocity distribution calculated from the inlet surface area and the air supply rate. It is referred to as a box-profile.

- A measured velocity profile is prescribed at a distance from the inlet surface. The velocities are fixed by manipulating the source term.

- The measured velocity profile is scaled to comply with the supply rate and the values are fixed at the inlet surface.

The inlet boundary values for turbulent quantities is also known influence the solution. In a high Reynolds number flow the effect of k and ϵ at the inlet boundary is often negligible due to the predominance of local production and destruction terms to transport terms. This does not apply to the low-velocity buoyancy affected flow of the present case. Turbulent kinetic energy is generated when the air enters through the perforations of the front plate and the shear stress caused by velocity gradients in vicinity of the inlet surface increases the level. An initial mixing takes place and the value of k decays rapidly due to dissipation and suppression of fluctuations by the stable stratification. The reduction of k takes place in a very short distance from the inlet surface and it can not be fully captured by the model. Visual observations suggest that the turbulence in the 'core region' of the supplied air is strongly reduced within 0.0-0.3 meter from the inlet device.

The inlet value of k is determined from an estimate of turbulent intensity (5-20 % of the mean inlet speed). Normally a value in the low range is chosen to compensate for the rapid decay which can not be captured due to insufficient grid refinement. To adopt a physical interpretation dissipation is specified corresponding to a desired value of turbulent viscosity or turbulent length scale. The turbulent length scale is taken as a proportion of the full height of the inlet device - usually in the range 2-10 cm.

As demonstrated by model results in chapter 7, an arbitrary chosen velocity profile and turbulent quantities at the inlet may tend to reduce prediction accuracy. By increasing the initial mixing the temperature gradient and subsequently the vertical acceleration is reduced and the velocities along the floor are underestimated.

The outlet has very limited effect on the flow field in general but it is important to ensure mass and heat conservation for the entire flow domain. The outlet velocity is found by dividing the supply air rate by the outlet area. The temperature of the exhaust air is either specified from measured values or left to adjust itself.

6.5 Heat sources

The main objective of applying a CFD-model in this work is to predict the air flow in front of the inlet device. This implies that the heat sources in the model principally serves the purpose of generating the required vertical temperature gradient. The thermal plumes do, however, act as a driving force and have a pronounced effect on the entire room air flow. Adequate measures must be taken to obtain the basic features of the plume in accordance with the experiments.

Shankar et. al. 1992 stress that estimates of the flow rate in thermal plumes in rooms ventilated by displacement ventilation are important. To obtain sufficient spreading of the ascending plume predicted by the k-ϵ model a very high grid resolution is needed and modifications for the generation of turbulent kinetic energy are recommended.

Schaelin et. al. 1992 calculate the temperature and velocity distribution in a thermal plume by the standard k-ϵ model and achieve good agreement with measurements. The number of grid nodes required in the vicinity of the heat source is also very large in this case.

Common to the authors is the large number of grid nodes used to model the plume separately. In the present work a similar procedure is excluded and a reduced version must be used.

The heat sources are represented as solid obstacles in the cartesian grid. Each of the computational cells which make up the obstacle is blocked by manipulating the source term and no convective or diffusive transport takes place across the cell surfaces. The dimensions, and thus the surface areas of the modelled heat sources, are approximated

in accordance with the experimental set up. The proportion of the supplied heat which is transferred by convection is distributed to the surrounding air volume. The convective heat is distributed to the adjacent cells depending on the surface of contact. The heat contribution enters the temperature equation through the source term and the derived air temperature increment of the adjacent cell depends solely on its volume. The rising plume is therefore strongly depending on the local grid refinement. The use of a rather coarse grid nevertheless results in a narrow plume penetrating to the ceiling for the small heat source and a diffuse plume disintegrating before reaching the ceiling for the large heat source.

The accordance with experimental observations indicates that this approach is a reasonable approximation. It should, however, be noted that a relatively large air volume is initially accelerated upwards and the increasing width of a plume is not accurately reproduced. The development of the plumes induced by the heat sources is shown in chapter 7.

Chapter 7

Model results and comparison with measurements

The purpose of applying CFD to model the air flow in the room is partly to gain insight into the overall air flow and partly to identify particular areas of the room where specified levels of key-parameters are exceeded and criteria for comfort are compromised. In this context it is important to distinguish between a qualitative assesment of the overall flow and a quantitative verification based on the exact distribution. In the former case the CFD results should be evaluated by applying a basic physical understanding of the flow while the latter case requires reliable measured data.

This chapter first adresses the performance of the numerical model with respect to overall features of the air flow and temperature distribution in a displacement ventilated room. The sensitivity of obtained results to different boundary conditions is investigated and finally predicted and measured velocity and temperature profiles are compared. The robustness and accuracy of the model is also tested for a modified turbulence model. Apart from comments on the agreement between model and measurements it is the objective to point out which model parameters are decisive for the prediction accuracy. The presentation of results leads to recommendations and a conclusion concerning the models applicability to practical problems.

7.1 Temperature and velocity field - overall model results

Characteristics of the flow field in a room with displacement ventilation is given in chapter 2 and this section presents model results in order to determine whether these overall patterns are captured by the numerical model. The figures at the same time offer interesting details of the air flow.

Fig.7.1 shows model results in terms of velocity vectors in the symmetry plane of the room - calculated with a high grid resolution (nx=40,ny=33,nz=30). It shows the inlet device to the left and the small heat source to the right. The overall air movement is induced by the injected cool air and the rising thermal plumes. A large proportion of the room air volume is stagnant. Despite the insignificant velocity level a horizontal air

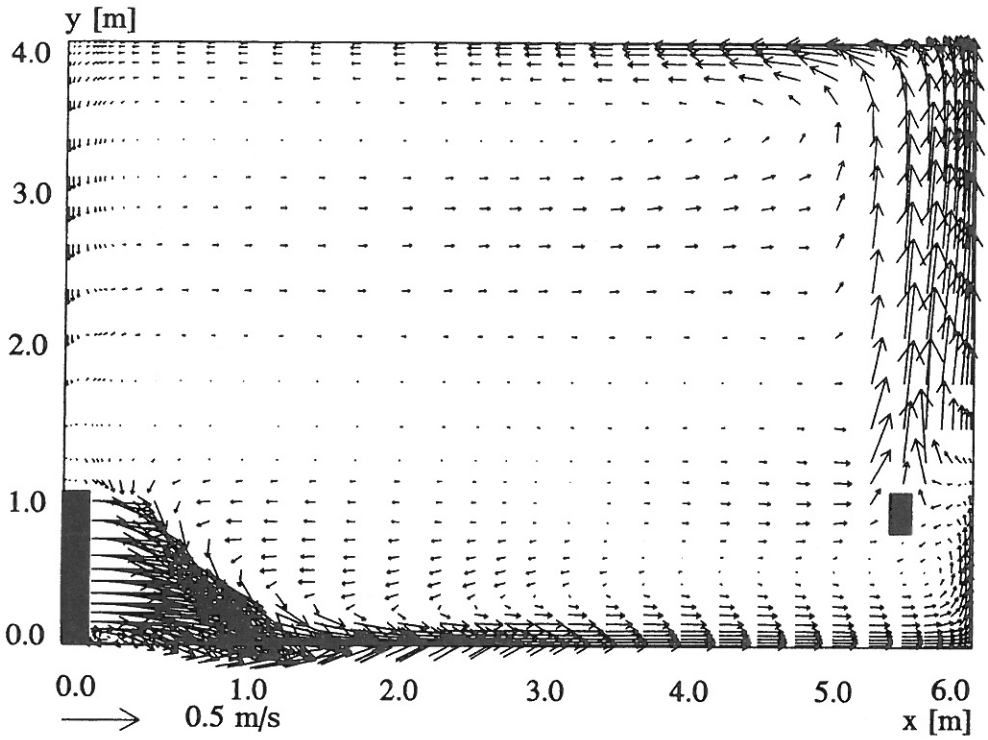

Figure 7.1 UV-vectorplot in the symmetry plane of the room (z=0.0m).

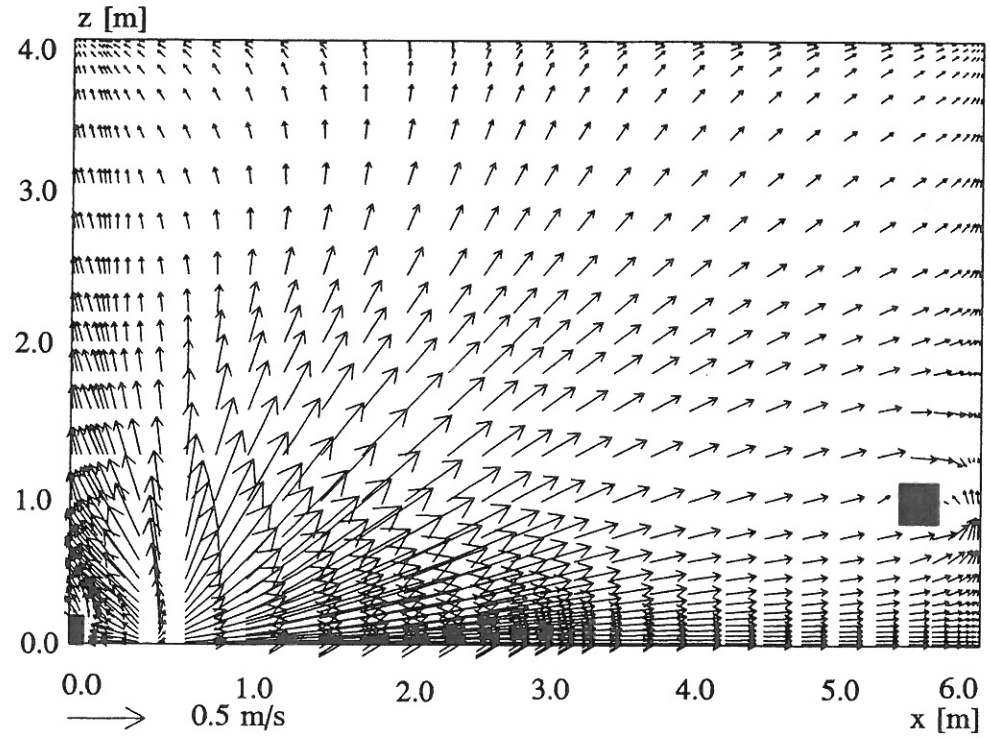

Figure 7.2 UW-vectorplot at floor level (y=0.03m).

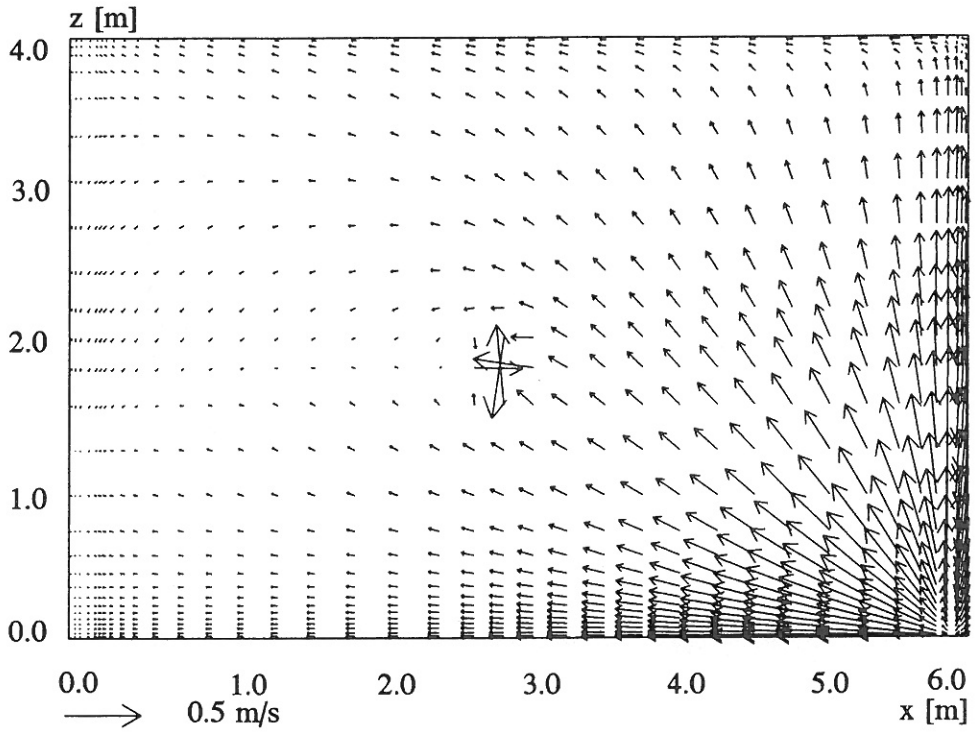

Figure 7.3 UW-vectorplot at the ceiling (y=3.98m).

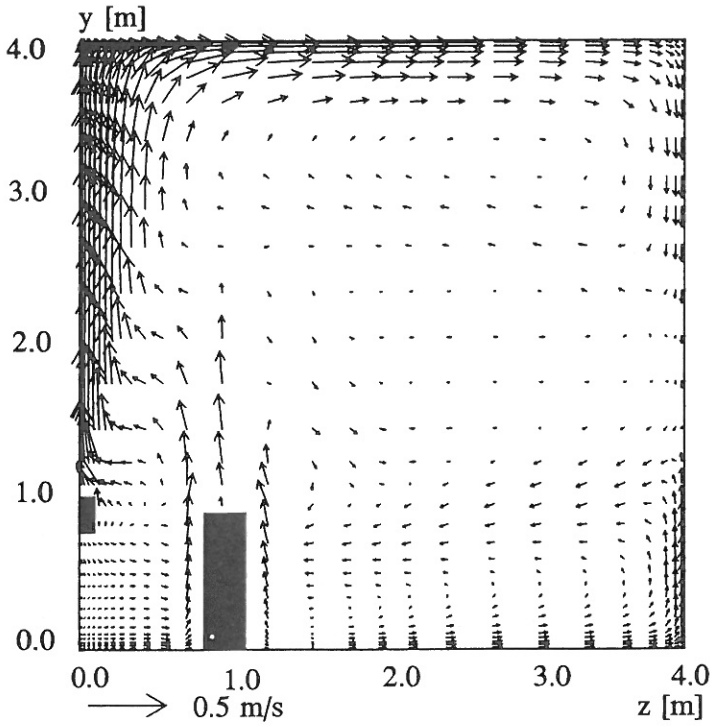

Figure 7.4 VW-vectorplot in plane with heat sources (x=5.54m).

movement clearly prevails implying stratified conditions. The buoyancy forces acting on the supplied air causes spreading in a thin layer across the floor and the characteristic velocity profiles are observed. Note also the small recirculation zone at the base of the inlet device.

A pressure gradient is established by the vertical contraction of the cool air and causes an approximately radial horizontal spreading - comparable to pouring e.g. water on the floor. This is clearly illustrated in fig. 7.2 where the inlet air impinges the floor in a short distance from the inlet device and a separation occurs. The large heat source which is standing at the floor is seen to the right.

The thermal plume rising above the small heat source is deflected as it reaches the ceiling and spreads horizontally similar to the cool air along the floor. It is demonstrated by fig.7.3 which also shows the swirling air motion close to the exhaust opening. The exhaust is only affecting a limited region close to the opening and not the flow in general.

Fig.7.4 shows the calculated flow around the heat sources. The thermal plumes generated by the two types of heat sources are evidently different. The main differences between the plumes are attributed to the differences in surface area and convective heat transfer to the surrounding air but they are also influenced by the grid size of the adjacent cells. The effect transferred per unit area is approximately 16 times larger for the small heat source than the large heat source, approximately 800 W/m^2 and 50 W/m^2, respectively. The plume above the small heat source transports the heated air volume to the ceiling where it is spread in a thin layer. The ascending air above the large heat source, on the other hand, reaches only 1.0-2.0 m upwards before it disintegrates. Rather crude assumptions have been made regarding the description of heat sources in the numerical model but the agreement with the visualization by smoke discussed in chapter 2 is fairly good.

From fig.7.5 it is seen that considerable temperature gradients appear close to the inlet device and heat source. Due to shear stress the supplied cool air volume mixes with the warmer surrounding room air and the temperature gradient is diminished. The dense air current is not only heated by entrainment of room air from above but also by heat flux from the floor and the temperature difference to the surrounding room air nearly vanishes. Except from the area close to the inlet device and the heat source the temperature difference in the full height of the room is less than 3°C.

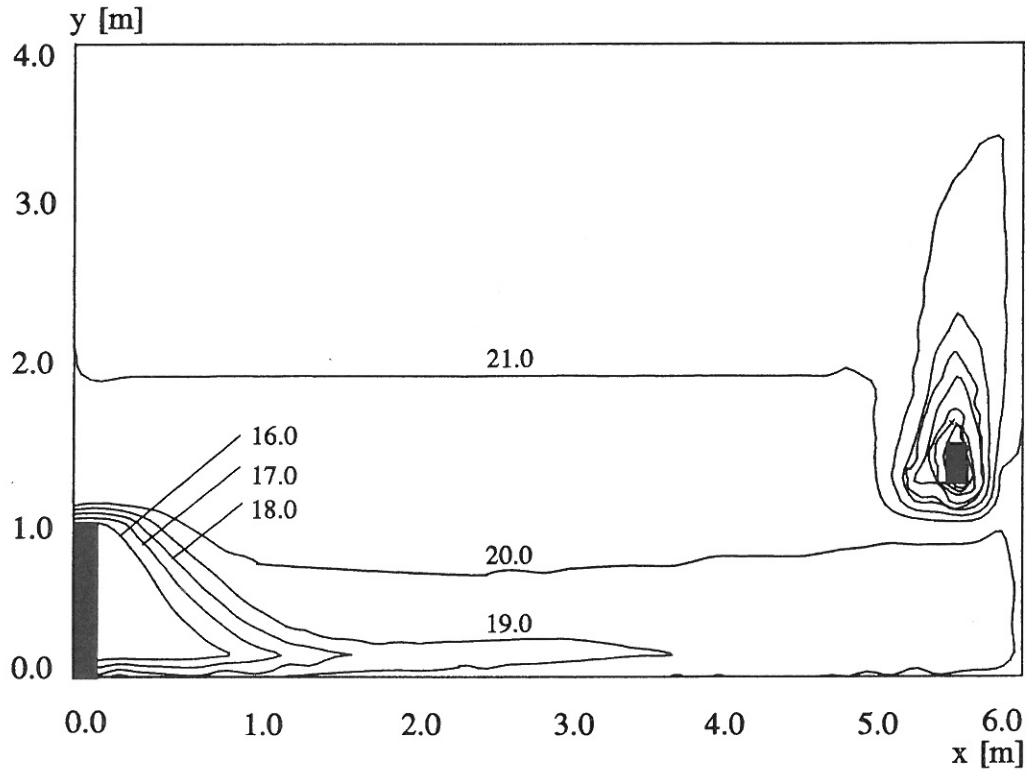

Figure 7.5 Isocurves for temperature in symmetry plane (z=0.0).

The overall patterns of the flow domain provided by the CFD-model are plausible and give valuable information about air and temperature distribution. Such apparently reasonable results are, however, obtained for a variety of boundary conditions and it is necessary to make a more detailed inspection in order to detect any discrepancies with the experimental data and to identify which factors are decisive to the results.

7.2 The effect of boundary conditions on the vertical temperature distribution

Large efforts have been done in order to improve turbulence models from the viewpoint that the inherent shortcomings which have been recognized are mainly responsible for the discrepancies encountered in application of CFD. The basic models for turbulent fluid flow are indeed only approximative but for practical applications the restrictions with respect to computational grid and limited information of boundary conditions may

be the main reason for the difference between model results and the experimental reality.

The vertical temperature gradient has a large influence on the flow field in the room in general and on the development of the flow along the floor in particular. The floor surface is heated by radiation from walls and ceiling and to less extent by conduction through the insulated floor. The layer of air adjacent to the surface is heated and the air temperature gradient across the height of the room is reduced. Approaches to include the redistribution of heat by applying different boundary conditions for temperature and radiation are discussed in the preceding chapter.

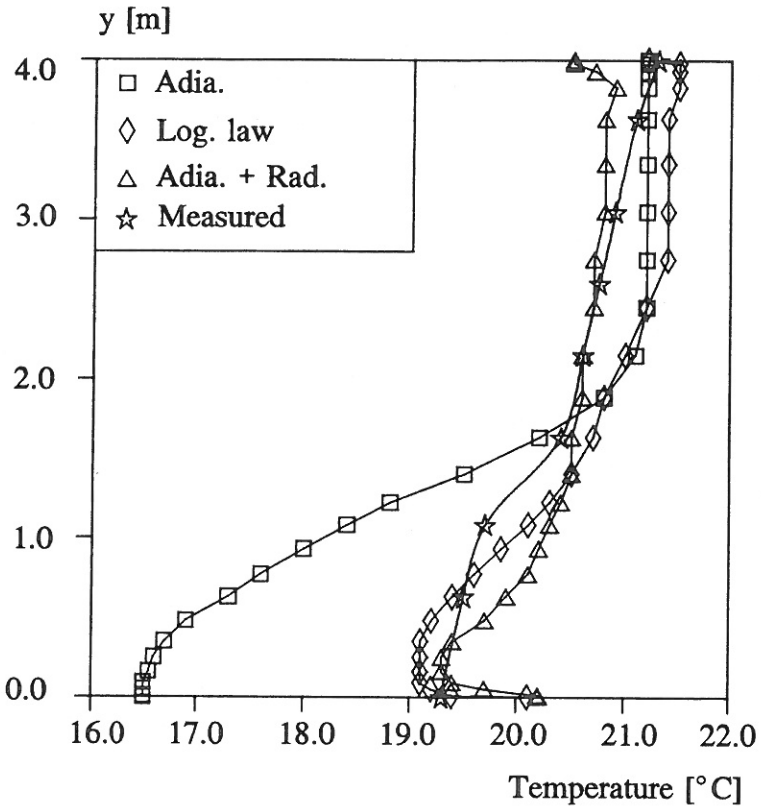

Figure 7.6 Vertical temperature profiles at (x,z)=(4.5 m,3.0 m).

The effect on the temperature field of adopting different strategies for describing temperature boundaries is illustrated by fig.7.6 and fig.7.7. They show measured and simulated vertical temperature profiles at a location where direct influence of heat sources and inlet device is avoided. The results obtained by applying three different boundary conditions for temperature are compared with measurements. The three versions are - adiabatic walls, logarithmic wall law in combination with prescribed

surface temperatures and an adiabatic wall assumption linked together with the DTM radiation model.

The adiabatic wall boundary is by far the easiest to implement but the agreement with measurements is very poor. The dense air current is only heated by the small amount of heat which is supplied by entrainment from the surrounding air resulting in too low temperature in the lower part of the room. The temperature differences are not leveled out and the profile becomes distinctly non-linear. Omission of the effect of radiation clearly leads to erroneous solutions.

The profiles obtained by applying logarithmic wall functions or the combination of adiabatic walls and the DTM radiation model exhibit a much higher degree of accordance with the experimental data. The standard of reference in terms of measured temperatures is limited but anyhow a reasonable agreement is achieved with respect to the temperature level while some deviation is found when comparing the exact profile shapes.

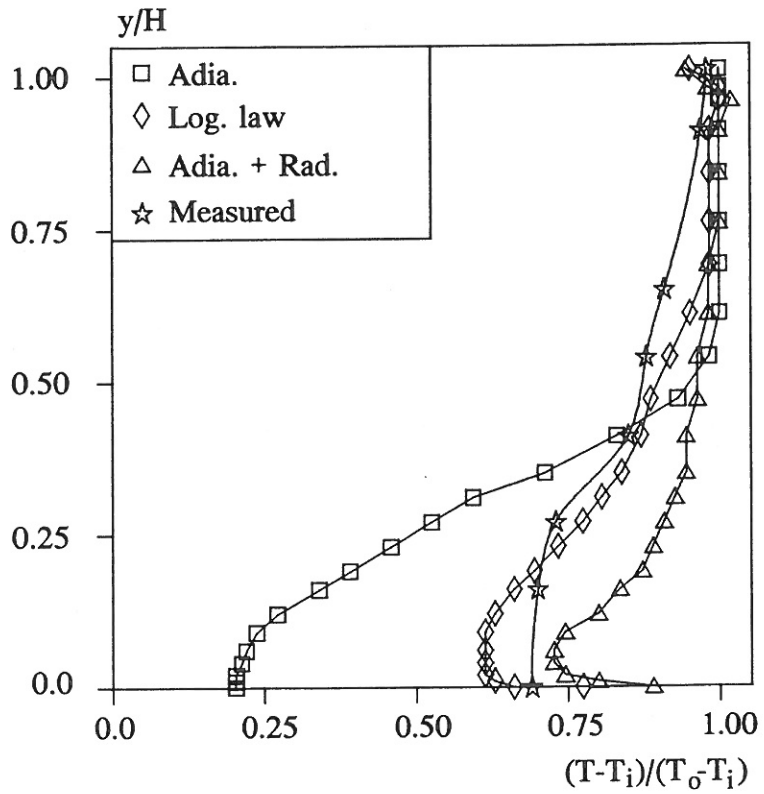

Figure 7.7 Non-dimensionalized temperature profiles at (x,z)=(4.5m,3.0m).

The temperature of the air adjacent to the floor increases due to heating by the floor. A considerable part of the 'cooling capacity', in terms of the temperature difference between outlet and inlet air, is 'spent' at the floor level. *Skistad 1989* applies a general 50 % rule (eq.(2.2)) implying that the temperature close to the floor equals the inlet temperature plus half the temperature difference between exhaust and inlet. In this case a value close to 70 % is more appropriate as it appears from the measurements and fig.7.7.

In the light of the temperature profiles obtained by different boundary conditions it is concluded that the simple approach of adiabatic walls yields incorrect temperature distribution implicating a false flow field. Satisfactory results with respect to temperature distribution is obtained provided radiation is accounted for - either indirectly by prescribing temperature at the room surfaces and calculating convective heat transfer coefficients or directly by adding a self-contained radiation model. Simplifications and adjustments are often required in consideration of the limitations on experimental information. It is important to point out that the computed heat transfer at the surfaces is sensitive to the emission coefficients in the radiation model, and to the convective heat transfer coefficients when the logarithmic wall law is applied. In the following section the problems associated with the use of wall functions are demonstrated.

7.3 Wall functions and heat transfer at walls

The heat fluxes at walls, ceiling and not least the floor are determined by the temperature difference between the near wall air and the surface and the convective heat transfer coefficients calculated from the wall functions. In chapter 6 the general shortcomings of the traditional wall functions (*Launder and Spalding 1974*) are described and it is pointed out that especially the grid dependency constitutes an unsolved problem.

The topic of this section is how the wall functions should be dealt with to achieve satisfactory estimates of convective heat transfer in the present case. The conditions are quite different at the vertical walls with natural convection and the horizontal floor with forced convection. The convective heat transfer coefficients, α_w, are typically in the range 2.0-4.0 W/m^{2}k for the walls while values in the range 3.0-6.0 W/m^{2}k are expected at the floor. The investigation of the traditional wall functions and the alternatives mentioned in chapter 6 has been confined to the floor surface because this

strongly affects the general temperature distribution and the development of the stratified flow along the floor.

Fig.7.8 shows the total heat supplied from the floor to the room air. Increasing the distance from the surface to the first grid node causes a decrease in the heat supplied from the floor to the room air for all investigated versions of wall functions. The heat flux calculated by the different wall functions seems to converge with decreasing distance between the wall and the first gridnode, y_p, while differences up to more than 20 % is found for relatively large y_p-values. The improved wall functions by *Yuan et. al. 1992* and *Chen 1988* increase the total heat transfer compared to the traditional version by *Launder et. al. 1974* and they are less dependent on near wall grid resolution. The problem ,however, is not eliminated and care should be taken with these versions as well. It may simply seem to be a question of adjusting the grid to obtain the desired heat transfer according to fig.(7.8) but values of the dimensionless wall distance, y^+, must be sufficiently large at the same time to ensure that the first grid node is situated ouside the viscous layer. Otherwise the increment in heat transfer only reflects the increment in temperature gradient appearing in the Fourier equation for heat transfer in stagnant air.

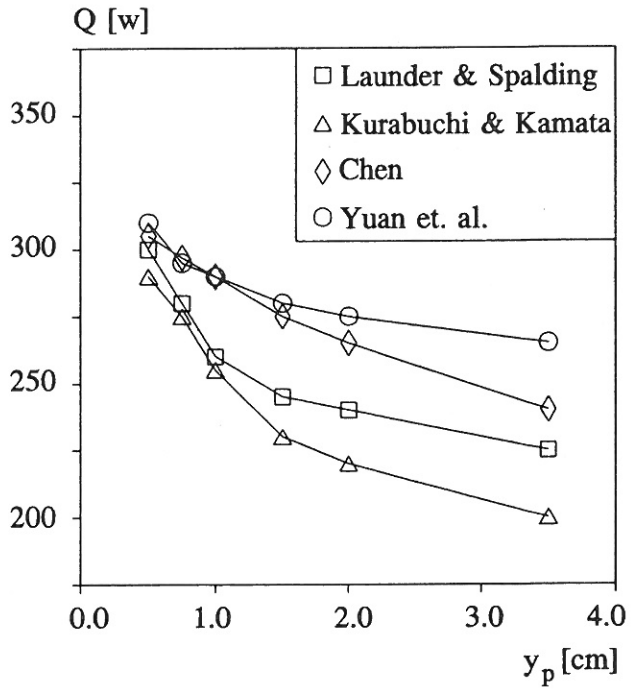

Figure 7.8 Total heat transfer from the floor versus distance to the first grid node.

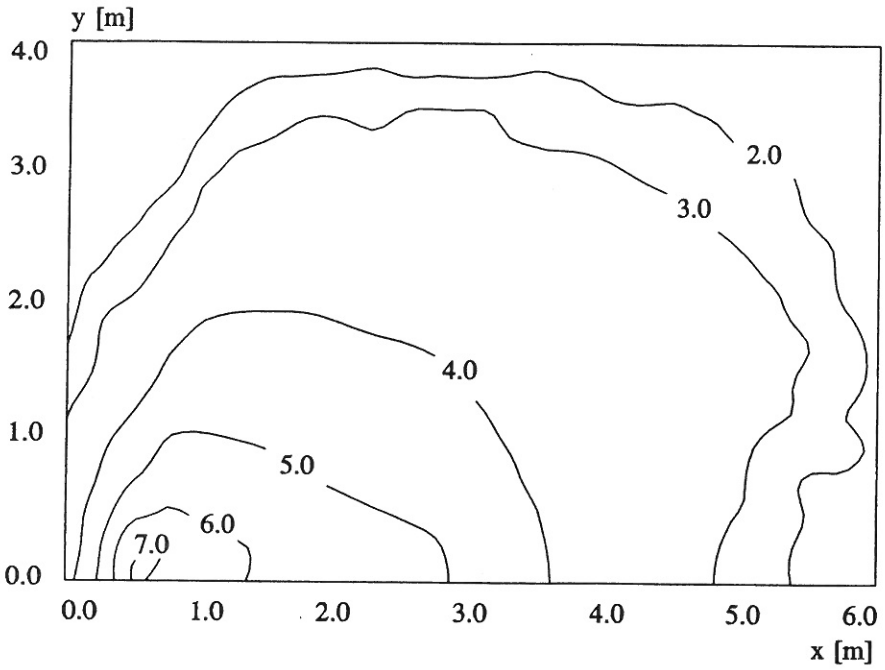

Figure 7.9 Convective heat transfer coefficients (W/m^2K) at the floor calculated by the wallfunctions of *Launder & Spalding 1974* (y_p=0.5cm).

Fig.7.9 is an iso-curve plot for α_w at the floor. The distribution of α_w is closely related to the air velocities along the floor - see fig.7.2. The values are slightly larger than expected close to the inlet device and slightly lower close to the walls. At the walls α_w is in the range 1.5-3.0 W/m^2k and at the ceiling 1.5-5.0 W/m^2k. All the tested cases show that heat is transferred from the air to the ceiling while the net heat transfer at the walls is close to zero. The heat loss at the upper part of the walls is approximately counterbalanced by the heat gain at the lower part of the room.

7.4 Damping functions

Damping functions for the suppression of turbulence by thermal stratification, f_b, and low-Reynolds number effects, f_{Rt}, are presented in chapter 4. The f_b-damping function serves to reduce the turbulent viscosity in areas where destruction of turbulent kinetic energy due to buoyancy takes place. This means that the reduction of turbulent mixing in areas with positive temperature gradients is intensified. The f_{Rt}-damping function reduces the turbulent viscosity in areas with low turbulent Reynolds numbers. In the stagnant areas with low air velocities the flow becomes laminar.

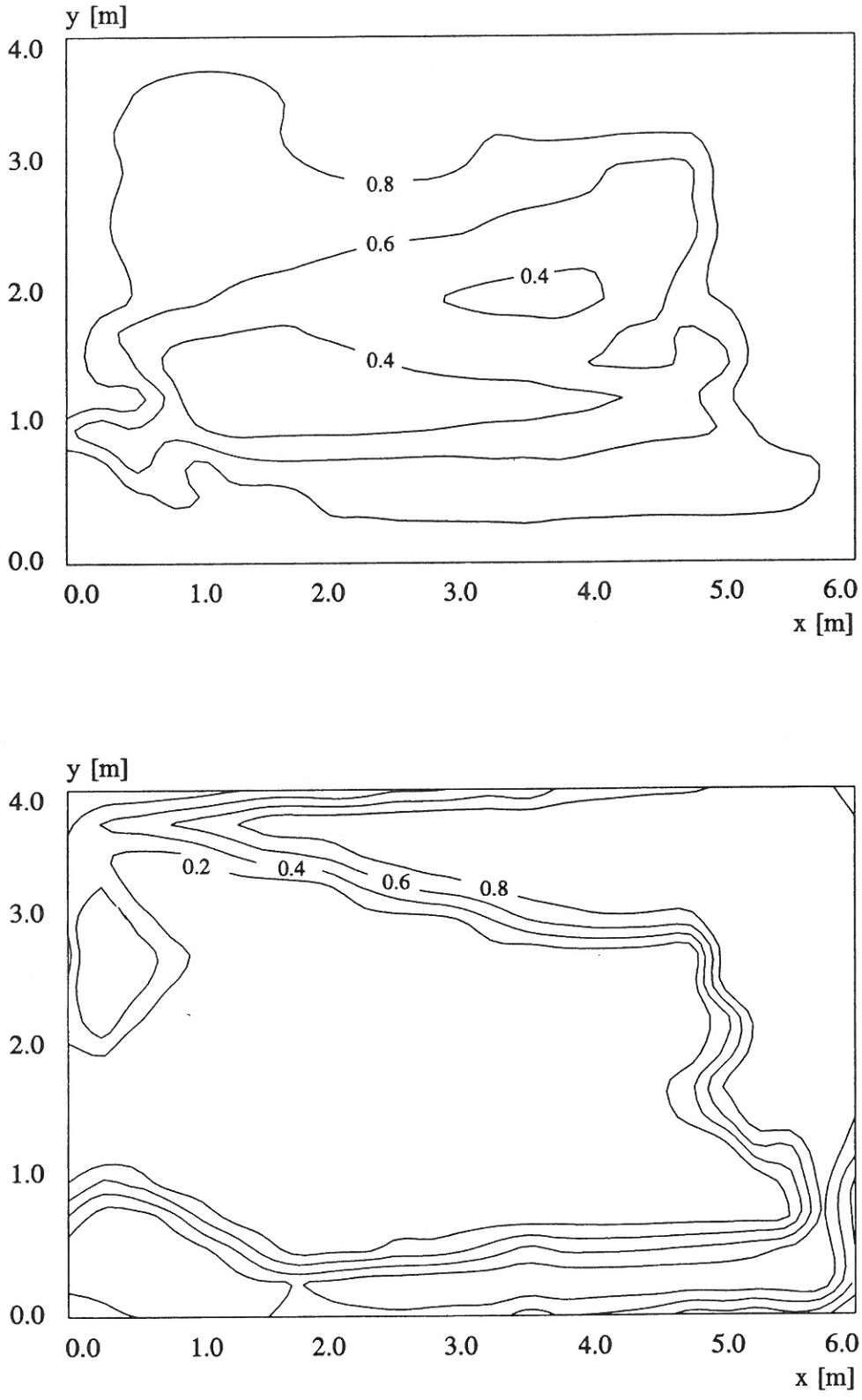

Figure 7.10 Values of f_b (upper) and f_{Rt} (lower) in the plane of symmetry (z=0.0 m).

Fig.7.10 shows where the respective dampingfunctions are active. The value 1.0 corresponds to no influence on the flow field and the value 0.0 corresponds to complete relaminarisation at the location concerned. The areas of the flow domain with the smallest values of the two types of damping functions coincide. The effect of f_b and f_{Rt} concur in the large stagnant air volume where laminar conditions subsequently prevail. The distribution of f_{Rt} agrees with the UV-vectorplot of fig.7.1. The strong effect of f_b is due to positive temperature gradients and small values of dissipation.

The damping functions are not directly affecting the flow field and they should be evaluated by the influence they exert on the turbulent viscosity. The velocity and temperature distribution in front of the inlet device depends on the turbulent mixing at the shear layer between injected air and surrounding room air. Consequently the reduction in turbulent viscosity by the damping functions in this region has been considered in fig.7.11.

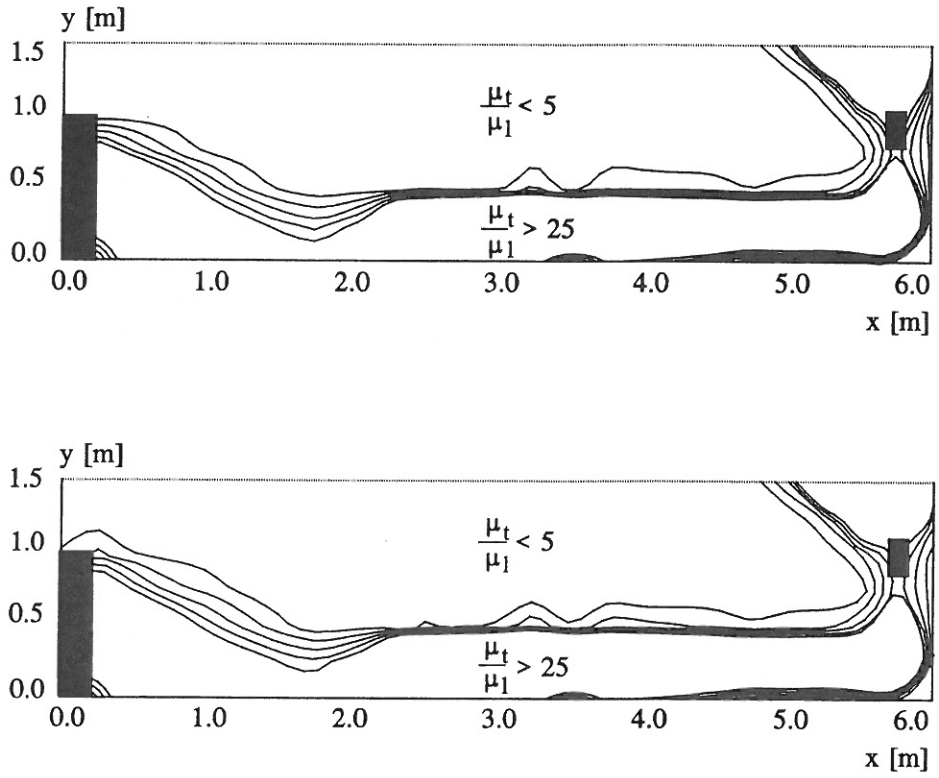

Figure 7.11 Isocurve plot of ratio between turbulent and laminar viscosity in the lower part of the room, z=0.0 - with damping functions (upper) and without (lower).

The change in turbulent viscosity by applying damping functions is not significant. The effect is confined to the stagnant zone and the high velocity regions at the inlet device and the heat source are left nearly unaffected. Comparisons between temperature and velocity data indicate accordingly that the damping functions only play a role in regions of the flow which are not of primary interest.

The results substantiate that large parts of the room air volume is approximately laminar and some model modifications are needed. This does however not imply that these modifications lead to considerable changes in computed velocities and temperatures in general. The benefit of using damping functions is thus negligible in this context and they are consequently left out in the model predictions presented in the proceeding sections.

7.5 Inlet boundary and maximum velocities

In the assessment of draught risk in a displacement ventilated room attention is usually focused on the region in front of the inlet device where the combination of low temperatures and high velocities causes comfort problems to occupants. It is important to predict the proportion of the floor area which is not suited for occupancy and take precautions in order to reduce it if necessary.

The development of the flow downstream of the inlet device is mainly determined by the inlet conditions and the vertical temperature gradient. The flow along the floor is decisive to the amount of heat transferred to the room air by convection and thus the vertical temperature profile. This coupling between velocity and temperature field stresses the importance of specifying appropriate inlet boundary conditions in the numerical model.

The geometry of the inlet device results in a very complex distribution of pressure, velocities, temperature and turbulent quantities in the air entering the room. The length scales of the perforations of the inlet surface compared to the length scales of the room makes it impossible to apply the sufficient resolution in space neither with respect to measurements nor with respect to computational grid in the numerical model. Simplifications are required and the purpose of this section is to investigate the correlation between values of maximum velocities calculated along the floor and description of the inlet boundary.

Velocity distribution and direction of the inlet velocity vector is treated coherently and thereupon the effect of k and ϵ at the inlet is adressed. Four combinations of velocity distribution and inlet velocity vector angle has been chosen in order to investigate the influence on the downstream velocity level along the floor. The test cases are presented in tab.7.1.

Case	Velocity distrib.	Angle of velocity vector
A	Uniform	0
B	Measured	0
C	Uniform	$-\pi/4$
D	Measured	$-\pi/4$

Table 7.1 Specification of test cases A-D.

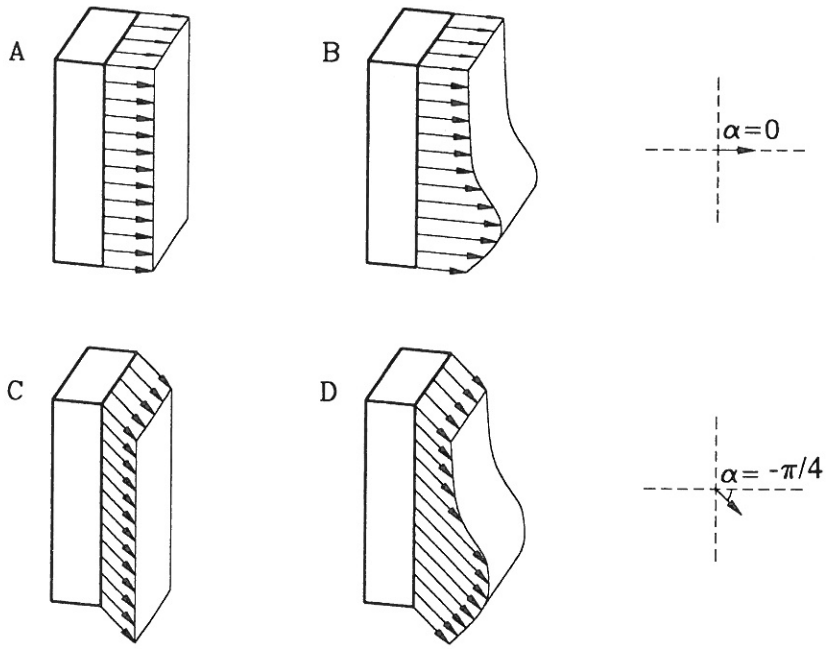

Figure 7.12 Illustration of test cases A-D.

Fig.7.13 shows the maximum velocity versus distance from the inlet device. The velocities are derived in the symmetry plane in the vertical distance 0-10 cm above the floor. The inlet air is accelerated and the highest velocity is found approximately 1.0 m from the inlet device. The maximum velocities then decay and deceleration occors close to the wall.

The highest predicted velocity is significantly lower than the measured value for all the cases A-D. If no information about the inlet velocity distribution is available a uniform 'box-profile' is usually assumed but fig.7.13 shows that this yields the poorest agreement with measurements. A considerable improvement is achieved by specifying an inlet velocity distribution similar to the measured and further improvement is obtained when the angle of the velocity vector is directed downwards. The example serves to illustrate the importance of adopting a correct description of the inlet boundary. The simplified and to some extent arbitrary test cases are ,however, not of universal validity and can not replace qualified measurements.

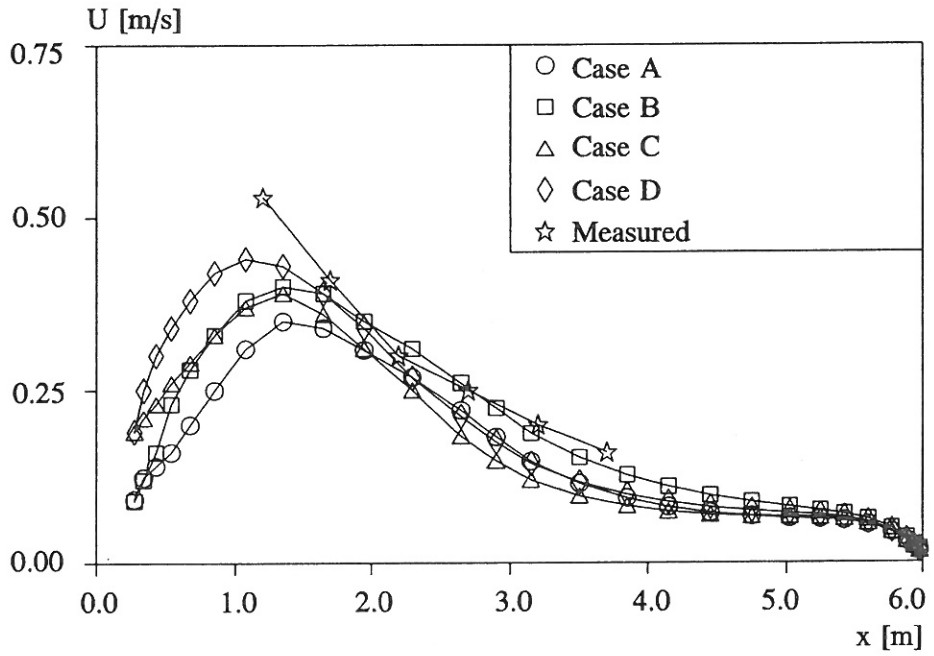

Figure 7.13 Maximum velocities in symmetry plane for the cases A-D.

The testcases E-H are chosen to study the effect of different levels of turbulent quantities in the supplied air on the maximum velocities. Two different levels of turbulence intensity, 5% and 10%, has been selected together with two turbulent length

scales, l, namely 0.02 m and 0.10 m as it appears from tab.7.2. The influence of inlet values of k and ϵ has been treated with a velocity distribution corresponding to case B.

Case	I [%]	k [m^2/s^2]	ϵ [m^2/s^3]	l [m]	μ_t/μ_l
E	5	$1.1\ 10^{-4}$	$6.0\ 10^{-5}$	0.02	1.3
F	10	$4.5\ 10^{-4}$	$4.8\ 10^{-4}$	0.02	2.5
G	5	$1.1\ 10^{-4}$	$1.2\ 10^{-5}$	0.10	6.0
H	10	$4.5\ 10^{-4}$	$9.5\ 10^{-5}$	0.10	12.8

Table 7.2 Specification of test cases E-H.

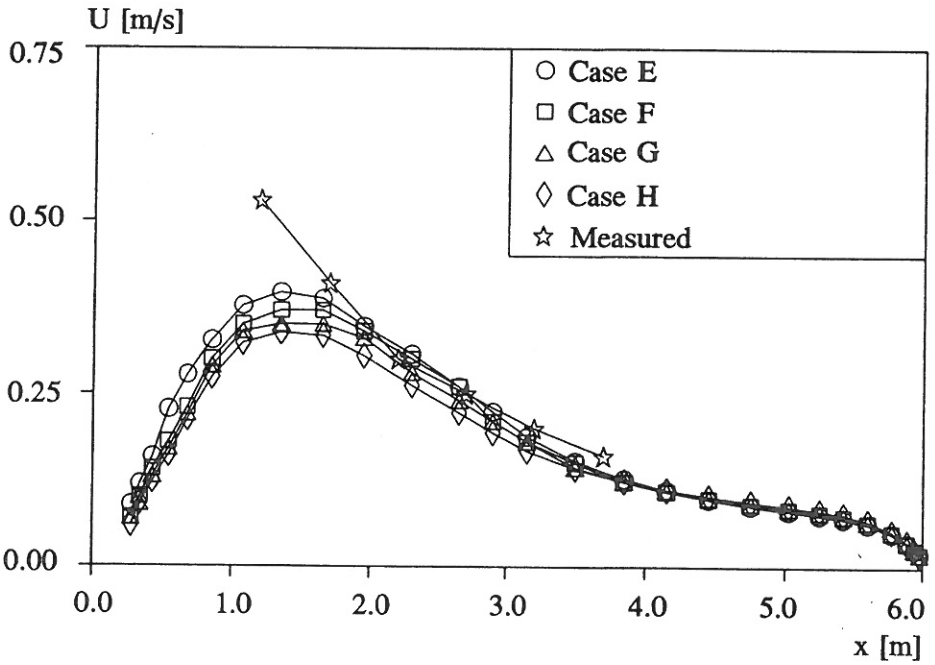

Figure 7.14 Maximum velocities in the symmetry plane for the cases E-H.

Again the measured peak velocity is higher than the simulated for all cases. It is not possible to identify the turbulent length scale as the key-parameter but the magnitude of the turbulent viscosity seems to affect the level of predicted maximum velocities in general and the peak velocities in particular. The best agreement with measurements is

found in case B where the supplied air is nearly laminar. The results indicate that the values of k and ϵ should be considered when dealing with this type of flow.

7.6 Velocity and temperature profiles in front of the inlet device

The maximum velocities along the floor are essential in the assessment of comfort conditions but in order to evaluate the capability of the numerical model to simulate the propagation of the dense air current it is necessary to consider the vertical distribution of velocities and temperature in the full height of the layer.

Fig.7.15 shows velocity profiles along the centre line of the inlet device. The peak velocity is underestimated close to the inlet device and the predicted velocities are slightly lower than the measured values in general. The modelled and measured profiles are similar in shape and the deviation is reduced with distance from the inlet.

Velocity and temperature fields are strongly correlated and the velocity profiles should be evaluated in connection with the temperature profiles in fig.7.16. The temperatures obtained by the numerical model are lower than the measurements - the differences are, however, less than 1.0 °C. Also for the temperatures the largest discrepancy is found close to the inlet device.

Fig.7.17 and fig.7.18 show temperature and velocity profiles for various streamline angles. The best agreement is found for streamlines close to the centre line, $\Theta = \pi/2$.

To sum up the information contained in fig.7.15-7.18 the vertical contraction of the cool injected air is not sufficiently strong in the model presumably due to underestimation of the temperature gradient close to the inlet device and the simplified description of the inlet boundary. The predicted maximum velocity close to the inlet device is consequently too low compared to measurements.

The measurements showed that the inlet device is capable of spreading the supply air in a radial pattern like a semicircular inlet device. This important feature is only partially captured by the CFD-model. The insufficient horizontal spreading is not only caused by the crude description of the inlet boundary and the underestimation of the vertical temperature gradient. The overestimation of turbulent kinetic energy, and thus turbulent viscosity, in the area where the supplied air impinges the floor also tends to reduce the air flow in the direction perpendicular to the inlet flow direction.

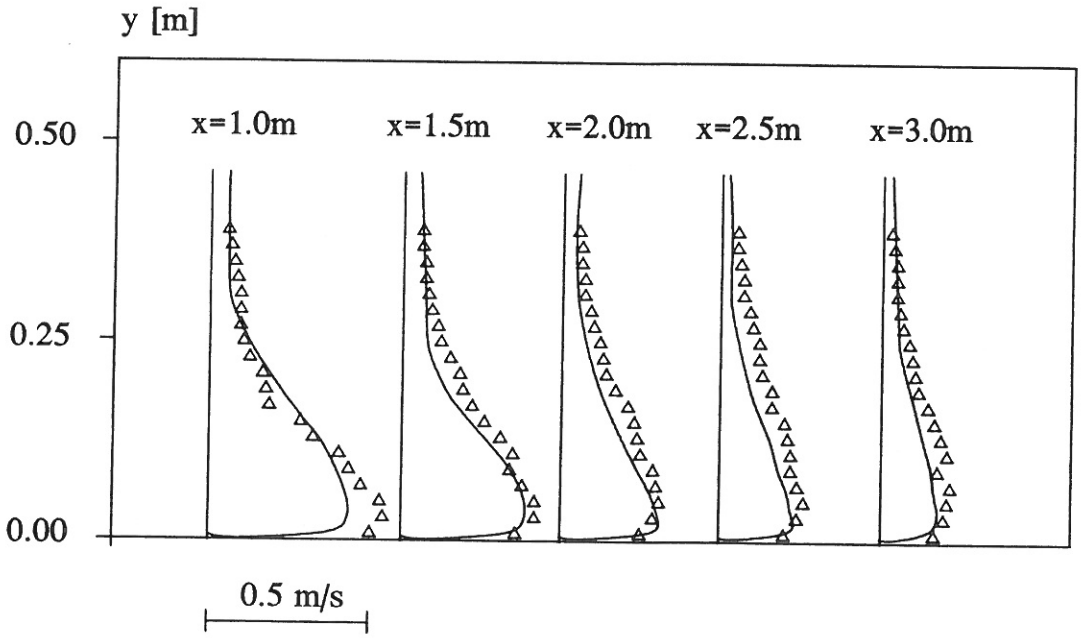

Figure 7.15 Velocity profiles in the symmetry plane (z=0.0m).

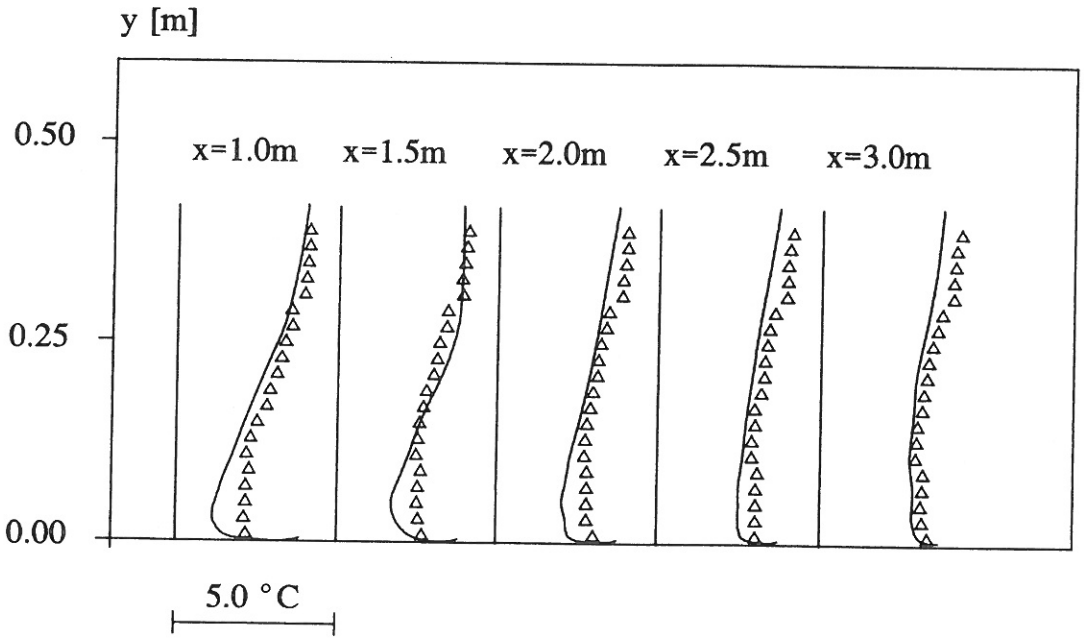

Figure 7.16 Temperature profiles in the symmetry plane (z=0.0 m) - the inlet temperature has been subtracted.

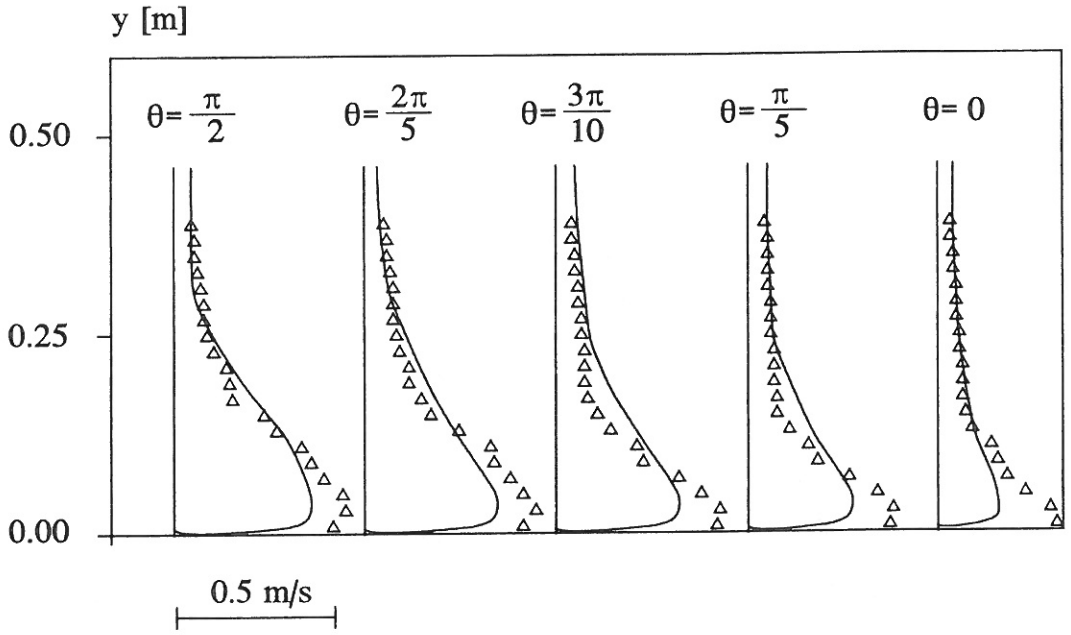

Figure 7.17 Velocity profiles within a radius of 1.0m from the inlet device.

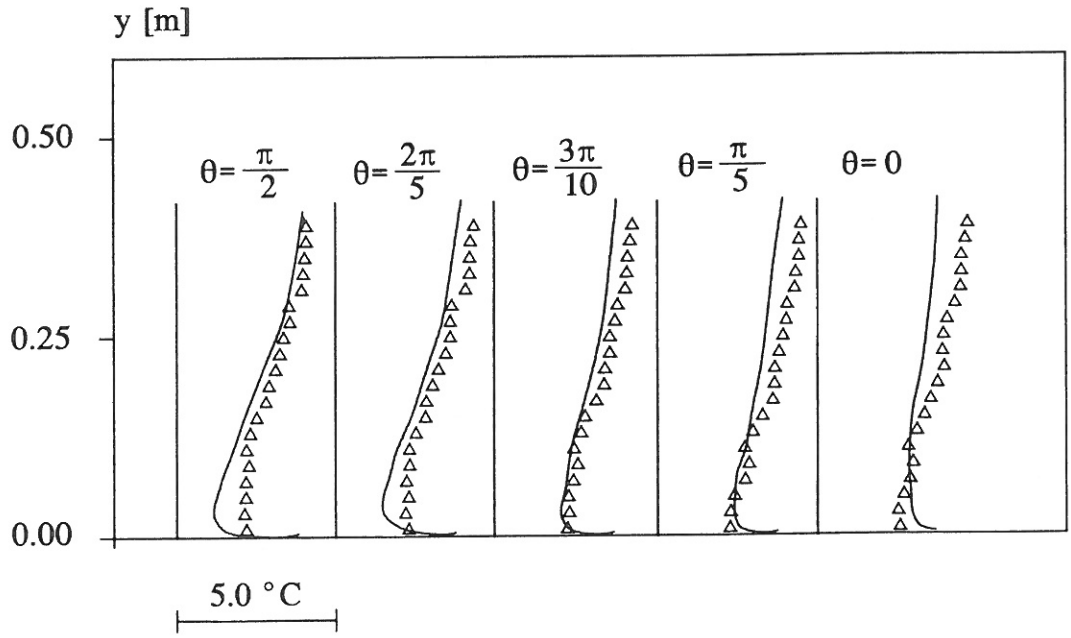

Figure 7.18 Temperature profiles within a radius of 1.0m from the inlet device - the inlet temperature has been subtracted.

7.7 Velocity decay and Archimedes number

The effect of Archimedes number on the predicted flow field remains to be treated. To test if the results obtained by the CFD-model comply with the basic correlations between velocities and Archimedes number a series of programme runs has been carried out with the model version containing the radiation model. A wide range of Archimedes numbers has been used to investigate if it is possible to identify a region in front of the inlet device where eq.(3.3) is valid i.e. where the relative maximum velocities decay proportionally to the reciprocal distance to the inlet device.

Fig.7.19 shows the maximum velocities in the centre line of the inlet device for different Archimedes numbers. The dashed lines with the slope -1 has been added to indicate where agreement between predictions and eq.(3.3) is obtained. For large Archimedes numbers the characteristic stratified flow along the floor is established in a relatively short distance from the inlet device and it is maintained until the opposite wall decelerates it. For decreasing Arkimedes numbers the range is reduced to r=2.0-5.0 m. The constant K in eq.(3.3) ranges from 7.5-11.3 in the cases presented in fig.7.19 and they are slightly larger that the values found for the measured data.

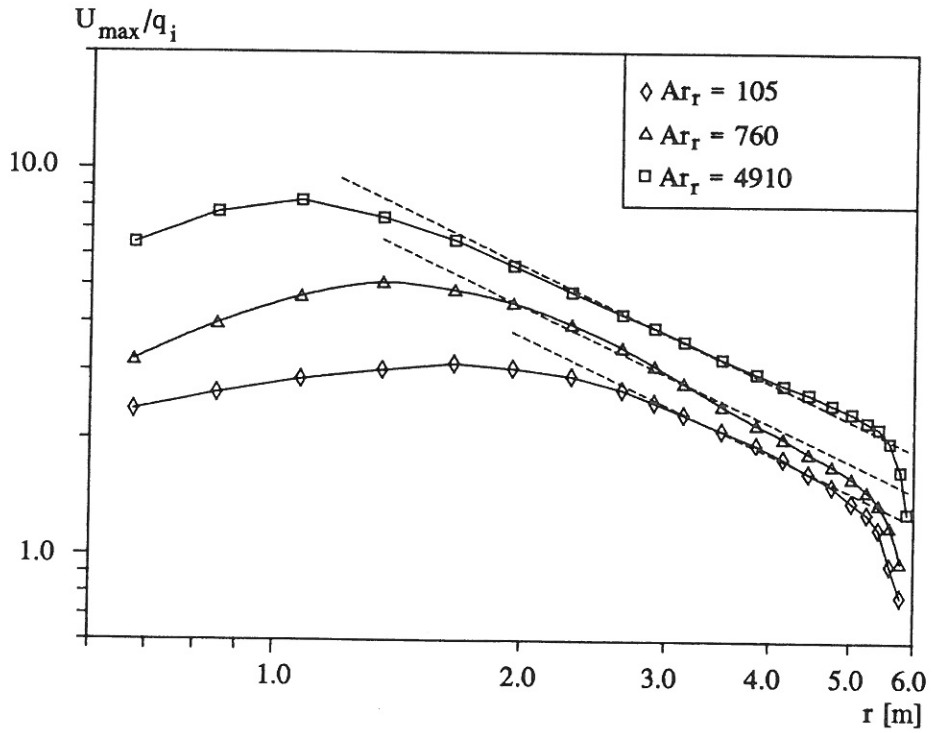

Figure 7.19 Predicted maximum velocities along the floor for different Arkimedes numbers.

Based on an equation for momentum conservation at the inlet device *Mathisen 1989* deduces the following relation

$$\frac{U_{max}}{U_i} = k_1 + k_2\sqrt{Ar} \tag{7.1}$$

The maximum velocity in front of the inlet device is a function of the squareroot of the Archimedes number where k_1 and k_2 are constants. Concerning eq.(3.3) it is implied by eq.(7.1) that

$$K(\theta,Ar_r) \sim k_1 + k_2\sqrt{Ar_r} \tag{7.2}$$

Fig.7.20 shows the K-values found by the curves for maximum velocities for different Archimedes numbers. Despite few K-values a linear increment with the squareroot of the reduced Arkimedes number is clearly seen. This supports that the maximum velocities along the floor predicted by the CFD-model agree with the theory in eq.(7.2) for a wide range of Archimedes numbers. To evaluate the exact velocity distribution supplementary measurements should be carried out.

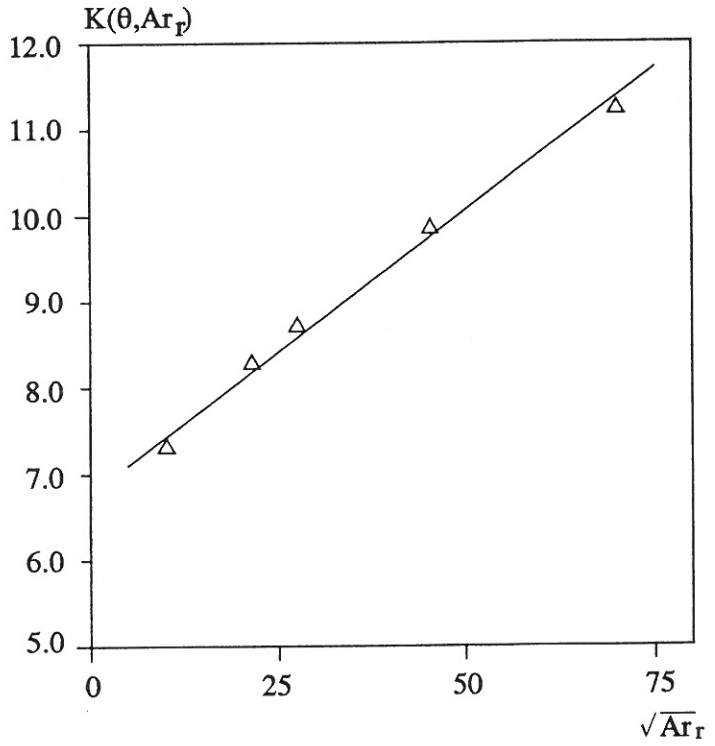

Figure 7.20 K-values versus the squareroot of reduced Arkimedes number.

7.8 Discussion

To make a final evaluation of the CFD-model the results presented in section 7.1-7.7 should be summed up.

The results obtained by the numerical model are satisfactory with respect to the overall features of the flow. The velocity and temperature distribution are in general in agreement with a qualitative assesment based on visual observations and descriptions found in various publications on the subject.

When attention is focused on the quantitative assesment of prediction accuracy in front of the inlet device a considerable sensitivity to different descriptions of boundary conditions is found. Calculation of heat flux at the walls and specification of the inlet boundary have a pronounced effect on the velocity and temperature fields and subsequently require special attention. Some of the boundary conditions applied in this work yield reasonable results and similar methods can be adopted in practical applications.

The modification of the turbulence model by damping functions exerts only minor influence on the interior flow domain and the effect on the velocities and temperatures close to the floor is negligible. Uncertainties attributed to limited experimental information and the coarseness of the computational grid involved in the description of boundary conditions override the importance of damping functions in the investigated cases.

The predicted velocity and temperature profiles in the dense air current along the floor deviate from the measured profiles. The discrepancy is substantial in the directions perpendicular to the inlet direction while a fair agreement is obtained along the centre line of the inlet device. The predicted velocities and temperatures are underestimated in general.

Considering the restrictions on grid refinement, the limitations of the turbulence model and the simplified specification of boundary conditions, the results are acceptable - and promising. Provided the description of boundary conditions is improved to achieve a broader range of validity, it can be concluded that the CFD-approach is a qualified tool for general as well as detailed investigations of the airflow and temperature distribution in rooms with displacement ventilation.

Chapter 8

Conclusion

The purpose of this study is to investigate air flow and temperature distribution in a room with displacement ventilation by means of full-scale measurements, semi-analytical models and a CFD-model. This section recapitulates the findings in the previous chapters and summarizes the main points.

The motivation to this work is found in the survey of the rather few investigations which has been carried out in rooms ventilated by the displacement principle. The limited existing knowledge concerning air flow in displacement ventilated room is a strong incentive to carry out full-scale measurements and at the same time analyze the flow field to enable an evaluation of different model approaches.

Based on visualization of the flow field by smoke, a line of procedure for the measurements has been determined. Detailed measurements of velocity and temperature profiles in front of the inlet device show that a distinct stratified flow is established close to the floor in less than 1.0 m from the inlet device. Furthermore, the measured data reveal that the temperature profiles at the walls are approximately linear which is not the case for the room air temperature profile. Finally, measured profiles of speed close to the inlet device exhibit large variations and indicate that the buoyancy forces and the initial entrainment are capable of transforming the velocity distribution in only a few centimeters from the inlet surface. It is difficult to obtain reliable measurements in this region due to the complexity of the flow field.

Based on the measured temperatures and velocities in the dense layer close to the floor an analysis is carried out which aims to investigate whether semi-analytical expressions deduced for 3-D jets can be modified to apply for the stratified flow in front of the inlet device.

Different proposals for calculating the velocity decay with distance from the inlet device are described, and the model of *Nielsen 1992* agrees very well with the measurements - not only for the center line of the inlet device, for which it was originally intended, but also for other streamline directions.

To account, not only for the maximum velocities, but for the complete vertical distribution of velocity and temperature an expression for a wall jet by *Verhoff 1963* was introduced. The velocity distribution is approximated very well by this expression. By introducing a correlation between the velocity and the temperature distribution it is investigated whether the temperature profile could be predicted as well. The measured data, however, indicate that this simplified correlation is not valid for the entire flow region along the floor.

Finally, an aspect of the stratified flow, which is believed to be crucial to the understanding of the flow mechanics, is treated. The measurements strongly imply that a supercritical and subcritical flow domain exist - separated by a 'density jump'. A more advanced description of the air current should thus recognize this important feature.

A second main effort is made with respect to the development and application of a CFD-model.

The theory for air flow and heat transfer including the k-ϵ turbulence model is briefly introduced and the governing equations are presented. The capabilities and limitations of the standard k-ϵ model applied to the buoyancy affected flow in a room with displacement ventilation are discussed and modifications in terms of damping functions are treated. The assumption of isotropic turbulence inherent in the eddy viscosity concept is identified as a significant shortcoming but the prospect of applying more advanced models is obstructed by the serious problems of numerical instability and increased demand for computing capacity. It is concluded that the k-ϵ model constitutes a suitable compromise.

The numerical procedure for solving the governing equations is covered extensively by a number of authors and is not described in detail in this report. Attention is focused on elements of the numerical method which influence the prediction accuracy and performance of the CFD-model. Difficulties are often encountered concerning convergence of the calculations. A number of factors influences the models ability to obtain a fully converged velocity and temperature field. They are discussed in relation to the specific type of flow and recommendations are presented.

The boundary conditions are important in flow simulations in rooms in general and in rooms with displacement ventilation in particular. The general problems associated with the specification of boundary conditions in the numerical model are discussed, but the role of radiation with respect to the boundary conditions for the temperature equation

and the necessary simplifications in the description of the inlet boundary, are the subjects of further investigations.

Three different types of temperature boundary conditions are presented. An adiabatic wall boundary disregarding radiation, a logarithmic wall law type estimating convective heat transfer coefficients and employing prescribed wall temperatures to implicitly account for radiation and finally a model version combining adiabatic walls with a self-contained radiation model. The applied Discrete Transfer radiation model is verified by comparison with the results obtained by the Monte Carlo method and extended logarithmic wall expressions - developed to remedy shortcomings of the traditional ones - are mentioned.

The predicted vertical temperature profiles obtained with the simple adiabatic wall boundary condition shows - as could be expected - considerable deviation from the measured ones. The remaining two approaches yield reasonable accordance between predicted and measured temperature profiles and are thus concluded to be applicable for modelling a displacement ventilated room.

The effect of specifying the inlet boundary in different ways is investigated. A uniform velocity distribution normal to the inlet surface is usually assumed due to the lack of experimental information. The velocity distribution is in fact non-uniform and the velocity vector is actually directed downwards. To introduce a higher degree of realism in the description of the inlet device different approaches have been employed. A series of tests including velocity distribution, angle of the inlet velocity vector and specification of turbulent quantities in the supply air shows that these factors affect the velocity level close to the floor. A measured velocity distribution together with a downwards directed velocity vector and low levels of turbulence intensity results in the highest velocities and the best agreement with measurements. A further improvement in the description of the inlet boundary is needed and the general validity should be tested.

The results obtained by the CFD-model emphasizes the importance of boundary conditions and the improvements of the solution by modifying the turbulence model, in terms of damping functions for buoyancy effects and low-Reynolds number effects, are quite insignificant with respect to the interior room air flow.

A detailed evaluation of the prediction accuracy is possible in the region close to the floor. The comparison between simulated and measured velocity and temperature profiles shows that both variables are slightly underestimated in general by the CFD-model. The largest deviation is found close to the inlet device due to too small vertical

contraction and horizontal spreading of the supplied air. The maximum deviation is, however, less than 20% in all cases which is considered to be satisfactory regarding the simplified inlet boundary condition.

It is furthermore demonstrated that solutions can be obtained for a wide range of Archimedes numbers. The characteristic stratified flow is established for in all the test cases and the velocity decay complies with the fundamental theory describing the relationship between decay rates and Archimedes number.

The work has clearly demonstrated that the difficulties associated with the specification of boundary conditions is a major drawback of applying CFD for this type of ventilated rooms. It is a problem even in a controlled experimental environment and it probably accounts for the most considerable contribution to discrepancies when a 'real' displacement ventilated room is modelled. The agreement with respect to the overall flow pattern may unfortunately lead the engineer to disregard this fact and accept local values of flow variables which deviate substantially from the reality.

Further improvement of the CFD-method is desirable but at the current stage it is applicable for many purposes. In *Jacobsen and Nielsen 1992* an example is given of how comfort conditions can be determined by applying CFD-results and by simply adding a transport-diffusion equation for a passive gas it is possible to consider aspects of contaminant distribution and air quality.

CFD is a useful tool to supplement and in some cases substitute experimental investigations. Provided a critical evaluation of the model results is performed confidence can be put in the CFD-method for predictions of air flow and temperature distribution in a displacement ventilated room.

References

Awbi H.B.
Application of Computional Fluid Dynamics in Room Ventilation, Building and Environment, vol. 24, 1989.

Baker A.J., Kelso P.E
On Validation of Computional Fluid Dynamics Procedures for Room Air Motion Prediction, ASHRAE transact. part 1, 1990.

Baturin V.
Fundamentals of Industrial Ventilation, Pergamon Press 1972.

Bradshaw P.
Turbulence - Topics in Applied Physics, vol. 12, Springer Verlag, London 1976.

Chen Q.
Indoor Airflow, Air Quality and Energy Consumption of Buildings, Ph.D thesis, Technicsche Universiteit Delft, Delft 1988.

Chikamoto T., Murakami S., Kato S.
Numerical Simulation of Velocity and Temperature Fields within Atrium based on Modified k-ϵ model Incorporating Damping effect due to Thermal Stratification, Proc. of International Symposium on Room Air Convection and Ventilation Effectiveness, Tokyo 1992.

Dagestad S.
Numerical Simulation of Stratified Flows with Different k-ϵ Turbulence models, Ph.D.-thesis, Norges Tekniske Høgskole, Trondheim 1991.

Davidson L.
Numerical Simulation of Turbulent Flow in Ventilated Rooms, Ph.D.-thesis, Chalmers University of Technology, Göteborg 1989.

Gibson M.M., Launder B.E.
On the Calculation of Horizontal Turbulent, Free Shear Flows Under Gravitational Influence, Journal of Heat Transfer, 1976.

Gosman A.D., Lockwood F.C., Megahed I.E.A., Shah N.G.
The Prediction of the Flow, Reaction, and heat transfer in the Combustion Chamber of a Glass Furnace, 18th Aerospace Sciences Meeting, Pasadena 1980.

Hossain M.S., Rodi W.
Mathematical Modelling of Vertical Mixing in Stratified Channel Flow, Proc. of Second International Symposium on Stratified Flows, Trondheim, 1980.

Ince N.Z., Launder B.E
On the Computation of Buoyance-driven Turbulent Flows in Rectangular Enclosures, International Journal of Heat and Fluid Flow, vol.10, 1989.

Jackman P.J.
Displacement Ventilation, Technical Memorandum 2/90, The Building Services Research and Information Association, 1990.

Jacobsen T.V., Nielsen P.V.
Velocity and Temperature Distribution in Flow from an Inlet Device in Rooms with Displacement Ventilation, Proc. of Roomvent, Aalborg 1992.

Jacobsen T.V., Nielsen P.V.
Numerical Modelling of Thermal Environment in a Displacement-Ventilated Room, Proc. of Indoor Air, vol.5, Helsinki 1993.

Jones W.P., Launder B.E.
The Prediction of Laminarization with a Two-equation Model of Turbulence, International Journal of Mass Heat Transfer, vol. 15, 1972.

Kofoed P.
Thermal Plumes in Ventilated Rooms, Ph.D.-thesis, Department of Building Technology and Structural Engineering, University of Aalborg, 1991.

Kurabuchi T., Kamata M.
Wall Boundary Conditions of Numerical Method of Non-isothermal Indoor Airflow - Natural Convection of a Vertical Heated Plate, Proc. of Annual Meeting of The Society of Heating, Airconditioning and Sanitary of Japan (in japanese), 1989.

Launder B.E., Spalding D.B.
The Computation of Turbulent Flows, Computional Methods of Applied Mechanical Engineering 3, 1974.

Launder B.E.
On the Effects of a Gravitational Field on the Turbulent Transport of Heat and Momentum, Journal of Fluid Mechanics, vol.67, 1975.

Lemaire A.D.
Simulation of testcase G - Displacement Ventilation, IEA Annex 20, Report No. AN20.1-NL-90-TNO-TPD11, Delft, 1991.

Lemaire A.D.
Measurement of testcase G - Displacement Ventilation, IEA Annex 20, Report No. AN20.1-NL-90-TNO-TPD15, Delft, 1991.

Leonard B.P.
A Stable and Accurate Convective Modelling Procedure Based on Quadratic Upstream Interpolation, Computer Methods in Applied Mechanics and Engineering, vol. 19, 1979.

Leschziner M.A.
Turbulence Modelling Challenges posed by Complex Flows, Proc. Roomvent, vol.1, Aalborg 1992.

Li Y., Sandberg M., Fuchs L.
Vertical Temperature Profiles in Rooms Ventilated by Displacement - Full-scale Measurement and Nodal Modelling, Proc. Indoor Air, Helsinki 1993.

Lockwood F.C., Shah N.G.
A new Radiation Solution Method for Incorporation in General Combustion Prediction Procedures, 18. International Symposium on Combustion, 1981.

Mathisen H.M, Skåret E.
Efficient Ventilation of Small Rooms, Proc. of 16th. Internatinal Congress of Refrigeration, Paris 1983.

Mathisen H.M.
Analysis and Evaluation of Displacement Ventilation, Ph.D.-thesis, Norges Tekniske Høgskole, Trondheim 1989.

Matsuo Y. , Yee J., Kurabuchi T., Kamata M.
Highly Accurate and Non-oscillatory Finite Difference Approximation Method for Convection Diffusion Equations, Proceedings of International Symposium on Room Air Convection and Ventilation Effectiveness, Tokyo 1992.

Melikov A., Derbiszewski B., Langkilde G.
Draught Risk in Rooms with Displacement Ventilation, Technical University of Denmark, 1989.

Murakami S., Kato S., Nakagawa H.
Numerical Prediction of Horizontal Nonisothermal 3-D Jet in Room based on the k-ϵ model, ASHRAE transactions, Vol.97, 1991.

Murakami S., Kato S., Ooka R.
Numerical Simulation of Horizontal Non-isothermal 3-D Jet in Room by DSM, Proc. Roomvent, vol. 1, Aalborg 1992.

Nallasamy M.
Turbulence Models and their Applications to the Prediction of Internal Flows, Computer and Fluids, vol.15, 1987.

Nielsen P.V., Restivo A., Whitelaw J.H.
Buoyancy-affected Flows in Ventilated Rooms, Journal of Numerical Heat Transfer, vol.2, 1979.

Nielsen P.V., Hoff L., Pedersen L.G.
Displacement Ventilation by Different Types of Diffusers, 9th AIVC conf., Gent, 1988.

Nielsen P.V.
Air Velocity at the Floor in a Room with Wall Mounted Air Terminal Device and Displacement Ventilation, Nordic Ventilation Group, Oslo 1990.

Nielsen P.V.
Velocity Distribution in the Flow from a Wall-Mounted Diffuser in Rooms with Displacement Ventilation, Proc. of Roomvent '92, Aalborg 1992.

Omori T., Taniguchi H., Kudo K.
Monte Carlo Simulation of Indoor Radiant Environment, International Journal for Numerical Methods in Engineering, vol.30, 1990.

Patankar S.V., Spalding D.B.
Heat and Mass Transfer in Boundary Layers, Morgan-Grampian, London 1967.

Patankar S.V., Spalding D.B.
A Calculation Procedure for Heat, Mass and Momentum Transfer in Three-dimensional Parabolic Flows, Journal of Heat and Mass Transfer, vol.15, 1972.

Patankar S.V.
Numerical Heat and Fluid Flow, McGraw-Hill, New York 1980.

Pedersen F.B.
Environmental Hydraulics - Stratified Flows, Lecture Notes on Coastal and Estaurine Studies, Springer Verlag 1986.

Rodi W.
Turbulence Models and their Application in Hydraulics, University of Karlsruhe, 1980.

Rodi W., Murakami S.
Turbulence Models for Practical Applications, Seisan-Kenkyu, vol.41, no.8, 1989.

Schlichting H.
Boundary Layer Theory, McGraw-Hill Book Company, 1968.

Schaelin A., Kofoed P.
Numerical Simulation of Thermal Plumes in Rooms, Proc. of Roomvent '92, Aalborg 1992.

Sandberg M., Lindström S.
A Model for Ventilation by Displacement, Proc. of Roomvent '87, Stockholm 1987.

Sandberg M., Mattson M.
The Mechanism of Spread of Negatively Buoyant Air from Low Velocity Air Terminals, Application of Fluid Mechanichs in Environment Protection 91, Wisla 1991.

Sandberg M., Holmberg S.
Spread of Supply Air from Low Velocity Air Terminals, Proc. Roomvent '90, Oslo 1991.

Sandberg M., Blomqvist C.
Displacement Ventilation in Office Rooms, ASHRAE Trans., Vancouver, 1989

Sandberg M.
Stratified Flow in Ventilated Rooms, The National Swedish Institute for Building Research, 1988.

Sandberg M.
Gravity Currents in Ventilated Rooms, The National Swedish Institute for Building Research, 1989.

Shankar V., Davidson L., Olsson E.
Ventilation by Displacement : Calculation of the Flow in Vertical Plumes, Proc. of Roomvent '92, Aalborg 1992.

Skistad H.
Fortrengningsventilasjon i komfortanlegg med lavimpuls lufttilførsel i oppholdssonerne, Norsk VVS Teknisk Forening, 1989. (in norwegian)

Skovgaard M., Nielsen P.V.
Modelling Complex Inlet Geometries in CFD - Applied to Air Flow in Ventilated Rooms, Proc. of the 12th AIVC conference, Warwick 1991.

Skovgaard M.
Turbulent Flow in Rooms Ventilated by the Mixing Principle, Ph.D.-thesis, Department of Building Technology and Structural Engineering, University of Aalborg, 1991.

Skåret E.
Ventilation by Displacement - Characterization and Design Implications, Ventilation '85, Elsevier Science Publishers B.V., 1986.

Skåret E.
Ventilation by Stratification and Displacement, Proc. of Second International Congress on Building Energy Management, Ames, 1986.

Spalding D.B.
A Novel Finite-Difference Formulation for Differential Expressions Involving First and Second Derivatives, Journal of Numerical Methods, vol.4, 1972.

Takemasa Y., Kurabuchi T., Kamata M.
Numerical Simulation of Indoor Air Temperature and Wall Heat Flow Distribution of a Heated and Cooled Room, Proc. of International Symposium on Room Air Convection and Ventilation Effectiveness, Tokyo 1992.

Tennekes H., Lumley J.L
A First Course in Turbulence, The Massachussets Institue of Technology, 1972.

Turner J.S.
Buoyancy effects in fluids, Cambridge University Press, Cambridge 1979.

Van Doormal J.P., Raithby G.D
Enchancements of the SIMPLE Method for Predicting Incompressible Fluid Flows, Journal of Numerical Heat Transfer, vol.7, 1984.

Verhoff A.
The Two-dimensional Turbulent Wall Jet w without an External Free Stream, Report no. 626, Princetown University, 1963.

Viollet P.L.
Turbulent Mixing in a Two-layer Stratified Shear Flow, Proc. of Second International Symposium on Stratified Flows, Trondheim, 1980.

Viollet P.L.
The modelling of turbulent recirculating flows for the purpose of reactor thermal-hydraulic analysis, Nuclear Engineering and Design, V.99, 1987.

Wilkinson D.L., Wood I.R
A Rapidly varied Flow Phenomenon in a Two-layer Flow, Journal of Fluid Mechanics, vol. 47, 1971.

Yuan X., Huber A., Schaelin A., Hachmann P., Moser A.
New Wall Functions for the Numerical Simulation of Air Flow Pattern in Rooms, Proc. Roomvent, vol.1, Aalborg 1992.

Nomenclature

Symbol	Description
A	Area, constant in wall jet equation
Ar	Archimedes number
Ar_l	Local Archimedes number
Ar_r	Reduced Archimedes number
a	Transport coefficient
α	Convective heat transfer coefficient, angle of velocity vector, underrelaxation coefficient
B	Constant in wall jet equation
b	Height of profile $\sim U_{max}/2$, buoyancy parameter
β	Volumetric expansion factor for air
C_μ, C_1, C_2, C_3	Constants in the k-ϵ turbulence model
c_p	Specific heat at constant pressure
Γ	Diffusion coefficient
δ_{ij}	Kronecker delta
E	Wall roughness function
erf	The errorfunction

ϵ	Dissipation rate of turbulent kinetic energy, emission coefficient
F_Δ	Densimetric Froude number
f_b	Buoyancy damping function
f_{Rt}	Low-Reynolds number damping function
G	Generation term
g	Gravitational acceleration
H	Height of room
h	Height of dense layer
I	Turbulence intensity, radiation intensity
K, K^*	Constants in equation for velocity decay
k	Turbulent kinetic energy
κ	Von Karman constant, gas absorption coefficient
l	Turbulent length scale
λ	Heat conductance
m	Exponent in velocity-temperature correlation equation
μ	Dynamic viscosity
θ	Streamline angle, horizontal angle
P	Pressure, production term
Pe	Peclet number

q	Airflow rate, radiative heat flux
Q	Convective heat transfer
r	Distance from inlet device
R	Residual
Re	Reynolds number
Ri	Richardson number
ρ	Density of air
S	Source term
σ	Prandtl number, Stefan-Boltzmann constant
T	Temperature
τ	Time, shear stress
ϕ	Arbitrary flow variable, vertical angle
u,v,w	Velocity fluctuations corresponding to x,y,z-directions, respectively
U,V,W	Time averaged velocity components corresponding to x,y,z-directions, respectively
U^+	Dimensionless velocity parallel to the wall
U_e	Entrainment velocity
U_f	Friction velocity
V	Volume

x,y,z	Cartesian coordinates
y^+	Dimensionless distance normal to the wall

Index	**Description**
e	Exhaust
f	Floor
i	Inlet
i,j,k	Indicators for coordinate direction in tensornotation
l	Laminar
nb	Neighbour cell
t	Turbulent
w, e, s, n, u, l	West, east, south, north, upper, lower - indicators for direction in a 3-D volume
*	Instantaneous value
1.1	Variable value 1.10m above the floor in the occupied zone

Appendix A - Wall functions

$$U^+ = \frac{U_p U^*}{U_f^2} = \frac{\ln(Ey^+)}{\kappa} \qquad y^+ = \frac{\rho U^* y_p}{\mu_l} \qquad T^+ = \frac{C_p \tau_w}{\alpha_w U_p} U$$

Launder and Spalding 1974 :

$$U^+ = \begin{cases} y^+ & y^+ < 11.6 \\ 2.3 ln y^+ + 5.1 & y^+ > 11.6 \end{cases}$$

$$T^+ = \begin{cases} \sigma_l y^+ & y^+ < 11.6 \\ \sigma_t (U^+ + P) = \sigma_t (2.3 ln y^+ + 3.2) & y^+ > 11.6 \end{cases}$$

Chen 1988 :

$$U^+ = \begin{cases} y^+ & y^+ < 8 \\ 3.5 \ln y^+ + 0.8 & 8 < y^+ < 40 \\ 2.3 ln y^+ + 5.1 & y^+ > 40 \end{cases}$$

$$T^+ = \begin{cases} \sigma_l y^+ & y^+ < 8 \\ 3.0 ln y^+ - 0.6 & 8 < y^+ < 40 \\ \sigma_t (2.3 ln y^+ + 3.2) & y^+ > 40 \end{cases}$$

Kurabuchi and Kamata 1989 :

$$U^+ = \begin{cases} y^+ & y^+ < 5 \\ 5.0 \ln y^+ - 3.1 & 5 < y^+ < 30 \\ 2.5 ln y^+ + 5.5 & y^+ > 30 \end{cases}$$

$$T^+ = \begin{cases} \sigma_l y^+ & y^+ < 5 \\ \sigma_t (5.0 ln y^+ - 3.1) & 5 < y^+ < 30 \\ \sigma_t (2.5 ln y^+ + 5.5) & y^+ > 30 \end{cases}$$

Moser et. al. 1992 :

$$U^+ = \begin{cases} y^+ & y^+ < 5 \\ 4.8\ln y^+ - 2.8 & 5 < y^+ < 16 \\ 3.5 ln y^+ + 1.0 & 16 < y^+ > 42 \\ 2.3 ln y^+ + 5.3 & y^+ > 42 \end{cases}$$

$$T^+ = \begin{cases} \sigma_l y^+ & y^+ < 5 \\ 4.2 ln y^+ - 3.1 & 5 < y^+ < 19 \\ 3.6 ln y^+ - 1.5 & 19 < y^+ < 45 \\ 2.1 ln y^+ + 4.1 & y^+ > 45 \end{cases}$$

Appendix B - Flow diagram for the TEAM CFD-code

General structure for the iterative calculation of variables :

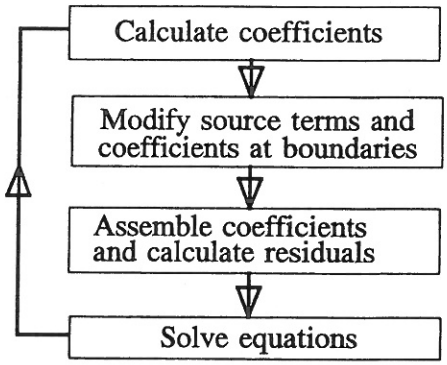

Over all structure of the TEAM-code :

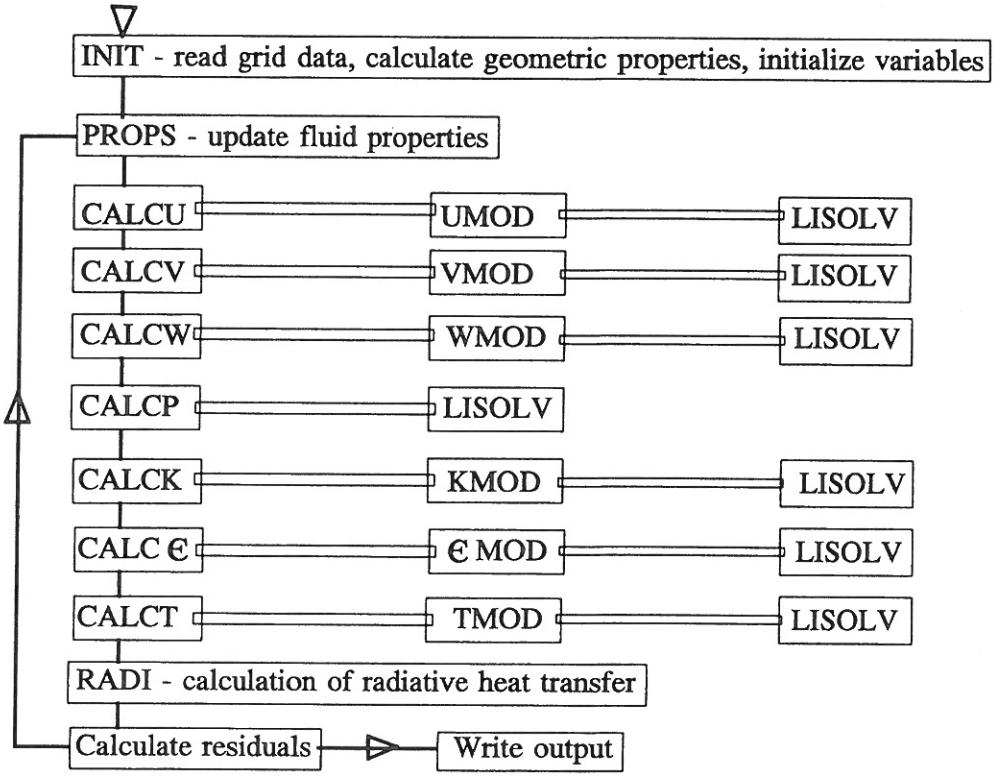

Sammenfatning

Denne Ph.D.-afhandling er udarbejdet som afslutning på forskningsprojektet "Luftstrømning og temperaturfordeling i lokaler med fortrængningsventilation". Det er projektets mål at afdække ventilationsprincippets strømningstekniske karakteristika ved hjælp af fuldskala målinger og en efterfølgende gennemføre en analyse hvor simple semi-empiriske modeller og en avanceret numerisk strømningsmodel tages i anvendelse.

Luftstrømningen i et lokale med fortrængningsventilation er drevet af den kølige indblæste luft og opdriftsstrømninger, der dannes ved varmekilder. I en given højde vil den tilførte luftmængde svare til den samlede luftmængde, der transporteres opad i disse opdriftsstrømninger. Her opstår en lagdeling, som adskiller den øvre zone med relativt høj temperatur og høj koncentration af eventuelle forurenende stoffer fra den nedre "rene" zone med relativt lav temperatur. Store dele af rummet er karakteriseret ved en meget ringe luftbevægelse, der foregår i horisontale lag p.gr.a temperaturgradienten. Desuden kan der ved væggene opstå betydelige opadrettede eller nedadrettede strømninger, hvis der er væsentlig temperaturforskel mellem vægflader og det tilstødende luftvolumen.

Den kølige luft tilføres via et vægmonteret armatur direkte i opholdszonen. Det tilstræbes at luften tilføres med lave hastigheder af komforthensyn. Opdriftskræfter forårsager en acceleration og vertikal kontraktion af det tilførte luftvolumen. Der sker en afbøjning idet den kølige luft rammer gulvet, og som følge heraf spredes luften horisontalt i et tyndt lag, der p.gr.a den termiske stratifikation kun i ringe grad opblandes med den øvrige rumluft.

At udnytte opdriftskræfter til at fortrænge et luftvolumen, og derved opnå tilstrækkelig luftkvalitet, har været udnyttet indenfor industriventilation i mange år, men fortrængningsventilation som selvstændigt begreb er først opstået for omtrent 10 år siden i Norge og Sverige. Rapporten gør rede for det forskningsarbejde, der har været udført med fortrængningsventilation, og det konkluderes at en decideret analyse af strømningsforholdene vil udgøre et væsentlig bidrag til den eksisterende viden.

Efterfølgende er målene for projektet konkretiseret og behovet for en dyberegående analyse af den stratificerede strømning foran indblæsningsarmaturet er fremhævet. På baggrund af målinger er det hensigten at undersøge hvorvidt modificerede udtryk fra

stråleventilation og/eller en avanceret numerisk strømningsmodel for hele strømningsfeltet er egnede redskaber til beskrivelse af strømningen.

I forbindelse med opbygning og verifikation af den numeriske model undersøges det hvilken rolle formuleringen af randbetingelser har på de opnåede resultater. Her er det vigtigt at belyse indblæsningsranden, hvor den komplekse opbygning af armaturet nødvendiggør en forsimplet beskrivelse. Strømningen er også i høj grad påvirket af det vertikale temperaturprofil, og strålingsudvekslingen mellem specielt gulv og loft må indeholdes i modellen på passende vis. Det er her væsentligt at anvise alternativer og undersøge hvad de måtte indebære i forhold til strømningen i rummet i almindelighed og i forhold til den stratificerede gulvstrømning i særdeleshed. Det er målet at præsentere anbefalinger omkring hvilke modelantagelser, der er afgørende for resultaterne og dermed nødvendige at inkludere og hvilke der kan lades ude af betragtning.

Målingerne er fortaget i et fuldskalarum udstyret med et Lindab COMDIF CDE-2010 armatur og henholdsvis en koncentreret varmekilde og to personsimulatorer. Forsøgsopstillingen er arrangeret således at rummets midterplan falder sammen med armaturets centerakse og udgør et symmetriplan.

Første skridt er gennemførelsen af en række røgforsøg, hvis primære formål er at fastlægge en procedure for gennemførelse af målingerne. Målinger af temperatur- og hastighedsprofiler i gulvstrømningen er foretaget i højden 0-30 cm over gulvfladen. I erkendelse af at strømningen fra armaturet er tilnærmelsesvis radiel indføres et polært koordinatsystem og målingerne gennemføres i "strømlinier" svarende til varierende afstand fra armaturet for fastholdt vinkel i forhold til armaturets centerakse.

Gulvstrømningen er opmålt for forskellige Arkimedes tal og herudover er der målt vertikale temperaturforløb i hele rummets højde, indvendige og udvendige temperaturprofiler på væggene, gulvtemperaturer og hastighedsfordelinger ved indblæsningsfladen.

Analysen af de målte data er først og fremmest koncentreret omkring hastighedsfaldet foran armaturet. Der præsenteres teorier opstillet af henholdsvis *Sandberg og Blomqvist 1989* og *Nielsen 1992*. Førstnævnte er ikke umiddelbart anvendelig i den praktiske analyse hvor imod sidstnævnte viser god overensstemmelse med målingerne. Oprindeligt er de anvendte udtryk opstillet for hastighedsfaldet i armaturets centerakse, men det demonstreres at de med god tilnærmelse kan udvides til at gælde for øvrige retninger i den 3-dimensionale gulvstrømning. Maksimalhastighederne kan bestemmes med god nøjagtighed og den efterfølgende analyse fokuserer på profilernes vertikale variation.

Det antages at profilerne er ligedannede og det undersøges om udtryk for hastighedsfordelingen i en vægstråle også kan anvendes for gulvstrømningen i et lokale med fortrængningsventilation. Desuden er det forsøgt at overføre en korrelation mellem hastigheder og temperaturer i en stråle til beskrivelse af temperatur profilet. På basis af måledata kan det konkluderes at hastighedsforløbet er godt beskrevet ved denne metode imens det vertikale temperaturforløb viser nogen afvigelse. Afsnittet afsluttes med en diskussion omkring den stærkt aftagende opblanding i den stratificerede strømning langs gulvet og der præsenteres måleresultater, der indikerer, at der optræder et henholdsvist sub-kritisk og super-kritisk domæne analogt til tilsvarende begreber indenfor hydraulikken.

I det efterfølgende afsnit redegøres for teorien for turbulent strømning. Den almindeligt anvendte k-ϵ model introduceres og de styrende differentialligninger opstilles. I gennemgangen lægges særlig vægt på de specifikke forhold i et lokale med fortrængningsventilation. Her tænkes på den udprægede indflydelse fra temperaturfeltet og lav-turbulente fænomener. Dæmpningsfunktioner til modifikation af turbulensmodellen beskrives og k-ϵ modellens styrker og svagheder opridses. Specielt antagelsen om isotrop turbulens udgør en begrænsning, men set i forhold til de væsentligt øgede krav til beregningskapacitet og de numeriske stabilitetsproblemer , der er forbundet med anvendelsen af mere avancerede alternativer, er k-ϵ modellen det bedst egnede kompromis.

Den numeriske løsningsmetode er i store træk beskrevet af *Patankar 1980*. Hovedpunkterne i processen er behandlet med særlig vægt på de valg der er foretaget. I diskretiseringen af de styrende ligninger er HYBRID-skemaet, der kombinerer "central difference" og "upwind difference", valgt fremfor det mere nøjagtige QUICK-skema p.gr.a. numeriske stabilitetsproblemer. Netop problemet med at opnå en konvergeret løsning - der samtidig er nøjagtig - omhandles og der fremhæves en række forhold, der bør tages i betragtning. Udformning af beregningsnet, linearisering af kildeled og valg af relaxationskoefficienter spiller her en vigtig rolle.

Randbetingelserne i den numeriske model er afgørende for det resulterende strømningsfelt og i det aktuelle tilfælde er væglove for temperatur- og impulsligninger, indblæsningsranden og beskrivelsen af varmekilderne af største betydning. De traditionelle væglove formuleret af *Launder and Spalding 1974* er blevet kritiseret og forslag til forbedrede versioner er undersøgt. Et hovedkritikpunkt er de beregnede konvektive varmeovergangskoefficienters afhængighed af beregningsnettet ved væggen.

Det er besluttet at undersøge tre vægrandbetingelser bestående af en simpel antagelse om adiabatiske vægge og ingen strålingsudveksling, adiabatiske vægge samt strålingsmodel og beregning af varmeovergang ved hjælp af temperaturvæglov og foreskreven temperaturfordeling på rummets flader. I den forbindelse testes forkellige væglove og der udvikles en strålingsmodel byggende på "Discrete Transfer Model" (DTM) beskrevet i *Lemaire 1991* og *Li 1992*.

På indblæsningsranden er effekten af at anvende et målt profil med uensartet hastighedsfordeling undersøgt og ud fra røgforsøgene er det endvidere fundet relevant at variere hastighedsvektorens retning ved indblæsningen.

Opdriftsstrømningerne over varmekilderne påvirker hele rumstrømningen og bla. *Shankar et. al. 1992* demonstrerer at k-ϵ modellen er i stand til at simulere strømningen når der anvendes et stort antal netpunkter. Det er imidlertid ikke muligt at benytte en sådan netopløsning når strømningen i hele rummet behandles. Derfor er beskrivelsen af varmekilderne forenklet med henblik på først og fremmest at opnå en overordnet overensstemmelse af hensyn til temperaturfordelingen i rummet.

Herefter præsenteres resultater opnået ved hjælp af den numeriske model og der sammenlignes med målinger. Det generelle strømningsbillede stemmer fuldt overens med observationerne under røgforsøgene. Faktisk kan detaljer i strømningsfeltet bedre iagttages i de detaljerede modelresultater. En overordnet kvalitativ overensstemmelse kan opnås for en række forskellige kombinationer af randbetingelser og en direkte sammenligning med måledata er nødvendig for at vurdere modellens beregningsnøjagtighed.

Effekten på den vertikale temperaturgradient af at anvende de tre ovenfor omtalte specifikationer af temperaturrandbetingelsen viser tydeligt at strålingen nødvendigvis må inkluderes i modellen. Kun ved væglove og foreskrevne fladetemperaturer samt versionen med separat strålingsmodel opnåes en rimelig tilnærmelse til rummets vertikale temperaturprofil. Temperaturniveauet er godt bestemt ved begge metoder, mens profilformerne er moderat afvigende i forhold til det målte.

Det er vist gennem anvendelse af fire forskellige væglove at den beregnede varmetilførsel ved gulvet afhænger af beregningsnettet i alle tilfælde. Flerlags væglove af *Chen 1988* og *Moser et. al. 1992* reducerer dog afhængigheden og resulterer generelt i højere varmeovergangskoefficienter og total varmeflux. Ofte er det nødvendigt at indføre et forholdsvist groft net ved væggene og man bør derfor være opmærksom på at de konvektive varmeovergangskoefficienter herved underestimeres.

Tilføjelsen af dæmpningsfunktioner i turbulensmodellen viser at diffusionen stort set er upåvirket med undtagelse af de stillestående områder. Der er derfor ikke nogen mærkbar nytte af at indføre disse og de er udeladt i det videre forløb.

En række testcases illustrerer at gulvstrømningens maksimalhastigheder som funktion af afstanden til indblæsningsarmaturet i udpræget grad er påvirket af indblæsningsranden. Den absolutte maksimalhastighed finder man i 2-5 cms højde over gulvet i en afstand af ca. 1.0 m fra armaturet. Her er hastigheden fra modellen lavere end den målte værdi i alle testcases, men der kan dog opnåes en rimelig overensstemmelse ved at anvende den målte hastighedsfordeling og en nedadrettet hastighedsvektor på indblæsningsranden. Desuden kan størrelsen af den turbulente kinetiske energi, dissipationen af turbulent energi og dermed den turbulente viskositet ved indblæsningsranden påvirke hastighedsniveauet. Resultaterne antyder at der bør specificeres en tilnærmelsesvis laminar tilstand.

Sammenligning af temperatur og hastighedsprofiler i hele gulvstrømningen viser at hastighederne og temperaturerne er let underestimerede i modellen og at den horisontale spredning langs gulvet ikke er tilstrækkelig stor. I armaturets centerakse kan man tale om en god tilnærmelse til målte værdier hvor imod retningen vinkelret på centeraksen viser en markant afvigelse.

Diskussionen af modelresultaterne munder ud i en konklusion, hvor det påpeges at de simple semi-empiriske modeller er velegnede til beskrivelse af gulvstrømningen men at en række usikre forhold gør det vanskeligt at anvende numeriske strømningsmodeller uden god indsigt i strømningsmæssige forhold og en passende reference i form af målinger. Den store informationsmængde der kan opnåes ved numeriske modeller gør dog metoden attraktiv og resultaterne viser at metoden har sin berettigelse hvis den følges op af en kritisk vurdering - helst i form af en verifikation.

Behandlingen af strømningen i rummet har vist at forholdene lokalt kan være komplekse og den eksisterende viden begrænset. Der kan kun opfordres til videre forskningsmæssig indsats både indenfor måling og modellering.

PH.D.-THESES ON INDOOR ENVIRONMENTAL TECHNOLOGY

THESIS NO. 1: P. Heiselberg: *Strømningsforhold i lokaler ventileret efter opblandings- og fortrængningsprincippet.* ISSN 0902-7513 R9015.

THESIS NO. 2: P. Kofoed: *Thermal Plumes in Ventilated Rooms.* ISSN 0902-7513 R9156.

THESIS NO. 3: M. Skovgaard: *Turbulent Flow in Rooms Ventilated by the Mixing Principle.* ISSN 0902-7513 R9145.

THESIS NO. 4: L. Germann: *REEXS - Reinforced Exhaust System* (in Danish). ISSN 0902-7513 R9154.

THESIS NO. 5: H. Overby: *Vertikale temperaturgradienter i rum med konvektive strømninger.* ISSN 0902-7513 R9312.

THESIS NO. 6: T. V. Jacobsen: *Airflow and Temperature Distribution in Rooms with Displacement Ventilation.* ISSN 0902-7513 R9328.

Department of Building Technology and Structural Engineering
The University of Aalborg, Sohngaardsholmsvej 57. DK 9000 Aalborg
Telephone: 45 98 15 85 22 Telefax: 45 98 14 82 43